CHAPTER 3

The Rotational Isomeric State Model

Carin A. Helfer and Wayne L. Mattice

Institute of Polymer Science, The University of Akron, Akron, OH 44235-3909

3.1 INTRODUCTION

Flexible macromolecules populate an enormous number of conformations at ordinary temperature, T. If ν stable conformations are available to each internal bond in a chain of n bonds, the chain can access ν^{n-2} conformations. When $\nu = 3$, as is appropriate for many simple polymers, the number of distinguishable conformations exceeds 10^{100} when $n > 211$. This number is achieved by polyethylene at the relatively low molecular weight of 2,984. Scientists and engineers need information about the average properties of specific chains with much larger values of n, where the conformation-dependent physical properties of interest depend on an appropriate average over a truly enormous number of conformations. Among the several models that have been proposed for averaging over this ensemble of conformations, the rotational isomeric state (RIS) model is unique in its combination of structural detail with computational efficiency. It incorporates as much structural detail (bond lengths, l, bond angles, θ, torsion angles, ϕ, differences in energy for conformations produced by rotation about a bond or pair of bonds) as most chemists are likely to desire. Figure 3.1 defines the values of θ and ϕ that are associated with bond i. This detailed description of the local chain structure is presented in a mathematical framework that often permits extremely fast calculation of the average values of many conformation-dependent physical properties of individual polymer chains in the amorphous bulk state and in dilute solution in a solvent chosen so that the excluded volume effect is negligible. The speed of the calculation follows from the formulation of the problem as the serial product of n matrices. Computers are easily trained to rapidly, and accurately, compute this serial product.

The most commonly calculated property is the mean square unperturbed dimension. It is usually represented by the mean square unperturbed end-to-end distance, $\langle r^2 \rangle_0$, obtained by averaging the square of the length of the end-to-end vector, $\mathbf{r}$, over all conformations under conditions where the chain is unperturbed by long-range interactions.

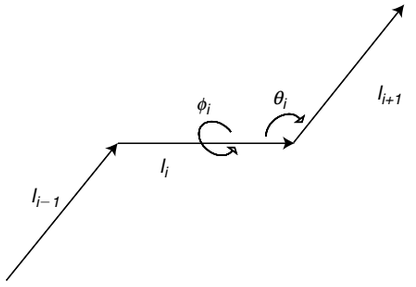

FIGURE 3.1. The definitions of θ_i and ϕ_i associated with bond *i*.

$$\mathbf{r} = \sum_{i=1}^{n} \mathbf{l}_i, \tag{3.1}$$

$$\langle r^2 \rangle_0 = \langle \mathbf{r} \cdot \mathbf{r} \rangle_0 = \sum_{i=1}^{n} l_i^2 + 2 \sum_{i=1}^{n-1} \sum_{j=i+1}^{n} \langle \mathbf{l}_i \cdot \mathbf{l}_j \rangle_0. \tag{3.2}$$

The double sum in Eq. (3.2) can be handled efficiently by matrix methods when the chain is in its unperturbed, or $\boldsymbol{\Theta}$, state. The result for $\langle r^2 \rangle_0$ is usually presented as the dimensionless characteristic ratio, C_n.

$$C_n = \frac{\langle r^2 \rangle_0}{nl^2}. \tag{3.3}$$

As defined in Eq. (3.3), C_n is the ratio of the mean square unperturbed end-to-end distance to the value expected for the freely jointed chain with the same number of bonds, of the same length. If the bonds in the chain are of different lengths, as in polyoxyethylene, l^2 in the denominator is replaced by the mean square bond length. For any flexible unperturbed chain, C_n approaches a limit, C_∞, as $n \to \infty$. The final approach to this limit is usually from below, but it can sometimes be from above. The latter situation can be encountered when C_n passes through a maximum at finite n [1].

The mean square unperturbed radius of gyration, $\langle s^2 \rangle_0$, is accessible by similar methods that rapidly evaluate and sum the mean square end-to-end distances for all of the subchains, denoted by $\langle r_{ij}^2 \rangle_0$, where i and j identify the chain atoms at the ends of the subchain. If all $n + 1$ chain atoms, indexed from 0 to n, can be taken to have the same mass, $\langle s^2 \rangle_0$ is given by the expression in Eq. (3.4).

$$\langle s^2 \rangle_0 = \frac{1}{(n+1)^2} \sum_{i=0}^{n-1} \sum_{j=i+1}^{n} \left\langle r_{ij}^2 \right\rangle_0. \tag{3.4}$$

If the chain is flexible, the RIS calculations produce $\langle s^2 \rangle_0 = \langle r^2 \rangle_0 / 6$ in the limit as $n \to \infty$, as expected [2]. The ratio $\langle r^2 \rangle_0 / \langle s^2 \rangle_0$ may differ from 6 at finite n because $\langle r^2 \rangle_0$ and $\langle s^2 \rangle_0$ do not have the same approach to their limiting behavior [1]. For many real chains, $\langle r^2 \rangle_0 / \langle s^2 \rangle_0 > 6$ at finite n, although $\langle r^2 \rangle_0 / \langle s^2 \rangle_0 \to 6$ as $n \to \infty$. The RIS model has no peer for the calculation of $\langle s^2 \rangle_0$ or $\langle r^2 \rangle_0$ as a function on n because it combines speed with structural detail. Numerous other conformation-dependent physical properties are accessible also from this model. This chapter will describe the RIS method, present a few illustrative results, and cite many of the RIS models for specific polymers that have been presented in the literature.

3.2 HISTORY AND NOTEWORTHY REVIEWS

The speed of calculations using the RIS model arises from its formulation of the problem as a serial product of matrices. The generator matrix technique, which lies at the heart of the calculation, predates the appearance of the RIS model by 10 years [3]. The application of the RIS technique to polymers is now over five decades old [4], although its appearance in the polymer literature did not begin to mushroom until a decade after its first appearance [5–9]. Because computers at that time did not have nearly the speed and widespread availability that is seen today, there was a strong motivation for formulation of the problem in a manner that allowed efficient calculation. With today's computers, the most popular calculations require no more than a few seconds of cpu time.

The first important general work on the RIS model is Flory's classic book, which first appeared in 1969 [10]. His book was followed 5 years later by an excellent review in *Macromolecules* that presented a more general and concise formulation of the RIS method [11]. Another book on the RIS model appeared during the year of the 25th anniversary of the first publication of Flory's original text [12]. It was soon followed by an exhaustive compilation, in a standardized format, of the RIS models presented in the literature over the four decades that ended in the mid-1990s [13].

3.3 RELATIONSHIP TO SIMPLER MODELS

The information incorporated in the RIS model and several simpler models is summarized in Table 3.1. The freely jointed chain has n bonds of length l, with no correlation whatsoever in the orientations of any pair of bonds. The contribution of the double sum in Eq. (3.2) is nil, and $C_n = 1$ at all values of n. Fixing the bond angle, but allowing free rotation about all bonds, produces the freely rotating chain. If $\theta \neq 90°$, C_n will depend on n. The asymptotic limit as $n \to \infty$ is $(1 - \cos\theta)/(1 + \cos\theta)$. If $\theta > 90°$, as is usually the case with real polymers, the freely rotating chain model yields $C_\infty > 1$. Energetic information, in the form of a torsional potential about the internal bonds, $E(\phi)$, is incorporated in the third model in Table 3.1. If the same symmetric torsion potential is applied independently to all internal bonds, the characteristic ratio depends on the average value of the cosine of the torsion angle. The term from the freely rotating chain is retained, and it is multiplied by another term that arises from the symmetric hindered rotation, $C_\infty = [(1-\cos\theta)/(1+\cos\theta)]\,[(1-\langle\cos\phi\rangle)/(1+\langle\cos\phi\rangle)]$.

TABLE 3.1. *Information incorporated in the RIS model and in several simpler models.*

Model	Geometric information[a]	Energetic information
Freely jointed chain	n, l	None
Freely rotating chain	n, l, θ	None
Simple chain with symmetric hindered rotation	n, l, θ,ϕ	First-order interactions (independent bonds, symmetric torsion)
RIS model	n, l, θ,ϕ	First- and higher-order interactions (interdependent bonds, torsion need not be symmetric)

[a]All bonds are assumed to be identical in the usual implementations of the first three models. The assumption of identical bonds is easily discarded in the RIS model.

Since $\langle\cos\phi\rangle$ depends on T, $\langle\cos\phi\rangle = \{\int \exp[-E(\phi)/kT]\, d\phi\}^{-1} \int \cos\phi \exp[-E(\phi)/kT]\, d\phi$, this model is the only one in this paragraph that explicitly says the mean square unperturbed dimensions are temperature dependent. The Boltzmann constant is denoted by k. All of the results in this paragraph assume that the bonds are identical.

In general, it is difficult or impossible to write the results for C_∞ with such simple closed-form expressions when the torsions become interdependent and the bonds are not all identical. However, Nature asks that we take account of the interdependence of the torsions, because nearly all of the real-world polymers have bonds that are subject to interdependent torsions. And many important polymers are made up of bonds with different lengths. The closest one can come to a general and simple expression is something of the form given in Eq. (3.5).

$$C_\infty = \lim_{n\to\infty} \frac{\boldsymbol{G}_1\boldsymbol{G}_2\cdots\boldsymbol{G}_n}{\mathbf{U}_1\mathbf{U}_2\cdots\mathbf{U}_n} = \lim_{n\to\infty} \frac{1}{Z_n}\boldsymbol{G}_1\boldsymbol{G}_2\cdots\boldsymbol{G}_n. \qquad (3.5)$$

As we shall see below, the denominator in Eq. (3.5) is the conformational partition function, Z_n, for the RIS model of the chain. It is constructed as a sum of Boltzmann factors that depend on T and the energies of the first- and higher-order interactions present in all of the conformations of the chain. Structural information does not appear explicitly in Z_n. However, a wealth of structural information (l, θ, ϕ) can appear in the numerator of Eq. (3.5). The numerator also contains all of the thermal and energetic information from Z_n. The combination of this information allows a rapid estimation of C_n, even at large n, because computers can rapidly calculate the serial matrix products that appear in the numerator and denominator of Eq. (3.5).

$\mathbf{U}_1 \ldots \mathbf{U}_n$ is a simpler serial product than $\boldsymbol{G}_1 \ldots \boldsymbol{G}_n$, because it does not include structural information explicitly. For this reason, the easiest introduction to the RIS model is to focus first on Z_n, rather than $\boldsymbol{G}_1 \ldots \boldsymbol{G}_n$.

3.4 THE ROTATIONAL ISOMERIC STATE APPROXIMATION

The basis for the RIS model is most easily seen if we consider a chain where the torsion angles at internal bonds are restricted to a small set of values. For many simple polymers, the RIS models use $\nu = 3$, but the model is sufficiently robust so that it can be used with other choices also. The number of conformations of a chain of n bonds is ν^{n-2}, which becomes enormous when n is large enough so that the molecule becomes of interest to polymer scientists. A pair of two consecutive bonds, bonds $i-1$ and i, has ν^2 conformations. The ν^2 conformations can be presented in tabular form, where the columns represent the ν conformations at bond i, and the rows represent the ν conformations at bond $i-1$. Each entry in the table corresponds to a specific choice of the conformations at these two bonds. In the RIS model, this table becomes a matrix. The elements in the matrix represent contributions to the statistical weights for the conformation adopted at bond i (which depends on the column in the matrix), for a specific choice of the conformation at the preceding bond (which depends on the row in the matrix).

3.5 THE STATISTICAL WEIGHT MATRIX

The statistical weight matrix for bond i, denoted $\mathbf{U}_i$, is usually formulated as the product of two matrices.

$$\mathbf{U}_i = \mathbf{V}_i\mathbf{D}_i. \qquad (3.6)$$

Interaction energies that depend only on the torsion at bond i are responsible for the statistical weights that appear along the main diagonal in $\mathbf{D}_i$. These interactions are termed first-order interactions because they depend on a single degree of freedom, ϕ_i. For the example of a polyethylene-like chain with a symmetric three-fold torsion potential, the rotational isomeric states are t, g^+, g^- (*trans*, *gauche*$^+$, *gauche*$^-$). In the approximation that all bonds are of the same length, all bond angles are tetrahedral, and the torsion angles for the t and $g^\pm$ states are 180° and $\pm 60^\circ$, the separation of the terminal atoms in a chain of three bonds is $(19/3)^{1/2}l$ in the t state, but this separation falls to $(11/3)^{1/2}l$ in the $g^\pm$ states. This change in separation usually produces different energies in the t and $g^\pm$ states. The influence of these energies on the conformation of the chain is taken into account in $\mathbf{D}$. Often a statistical weight is calculated from the corresponding energy as a Boltzmann factor, $w = \exp(-E/RT)$. The t state is usually taken as the reference point, with $E_t = 0$

and a statistical weight of one, and the g states have a statistical weight of $\sigma = \exp[-(E_g - E_t)/RT]$ if the torsion is symmetric, with $E_{g+} = E_{g-}$. A pre-exponential factor may also be necessary if the t and $g^{\pm}$ wells have significantly different shapes. When the order of indexing of the rows and columns is t, g^+, g^-, this diagonal matrix takes the form shown in Eq. (3.7).

$$\mathbf{D}_i = \text{diag}(1,\sigma,\sigma) = \begin{bmatrix} 1 & 0 & 0 \\ 0 & \sigma & 0 \\ 0 & 0 & \sigma \end{bmatrix}, \quad 1 < i < n. \tag{3.7}$$

Real chains often have $\sigma < 1$, as in polyethylene [14], but a few chains, such as polyoxymethylene, have $\sigma > 1$ [15].

The second-order interactions depend jointly on ϕ_{i-1} and ϕ_i. For a simple chain with $\nu = 3$ and symmetric torsion about its internal bonds, the second-order interactions in the tg^+, tg^-, g^+t, and g^-t states are identical, as are the interactions in the g^+g^+ and g^-g^- states, and the interactions in the g^+g^- and g^-g^+ states. The general form of $\mathbf{V}_i$ under these conditions appears in Eq. (3.8), where the order of indexing is t, g^+, g^- for both rows and columns, and the reference point for the second-order interactions is any of the four conformations where one bond is t and the other is g.

$$\mathbf{V}_i = \begin{bmatrix} \tau & 1 & 1 \\ 1 & \psi & \omega \\ 1 & \omega & \psi \end{bmatrix}, \quad 2 < i < n. \tag{3.8}$$

The state at bond $i-1$ indexes the rows, and the state at bond i indexes the columns.

Figure 3.2 depicts the four possible separations of the terminal atoms in a chain of four bonds when all bonds are of the same length, bond angles are tetrahedral, and the torsion angles for the t and $g^{\pm}$ states are 180° and ±60°. By far the shortest separation is seen when the two internal bonds adopt g states of opposite sign. This short distance causes most real chains to have severely repulsive second-order interactions in the g^+g^- and g^-g^+ conformations, producing $\omega < 1$, as in both polyethylene and polyoxyethylene. Often the other second-order interactions are weak enough so that little error is introduced if they are ignored, which frequently leads to the approximation $\tau = \psi = 1$.

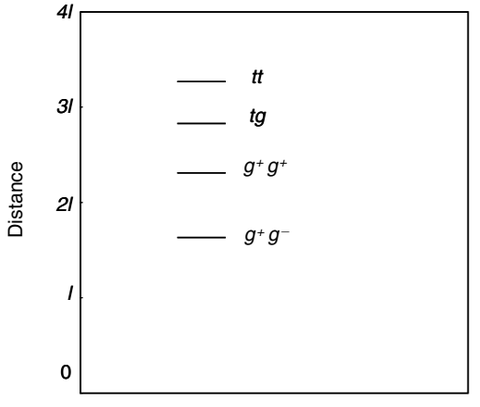

FIGURE 3.2. The four distinguishable separations of the terminal atoms in a chain of four bonds when all bonds are of the same length, l, all bond angles are tetrahedral, and the three states at each internal bond have torsion angles of 180° (t) or ± 60° (g^+ and g^-).

The statistical weight matrix incorporates the first- and second-order interactions, according to Eq. (3.6). For the chain with a symmetric three-fold torsion potential and pairwise interdependent bonds, $\mathbf{U}_i$ adopts the form in Eq. (3.9).

$$\mathbf{U}_i = \begin{bmatrix} \tau & \sigma & \sigma \\ 1 & \sigma\psi & \sigma\omega \\ 1 & \sigma\omega & \sigma\psi \end{bmatrix}, \; 2 < i < n. \tag{3.9}$$

The first rotatable bond in the chain, with $i = 2$, is a special case because there is no preceding rotatable bond for use in defining the statistical weights to be incorporated in $\mathbf{V}_2$. This situation is handled by formulating $\mathbf{U}_2$ using only the statistical weights for first-order interactions, which is achieved by using a value of 1 for every element in $\mathbf{V}_2$.

For the simple chain considered in the examples presented in Eqs. (3.7)–(3.9), all of the $\mathbf{U}_i$ are square and identical [14]. In polyoxymethylene, all of the $\mathbf{U}_i$ are square, but there are two square $\mathbf{U}_i$ with distinctly different numerical values of the elements [15]. Half of the statistical weight matrices for polyoxymethylene incorporate second-order interactions between pairs of oxygen atoms, and the other half incorporate second-order interactions between pairs of methylene groups. For other polymers, such as the polycarbonate of bisphenol A [16], some of the $\mathbf{U}_i$ may be rectangular but not square, because there is a different number of rotational isomeric states at bonds $i-1$ and i. The RIS model does not require that all bonds adopt the same value for ν.

3.6 THE CONFORMATIONAL PARTITION FUNCTION, Z_n

The conformational partition function, in the RIS approximation, is the sum of the statistical weights for the ν^{n-2} conformations in the RIS model. The terminal row and column vectors must be formulated so that they will extract the desired sum of the statistical weights of all conformations from $\mathbf{V_2D_2} \ldots \mathbf{V}_{n-1}\mathbf{D}_{n-1}$.

$$\begin{aligned} Z_n &= \mathbf{J}^*\mathbf{V}_2\mathbf{D}_2\mathbf{V}_3\mathbf{D}_3 \ldots \mathbf{V}_{n-1}\mathbf{D}_{n-1}\mathbf{J} \\ &= \mathbf{J}^*\mathbf{U}_2\mathbf{U_3} \ldots \mathbf{U}_{n-1}\mathbf{J}. \end{aligned} \tag{3.10}$$

$\mathbf{J}^*$ denotes a row of ν elements in which the first element is 1 and all following elements are 0, and $\mathbf{J}$ denotes a column of ν elements in which every element is 1. The statistical weight matrix $\mathbf{U}_i$, $1 < i < n$, is the product $\mathbf{V}_i\mathbf{D}_i$. Often $\mathbf{J}^*$ and $\mathbf{J}$ are written instead as $\mathbf{U}_1$ and $\mathbf{U}_n$ [11].

$$Z_n = \mathbf{U}_1\mathbf{U}_2\mathbf{U}_3 \ldots \mathbf{U}_{n-1}\mathbf{U}_n = \prod_{i=1}^{n} \mathbf{U}_i. \tag{3.11}$$

As a specific example, Z_n for a polyethylene chain can be calculated by the combination of Eqs. (3.9) and (3.11), in the approximation where $\tau = \psi = 1$ [14].

$$Z_n = [1 \quad 0 \quad 0] \begin{bmatrix} 1 & \sigma & \sigma \\ 1 & \sigma & \sigma \\ 1 & \sigma & \sigma \end{bmatrix} \begin{bmatrix} 1 & \sigma & \sigma \\ 1 & \sigma & \sigma\omega \\ 1 & \sigma\omega & \sigma \end{bmatrix}^{n-3} \begin{bmatrix} 1 \\ 1 \\ 1 \end{bmatrix} = \mathbf{J}^* \begin{bmatrix} 1 & \sigma & \sigma \\ 1 & \sigma & \sigma\omega \\ 1 & \sigma\omega & \sigma \end{bmatrix}^{n-2} \mathbf{J}. \tag{3.12}$$

For ethyl terminated polyoxyethylene, the main portion of the calculation employs a repetition of three distinct statistical weight matrices, containing two distinct σ's and two distinct ω's [15].

$$Z_n = \mathbf{J}^* \begin{bmatrix} 1 & \sigma_a & \sigma_a \\ 1 & \sigma_a & \sigma_a \\ 1 & \sigma_a & \sigma_a \end{bmatrix} \left(\begin{bmatrix} 1 & \sigma_a & \sigma_a \\ 1 & \sigma_a & \sigma_a\omega_a \\ 1 & \sigma_a\omega_a & \sigma_a \end{bmatrix} \begin{bmatrix} 1 & \sigma_b & \sigma_b \\ 1 & \sigma_b & \sigma_b\omega_b \\ 1 & \sigma_b\omega_b & \sigma_b \end{bmatrix} \begin{bmatrix} 1 & \sigma_a & \sigma_a \\ 1 & \sigma_a & \sigma_a\omega_b \\ 1 & \sigma_a\omega_b & \sigma_a \end{bmatrix} \right)^{(n-4)/3} \begin{bmatrix} 1 & \sigma_a & \sigma_a \\ 1 & \sigma_a & \sigma_a\omega_a \\ 1 & \sigma_a\omega_a & \sigma_a \end{bmatrix} \mathbf{J}. \tag{3.13}$$

Here σ_a and σ_b denote the statistical weights for the first-order interaction of two methylene groups and two oxygen atoms, respectively, in g states. The statistical weights for the second-order interactions of two methylene groups and a methylene group with an oxygen atom in $g^{\pm}g^{\mp}$ states are denoted by ω_a and ω_b, respectively.

Table 3.2 summarizes RIS models for several chains with pair-wise interdependent bonds subject to a symmetric three-fold torsion potential, such that $\mathbf{U}$ is given by Eq. (3.9). The torsion angles are 180° and $\pm(60^\circ + \Delta\phi)$. Every entry has $E_\omega < 0$. This energy is listed as being infinite when the population of the g^+g^- and g^-g^+ states is so small that it can be ignored. In contrast with E_ω, the table contains entries for E_σ that are of either sign.

Table 3.3 summarizes selected literature citations for RIS models for homopolymers with 1–7 bonds per repeat unit, with all bonds subject to symmetric torsions. The list in Table 3.3 terminates with poly(6-aminocaproamide), nylon 6, although RIS models for chains with much longer repeat units have been reported in the literature [13]. The selection of entries in Table 3.3 is based in part on recognizing contributions of historical interest, and in part on more recent models that exploit computational methods and experiments that were not readily available during the early days of the development of RIS models. It does not include all applications of the RIS model to a given polymer. In some cases this number would be huge. For example, there are well over 100 applications of RIS models for polyethylene in the literature.

TABLE 3.2. *RIS models for several chains with pair-wise interdependent bonds subject to a symmetric threefold torsion potential and $E_\tau = E_\psi = 0$. Lengths in nm, angles in degrees, energies in kJ/mol.*

Polymer	Bond	l	θ	$\Delta\phi$	E_σ	E_ω	Reference
Polymethylene	C–C	0.153	112	7.3±3	1.1–1.9	5.4–6.7	[14]
Polymethylene	C–C	0.153	112	0±3	1.8–2.5	7.1–8.0	[14]
Polyoxymethylene	C–O	0.142	112	5	−5.9	∞	[15]
	O–C	0.142	112	5	−5.9	6.3	
Polydimethylsilmethylene	Si–C	0.190	115	0	0	∞	[17]
	C–Si	0.190	109.5	0	0	0.80	
Polydimethylsiloxane	Si–O	0.164	143	0	3.6	∞	[18]
	O–Si	0.164	110	0	3.6	4.2	
Polyoxyethylene	C–O	0.143	111.5	10	−1.7 to −2.1	1.7	[15]
	O–C	0.143	111.5	10	−1.7 to −2.1	∞	
	C–C	0.153	111.5	10	3.8	1.7	
Poly(trimethylene oxide)	O–C	0.143	111.5	10	3.8	∞	[15]
	C–C	0.153	111.5	0	−1.7	∞	
	C–C	0.153	111.5	0	−1.7	2.5	
	C–O	0.143	111.5	10	3.8	∞	

TABLE 3.3. *Selected literature citations for RIS models of polymers without rings in the backbone and with bonds subject to symmetric torsions. x denotes the number of chain atoms in the repeat unit. For a given value of x, the models are listed in the order of increasing molecular weight of the repeat unit specified in the third column.*

x	Polymer	Repeat unit	References
1	Polymethylene, polyethylene	$-CH_2-$	[14,19]
	Polysilane	$-SiH_2-$	[20]
	Polymeric sulfur	–S–	[21–23]
	Polytetrafluoroethylene	$-CF_2-$	[24–26]
	Polydimethylsilylene	$-Si(CH_3)_2-$	[20]
	Polymeric selenium	–Se–	[21–23, 27]
2	Polyoxymethylene	$-CH_2-O-$	[15,28,29]
	Polysilylenemethylene	CH_2SiH_2	[30]
	Polydihydrogensiloxane	$OSiH_2$	[31]
	Polyisobutylene	$-CH_2-C(CH_3)_2-$	[32–35]
	Polyvinylidene fluoride	$-CH_2-CF_2-$	[36,37]
	Polydimethylsilylenemethylene	$-CH_2-Si(CH_3)_2-$	[17,30,38]
	Polydimethylsiloxane	$-O-Si(CH_3)_2-$	[18,39]
	Polyphosphate	$-O-PO_2-$	[40]
	Polyvinylidene chloride	$-CH_2-CCl_2-$	[41]
	Polydichlorophosphazene	$-N-PCl_2-$	[42]
	Polyvinylidene bromide	$-CH_2-CBr_2-$	[36]
	Polydiphenylsiloxane	$-O-Si(C_6H_5)_2-$	[43]
3	Polyoxyethylene	$-O-CH_2-CH_2-$	[15,44–46]
	Polyglycine	$-NH-CH_2-CO-$	[47]
	Polythiaethylene	$-S-CH_2-CH_2-$	[48,49]
	Poly(oxy-1,1-dimethylethylene)	$-O-CH_2-CH(CH_3)_2-$	[50]
4	Poly(1,4-*cis*-butadiene)	$-CH_2-CH=CH-CH_2-$	[51–54]
	Poly(1,4-*trans*-butadiene)	$-CH_2-CH=CH-CH_2-$	[53–56]
	Poly(trimethylene oxide)	$-CH_2-CH_2-CH_2-O-$	[15]
	Poly(1,4-*cis*-isoprene)	$-CH_2-CH=C(CH_3)-CH_2-$	[51,52,57]
	Poly(1,4-*trans*-isoprene)	$-CH_2-CH=C(CH_3)-CH_2-$	[53,55,56]
	Poly(trimethylene sulfide)	$-CH_2-CH_2-CH_2-S-$	[58]
	Poly(3,3-dimethyloxetane)	$-O-CH_2-C(CH_3)_2-CH_2-$	[59,60]
	Poly(3,3-dimethylthietane)	$-S-CH_2-C(CH_3)_2-CH_2-$	[61]
5	Poly(tetramethylene oxide)	$-CH_2-CH_2-CH_2-CH_2-O-$	[15]
	Poly(1,3-dioxolane)	$-CH_2-CH_2-O-CH_2-O-$	[62]
6	Poly(pentamethylene sulfide)	$-S-CH_2-CH_2-CH_2-CH_2-CH_2-$	[63]
	Poly(thiodiethylene glycol)	$-O-CH_2-CH_2-S-CH_2-CH_2-$	[64]
7	Poly(hexamethylene oxide)	$-O-CH_2-CH_2-CH_2-CH_2-CH_2-CH_2-$	[65]
	Poly(6-aminocaproamide)	$-NH-CH_2-CH_2-CH_2-CH_2-CH_2-CO-$	[66]

3.7 THE STEREOCHEMICAL SEQUENCE IN VINYL POLYMERS

Vinyl polymers, for which polypropylene serves as a prototype, present some additional issues not encountered in chains with symmetric torsions. The physical properties of these chains depend on the stereochemical composition and stereochemical sequence of the chain, and this dependence must be reflected in Z. Two equivalent methods have been used for description of the stereochemistry of vinyl polymers. One approach uses pseudoasymmetric centers [67]. Although the fragment denoted by $-CH_2-CHR-CH_2-$ does not contain a chiral center, it can be treated as though it were chiral if one CH_2 group is distinguished from the other. This distinction is drawn when the bonds in the chain are indexed from one end to the other, because then the CH_2-CHR bond preceding the pseudoasymmetric center bears a different index from the following $CHR-CH_2$ bond. The –CHR-group is defined here to be in the d (l) configuration if the z component of the nonhydrogen substituent is positive (negative) in a local coordinate system for the $CHR-CH_2$ bond. This local coordinate system is defined as follows: The x-axis for the $CHR-CH_2$ bond is parallel with the bond and oriented from CHR to CH_2. The y-axis is in the plane of the chain atoms in $-CH_2-CHR-CH_2-$, and oriented with a positive projection on the x-axis for the preceding CH_2-CHR bond, which points from CH_2 to CHR. The z-axis completes a right-handed Cartesian coordinate system. Alternatively (and equivalently), the stereochemical sequence can be described

as sequences of *meso* diads (two successive identical pseudoasymmetric centers) and/or *racemo* diads (two successive nonidentical pseudoasymmetric centers) [67].

Statistical weight matrices that include all first- and second-order interactions can be formulated using Eq. (3.6) and the additional matrix defined in Eq. (3.14).

$$\mathbf{Q} = \begin{bmatrix} 1 & 0 & 0 \\ 0 & 0 & 1 \\ 0 & 1 & 0 \end{bmatrix}. \tag{3.14}$$

$\mathbf{Q}$ has the useful property that $\mathbf{Q}^2 = \mathbf{E}$, where $\mathbf{E}$ denotes the identity matrix. For a vinyl polymer with a nonarticulated side chain (such as a halogen atom), the $-$CHR$-$CH$_2-$ bond immediately following a pseudoasymmetric center has a $\mathbf{D}$ matrix that is either

$$\mathbf{D}_d = \text{diag}(\eta,1,\tau) \tag{3.15}$$

or

$$\mathbf{D}_l = \text{diag}(\eta,\tau,1) = \mathbf{Q}\mathbf{D}_d\mathbf{Q}, \tag{3.16}$$

depending on whether the CHR is a *d* or *l* pseudoasymmetric center. The three-rotational isomeric states are t,g^+, and g^-, in that order. The conformation weighted by τ has two first-order interactions, which occur between the underlined pairs of atoms in $\underline{\text{C}}\text{H}_2-\text{CHR}-\text{CH}_2-\underline{\text{C}}$ and $\text{CH}_2-\text{CH}\underline{\text{R}}-\text{CH}_2-\underline{\text{C}}$ (this τ is different from the one used in Eq. (3.9)). The conformation with only the second of these first-order interactions is weighted by η, and the conformation with only the first of these first-order interaction is the reference point, with a statistical weight of 1. The most important second-order interactions are independent of the configuration of the side chain because they only involve atoms in the main chain.

$$\mathbf{V}_d = \mathbf{V}_l = \begin{bmatrix} 1 & 1 & 1 \\ 1 & 1 & \omega \\ 1 & \omega & 1 \end{bmatrix}. \tag{3.17}$$

The complete statistical weight matrices for this bond in the two stereochemical configurations are obtained as $\mathbf{VD}$, from Eq. (3.6).

$$\mathbf{U}_d = \mathbf{Q}\mathbf{U}_l\mathbf{Q} = \begin{bmatrix} \eta & 1 & \tau \\ \eta & 1 & \tau\omega \\ \eta & \omega & \tau \end{bmatrix}. \tag{3.18}$$

Proceeding in the same manner, there are four possible statistical weight matrices for the CH$_2-$CHR bond immediately before a pseudoasymmetric center, depending on the stereochemistry at this center and the preceding pseudoasymmetric center. If both pseudoasymmetric centers have the same chirality, the two possibilities, $\mathbf{U}_{dd}$ and $\mathbf{U}_{ll}$, can be interconverted using $\mathbf{Q}$.

$$\mathbf{U}_{dd} = \mathbf{Q}\mathbf{U}_{ll}\mathbf{Q} = \begin{bmatrix} \eta\omega_{\text{RR}} & \tau\omega_{\text{CR}} & 1 \\ \eta & \tau\omega_{\text{CR}} & \omega_{\text{CC}} \\ \eta\omega_{\text{CR}} & \tau\omega_{\text{CC}}\omega_{\text{RR}} & \omega_{\text{CR}} \end{bmatrix}. \tag{3.19}$$

The double subscript on ω shows whether the second-order interaction is between two groups in the backbone, ω_{CC}, two side chains, ω_{RR}, or a side chain and a group in the backbone, ω_{CR}. If the two pseudoasymmetric centers have opposite chirality, the two possibilities are given in Eq. (3.20).

$$\mathbf{U}_{dl} = \mathbf{Q}\mathbf{U}_{ld}\mathbf{Q} = \begin{bmatrix} \eta & \omega_{\text{CR}} & \tau\omega_{\text{RR}} \\ \eta\omega_{\text{CR}} & 1 & \tau\omega_{\text{CC}} \\ \eta\omega_{\text{RR}} & \omega_{\text{CC}} & \tau\omega_{\text{CR}}^2 \end{bmatrix}. \tag{3.20}$$

When pseudoasymmetric centers are used for the description of the stereochemical sequence, six distinct statistical weight matrices, Eqs. (3.18)–(3.20), are required. They can be replaced by a total of three statistical weight matrices, denoted by $\mathbf{U}_p$,$\mathbf{U}_m$, and $\mathbf{U}_r$, if the stereochemical sequence is described instead as a sequence of *meso* and *racemo* diads.

$$\mathbf{U}_p = \mathbf{Q}\mathbf{U}_d = \mathbf{U}_l\mathbf{Q}, \tag{3.21}$$

$$\mathbf{U}_m = \mathbf{U}_{dd}\mathbf{Q} = \mathbf{Q}\mathbf{U}_{ll}, \tag{3.22}$$

$$\mathbf{U}_r = \mathbf{U}_{dl} = \mathbf{Q}\mathbf{U}_{ld}\mathbf{Q}. \tag{3.23}$$

The conformational partition function for a vinyl polymer of specified stereochemical sequence is formulated as a string of matrices where every second matrix is $\mathbf{U}_p$, and the intervening matrices are either $\mathbf{U}_m$ or $\mathbf{U}_r$, depending on the sequence of the diads in the chain. The definitions of the rotational isomeric states must change also when Eqs. (3.21)–(3.23) are used. Instead of using the t,g^+, and g^- states that are appropriate for *d* and *l* pseudoasymmetric centers, one uses t, g, and $\bar{g}$ states for *meso* and *racemo* diads. The *gauche* state that has τ in its statistical weight is denoted by $\bar{g}$, and the other *gauche* state is denoted simply by g. Indexing of rows and columns in $\mathbf{U}_p$,$\mathbf{U}_m$, and $\mathbf{U}_r$ is in the sequence t, g, $\bar{g}$.

Several vinyl polymers, such as polystyrene, have statistical weights such that τ and all of the ω's are much smaller than 1. Under these circumstances little error may be introduced if the $\bar{g}$ state is ignored because its statistical weight always includes $\tau\omega$. This simplification allows construction of Z with 2×2 matrices where the rows and columns are indexed t, g [68].

$$\mathbf{U}_p = \begin{bmatrix} 1 & 1 \\ 1 & \omega \end{bmatrix}, \tag{3.24}$$

$$\mathbf{U}_m = \begin{bmatrix} \eta^2\omega_{\text{RR}} & \eta \\ \eta & \omega_{\text{CC}} \end{bmatrix}, \tag{3.25}$$

$$\mathbf{U}_r = \begin{bmatrix} \eta^2 & \eta\omega_{\text{CR}} \\ \eta\omega_{\text{CR}} & 1 \end{bmatrix}. \tag{3.26}$$

In these three equations, all of the statistical weights for first-order interactions in the diad have been placed in $\mathbf{U}_m$ and $\mathbf{U}_r$. The $\mathbf{U}_p\mathbf{U}_m$ sequence shows that an isotactic chain can avoid conformations weighted by ω (a very small number in most polymers) if it adopts an ordered sequence that is either *tg* or *gt*, which is consistent with the commonly observed chain conformation in crystalline isotactic

polymers. In contrast, the $\mathbf{U}_p\mathbf{U}_r$ sequence shows that a syndiotactic chain is more likely to crystallize in either the *tt* or *gg* conformation, because these conformations do not require weighing with ω.

Literature citations for RIS models for several vinyl polymers, as well as related polymers for which stereochemical compositions and stereochemical sequences are issues, are summarized in Table 3.4.

3.8 EXTRACTION OF USEFUL INFORMATION FROM Z_n

The conformational partition function is subject to the same types of manipulations as are other partition functions encountered in statistical mechanics. Thus the average conformational energy of the chain is obtained from the temperature dependence of Z_n.

$$\langle E\rangle - E_0 = kT^2\left(\frac{\partial \ln Z_n}{\partial T}\right). \tag{3.27}$$

Z_n depends on T because the elements of the statistical weight matrices are Boltzmann factors. The conformational entropy is obtained from this result and $\ln Z_n$.

$$S = \frac{\langle E\rangle - E_0}{T} + k\ln Z_n. \tag{3.28}$$

The same approach can be used to deduce average conformations of local portions of the chain. The probability that bond i is in a particular rotational isomeric state, η, is obtained by dividing Z_n into the sum of the statistical weights of all conformations where this bond is in the desired state.

$$p_{\eta;i} = Z^{-1}\mathbf{U}_1\mathbf{U}_2\cdots\mathbf{U}_{i-1}\mathbf{U}'_{\eta;i}\mathbf{U}_{i+1}\cdots\mathbf{U}_n. \tag{3.29}$$

The modified statistical weight matrix denoted by $\mathbf{U}'_{\eta;i}$ is obtained by zeroing all columns of $\mathbf{U}_i$ except the column that indexes the desired state, η. This operation has the effect of ignoring the statistical weights of all conformations of the chain where bond i is not in the desired state, while keeping intact the statistical weights of all chain

Table 3.4. *RIS models for selected vinyl polymers and related polymers for which stereochemical composition and stereochemical sequence are issues. Chains are listed in the order of the molecular weight of their repeat unit.*

Polymer	Repeat unit	References
Polypropylene	$-CH_2-CH(CH_3)-$	[69–72]
Poly(vinyl alcohol)	$-CH_2-CH(OH)-$	[73,74]
Poly(vinyl fluoride)	$-CH_2-CHF-$	[75]
Poly(1-butene)[a]	$-CH_2-CH(C_2H_5)-$	[76]
Polysilapropylene	$-CH_2-SiH(CH_3)-$	[77]
Poly(propylene oxide)	$-O-CH_2-CH(CH_3)-$	[78,79]
Poly(vinyl methyl ether)[a]	$-CH_2-CH(OCH_3)-$	[80]
Poly(vinyl chloride)	$-CH_2-CHCl-$	[81,82]
Poly(methyl vinyl ketone)	$-CH_2-CH(COCH_3)-$	[83]
Poly(propylene sulfide)	$-S-CH_2-CH(CH_3)-$	[79,84,85]
Poly(trifluoroethylene)	$-CF_2-CHF-$	[75]
Head-to-head, tail-to-tail polypropylene[b]	$-CH_2-CH(CH_3)-CH(CH_3)-CH_2-$	[86]
Poly(vinyl acetate)	$-CH_2-CH(OCOCH_3)-$	[87]
Poly(methyl acrylate)	$-CH_2-CH(COOCH_3)-$	[88–90]
Poly(tert-butyl vinyl ketone)	$-CH_2-CH[COC(CH_3)_3]-$	[91]
Poly(methyl methacrylate)	$-CH_2-C(CH_3)(COOCH_3)-$	[92–94]
Poly(methyl phenyl siloxane)	$-O-Si(CH_3)(C_6H_5)-$	[95]
Polystyrene	$-CH_2-CH(C_6H_5)-$	[68,96,97]
Poly(2-vinylpyrridine)	$-CH_2-CH(C_5NH_4)-$	[98]
Poly(vinyl bromide)	$-CH_2-CHBr-$	[99]
Poly(*N*-vinyl pyrrolidone)	$-CH_2-CH(C_4NOH_6)-$	[100]
Poly(α-methylstyrene)	$-CH_2-C(CH_3)(C_6H_5)-$	[101]
Polysilastyrene	$-SiH_2-SiH(C_6H_5)-$	[102,103]
Poly(*p*-chlorostyrene)	$-CH_2-CH(C_6H_4Cl)-$	[104]
Poly(phenyl acrylate)	$-CH_2-CH(COOC_6H_5)-$	[105]
Poly(*N*-vinyl carbazole)	$-CH_2-CH(C_{12}NH_8)-$	[106,107]
Poly(methylphenylsilylene)	$-Si(CH_3)(C_6H_5)-$	[102,108]
Asymmetrically substituted polysilylenemethylene[a]	$-CH_2-Si(CH_3)[O(CH_2)_3OC_6H_4C_6H_5]-$	[109]

[a] These articulated side chains require more elaborate methods that are extensions of the simpler ones described in this Chapter.
[b] Hydrogenated poly(2,3-dimethylbutadiene).

conformations where this bond is in state η. The $p_{\eta;i}$ are useful in the interpretation of conformation-dependent properties of polymers that are highly local in origin. Examples are the coupling constants in NMR spectra [110], as evaluated by a Karplus relationship [111–114], and the optical activity of chiral vinyl polymers [115].

An extension of this approach yields the probability that bonds $i-1$ and i are simultaneously in states ξ and η, respectively.

$$p_{\xi\eta;i} = Z^{-1}\mathbf{U}_1\mathbf{U}_2\cdots\mathbf{U}_{i-1}\mathbf{U}'_{\xi\eta;i}\mathbf{U}_{i+1}\cdots\mathbf{U}_n. \tag{3.30}$$

The matrix $\mathbf{U}'_{\xi\eta;i}$ is obtained from $\mathbf{U}_i$ by zeroing every element except the one in the row and column indexed by ξ and η, respectively.

A useful method for calculating the probabilities for longer sequences of bonds, in the approximation where there is interdependence of nearest-neighbor pairs of bonds, makes use of another probability that can be calculated from the results of Eqs. (3.29) and (3.30).

$$q_{\xi\eta;i} = p_{\xi\eta;i}/p_{\xi;i-1}. \tag{3.31}$$

This term is the probability that bond i is in state η, given that bond $i-1$ is in state ξ. (This restriction on the state at bond $i-1$ was absent in the definition of $p_{\xi\eta;i}$.) The differences in $q_{\xi\eta;i}$ and $p_{\xi\eta;i}$ are apparent from examination of the types of summations that must be performed in order to achieve unit probability.

$$\sum_{\xi=1}^{\nu}\sum_{\eta=1}^{\nu} p_{\xi\eta;i} = 1, \tag{3.32}$$

$$\sum_{\eta=1}^{\nu} q_{\xi\eta;i} = 1. \tag{3.33}$$

The normalization is achieved differently for $p_{\xi\eta;i}$ and $q_{\xi\eta;i}$. If $\sigma = 0.543$ and $\omega = 0.087$, a C–C bond in the middle of a long polyethylene chain has the following values for these probabilities, where each set of probabilities is presented in the form of a 3×3 matrix with rows and columns indexed in the order t, g^+, g^-.

$$\mathbf{p}_{\xi\eta;i} = \begin{bmatrix} 0.321 & 0.138 & 0.138 \\ 0.138 & 0.0591 & 0.00516 \\ 0.138 & 0.00516 & 0.0591 \end{bmatrix}, \tag{3.34}$$

$$\mathbf{q}_{\xi\eta;i} = \begin{bmatrix} 0.538 & 0.231 & 0.231 \\ 0.682 & 0.292 & 0.026 \\ 0.682 & 0.026 & 0.292 \end{bmatrix}. \tag{3.35}$$

The elements in Eq. (3.34) illustrate the importance of the interdependence of the bonds in polyethylene. The probability for a pair of bonds in g states depends strongly on whether they are of the same or opposite sign. The interdependence of the bonds is also apparent in Eq. (3.35). If the bonds were independent, all rows of $\mathbf{q}_{\xi\eta;i}$ would be identical.

The probability that bonds $i-2$, $i-1$, and i are in states ζ, ξ, and η, respectively, is given by $p_{\zeta;i-2}q_{\zeta\xi;i-1}q_{\xi\eta;i}$, which results from the logical extension of Eq. (3.30). This approach can be extended to the probabilities for observations of longer sequences of bonds in specified states.

3.9 VIRTUAL BONDS

Many important chains contain bonds that are locked into a single conformation due to restrictions imposed by ring formation, as in the benzene ring of poly(ethylene terephthalate), or electronic structures (as in the amide unit of nylon-6, which strongly prefers the planar *trans* conformation). These rigid units are often treated with virtual bonds, where a single virtual bond spans the rigid unit. Several instances where virtual bonds have been used are summarized in Table 3.5.

3.10 MATRIX EXPRESSION FOR THE DIMENSIONS OF A SPECIFIED CONFORMATION

The geometry for a specified conformation of a chain of n bonds is formulated in a manner that will facilitate averaging of the result with the aid of the information contained in Z_n. We will defer the averaging process until the next section, and focus here on a single conformation. The statistical weight of this conformation is irrelevant in the present section, but it will become highly relevant in the next section.

The local Cartesian coordinate system depicted in Fig. 3.3 is affixed to each bond in the chain. Bond i runs from chain atom $i-1$ to chain atom i. The x-axis for this bond is parallel with the bond, and oriented from chain atom $i-1$ to chain atom i. The y-axis is in the plane of bonds i and $i-1$, and oriented with a positive projection on bond $i-1$. The z-axis completes a right-handed Cartesian coordinate system. Since the first bond does not have a previous bond for use in defining the y-axis, an imaginary zeroth bond is used. This bond is oriented such that it produces a *trans* state

TABLE 3.5. *Examples of the use of virtual bonds in the construction of RIS models.*

Rigid unit	Examples	References
Aromatic ring	Polybenzoxazine	[116]
	Polycarbonates	[16,117]
	Polyesters	[118–120]
	Polypyrrole	[121]
Aliphatic ring	Polysaccharides	[122–124]
	Nucleic acids	[125]
Amide group	Poly(amino acids)	[126–128]
Ester group	Poly(lactic acid)	[129]
$CH_2CH{=}CHCH_2$ unit	Polybutadiene	[51]

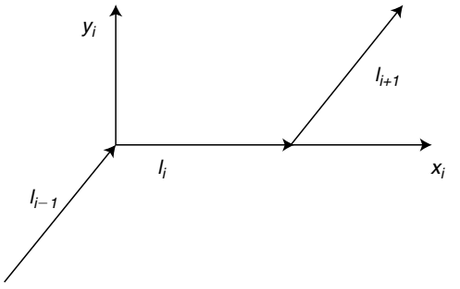

FIGURE 3.3. Local coordinate system for bond *i*. The *x* and *y* axes are drawn on the figure. The *z*-axis (not drawn) completes a right-handed Cartesian coordinate system.

at the first bond. With these definitions of the local coordinate systems, a bond vector in its own coordinate system can be quickly written.

$$\mathbf{l}_i = \begin{bmatrix} l \\ 0 \\ 0 \end{bmatrix} \tag{3.36}$$

The matrix that transforms a vector from its representation in the coordinate system of bond $i+1$ into its representation in bond i is denoted $\mathbf{T}_i$. It depends on the angle made by these two bonds and the torsion at bond i.

$$\mathbf{T}_i = \begin{bmatrix} -\cos\theta & \sin\theta & 0 \\ -\sin\theta\cos\phi & -\cos\theta\cos\phi & -\sin\phi \\ -\sin\theta\sin\phi & -\cos\theta\sin\phi & \cos\phi \end{bmatrix}. \tag{3.37}$$

The expression for $\mathbf{l}_{i+1}$ in the coordinate system of bond i is $\mathbf{T}_i\mathbf{l}_{i+1}$. With this notation, the end-to-end vector in a specified conformation can be written as a serial product of n matrices constructed from $\mathbf{T}$ and $\mathbf{l}$ [11].

$$\begin{aligned} \mathbf{r} &= [\,\mathbf{T}_1 \quad \mathbf{l}_1\,] \begin{bmatrix} \mathbf{T}_2 & \mathbf{l}_2 \\ \mathbf{0} & 1 \end{bmatrix} \cdots \begin{bmatrix} \mathbf{T}_{n-1} & \mathbf{l}_{n-1} \\ \mathbf{0} & 1 \end{bmatrix} \begin{bmatrix} \mathbf{l}_n \\ 1 \end{bmatrix} \\ &= \mathbf{A}_1\mathbf{A}_2\cdots\mathbf{A}_{n-1}\mathbf{A}_n. \end{aligned} \tag{3.38}$$

All of the geometric information (l_i, θ_i, ϕ_i) pertinent to bond i appears in $\mathbf{A}_i$. The squared end-to-end distance and squared radius of gyration can be calculated using exactly the same information, but with the information presented in larger matrices.

$$r^2 = [\,1 \quad 2\mathbf{l}_1^{\mathrm{T}}\mathbf{T}_1 \quad l_1^2\,] \begin{bmatrix} 1 & 2\mathbf{l}_2^{\mathrm{T}}\mathbf{T}_2 & l_2^2 \\ \mathbf{0} & \mathbf{T}_2 & \mathbf{l}_2 \\ 0 & \mathbf{0} & 1 \end{bmatrix} \cdots \begin{bmatrix} 1 & 2\mathbf{l}_{n-1}^{\mathrm{T}}\mathbf{T}_{n-1} & l_{n-1}^2 \\ \mathbf{0} & \mathbf{T}_{n-1} & \mathbf{l}_{n-1} \\ 0 & \mathbf{0} & 1 \end{bmatrix} \begin{bmatrix} l_n^2 \\ \mathbf{l}_n \\ 1 \end{bmatrix} = \mathbf{G}_1\mathbf{G}_2\cdots\mathbf{G}_{n-1}\mathbf{G}_n. \tag{3.39}$$

The expression for s^2 is written in the approximation where all of the chain atoms can be taken to be of the same mass.

$$s^2 = (n+1)^{-2}\mathbf{H}_1\mathbf{H}_2\ldots\mathbf{H}_{n-1}\mathbf{H}_n. \tag{3.40}$$

Matrices $\mathbf{H}_1$ and $\mathbf{H}_n$ are written as the first row and last column, respectively, of the general expression for $\mathbf{H}_{i,1} < i < n$, as was true also for $\mathbf{G}$ [11].

$$\mathbf{H}_i = \begin{bmatrix} 1 & 1 & 2\mathbf{l}_i^{\mathrm{T}}\mathbf{T}_i & l_i^2 & l_i^2 \\ 0 & 1 & 2\mathbf{l}_i^{\mathrm{T}}\mathrm{T}_i & l_i^2 & l_i^2 \\ \mathbf{0} & \mathbf{0} & \mathbf{T}_i & \mathbf{l}_i & \mathbf{l}_i \\ 0 & 0 & \mathbf{0} & 1 & 1 \\ 0 & 0 & \mathbf{0} & 0 & 1 \end{bmatrix}, \quad 1 < i < n. \tag{3.41}$$

The squared dipole moment, μ^2, of polar chains such as polyoxymethylene can be treated using a simple modification of Eq. (3.39). The bond vector, $\mathbf{l}_i$, for bond i is replaced by the dipole moment vector, $\mathbf{m}_i$, for the same bond [15]. For polyoxymethylene, the bond vectors are connected in a head-to-tail fashion, but the bond dipole moment vectors are connected in a head-to-head, tail-to-tail fashion, with the oxygen atom being at the negative end of $\mathbf{m}_i$. Extension to polyoxyethylene requires that some of the $\mathbf{m}_i$ be null vectors, as would be the case for the CH_2–CH_2 bond [15]. In some chains, such as poly(vinyl chloride), the important $\mathbf{m}_i$ are not aligned with the $\mathbf{l}_i$ [130].

3.11 AVERAGING THE DIMENSIONS OVER ALL THE CONFORMATIONS IN $\mathbf{Z_n}$

The matrices denoted by $\mathbf{A}_i$, $\mathbf{G}_i$, and $\mathbf{H}_i(1 < i < n)$ in Eqs. (3.38)–(3.40) depend on the rotational isomeric state assigned to bond i through the appearance of ϕ_i in $\mathbf{T}_i$. The states at this bond also index the columns of $\mathbf{U}_i$. We now seek a pairing of the appropriate statistical weight from $\mathbf{U}_i$ with the geometry in $\mathbf{T}_i$. This objective is achieved by expansion of each element in $\mathbf{U}_i$ through multiplication of each of its elements by the appropriate $\mathbf{A}_i$, $\mathbf{G}_i$, or $\mathbf{H}_i$, depending on whether the target of the calculation is $\langle\mathbf{r}\rangle_0$, $\langle r^2\rangle_0$, or $\langle s^2\rangle_0$. As an example, the calculation of $\langle r^2\rangle_0$ can be written as a serial product of n $\mathbf{G}$ matrices [11].

$$\langle r^2\rangle_0 = Z^{-1}\boldsymbol{G}_1\boldsymbol{G}_2\ldots\boldsymbol{G}_{n-1}\boldsymbol{G}_n. \tag{3.42}$$

The internal $\boldsymbol{G}_i$ are constructed by expansion of each element in $\mathbf{U}_i$, denoted $u_{\xi\eta}$, by $\boldsymbol{G}_\eta$, such that $\boldsymbol{G}_i$ becomes a $5\nu \times 5\nu$ matrix, whereas $\mathbf{U}_i$ was a $\nu \times \nu$ matrix. The terminal $\boldsymbol{G}_i$ are either a row or column of 5ν elements. When $\nu = 3$, the $\mathbf{G}$ matrices take the forms shown in Eqs. (3.43)–(3.45).

$$\boldsymbol{G}_1 = \begin{bmatrix} 1 & 2l_1^T\mathbf{T}_1 & l_1^2 & 0 & \cdots & 0 \end{bmatrix}, \tag{3.43}$$

$$\boldsymbol{G}_i = \begin{bmatrix} u_{11}\boldsymbol{G}_t & u_{12}\boldsymbol{G}_{g^+} & u_{13}\boldsymbol{G}_{g^-} \\ u_{21}\boldsymbol{G}_t & u_{22}\boldsymbol{G}_{g^+} & u_{23}\boldsymbol{G}_{g^-} \\ u_{31}\boldsymbol{G}_t & u_{32}\boldsymbol{G}_{g^+} & u_{33}\boldsymbol{G}_{g^-} \end{bmatrix}, \quad 1 < i < n, \quad (3.44)$$

$$\boldsymbol{G}_n = \begin{bmatrix} l_n^2 \\ \mathbf{l}_n \\ 1 \\ l_n^2 \\ \mathbf{l}_n \\ 1 \\ l_n^2 \\ \mathbf{l}_n \\ 1 \end{bmatrix}. \quad (3.45)$$

3.12 USE OF C_n FOR CALCULATION OF C_∞

The results of an illustrative calculation are depicted in Fig. 3.4. The chain has $\theta = 112°$, $\nu = 3$, and $\phi = 180°$ and $\pm 60°$. The statistical weight matrix for all internal bonds is given by Eq. (3.9) with $\tau = \psi = 1$. When σ and ω are also 1, the chain has the same C_n as the freely rotating chain with the same bond angle. Imposition of a symmetric torsional potential that penalizes the g states, with $\sigma = 0.4$, increases the C_n. Introduction of a pair-wise interdependence, via $\sigma = 0.4$ and $\omega = 0.1$, produces a further increase in C_n. Obviously, the interdependence of the bonds can have a strong effect on the unperturbed dimensions of the chain.

The value of C_∞ can be reliably determined from the results depicted in Fig. 3.4 if $\sigma = \omega = 1$, but the limiting value is less reliably defined when $\sigma = 0.4$ and $\omega = 0.1$. This problem is alleviated by plotting the same data in another manner, as shown in Fig. 3.5. The linear extrapolation of the data to $1/n = 0$ leads unambiguously to the value for C_∞. This linear extrapolation is theoretically justified both for $\langle r^2 \rangle_0 / nl^2$ and for $\langle s^2 \rangle_0 / nl^2$ [1] and also for the corresponding ratio constructed from the mean square unperturbed dipole moment, $\langle \mu^2 \rangle_0 / nm^2$ [131].

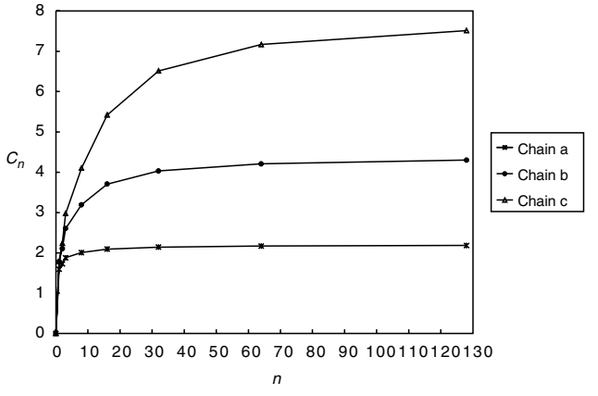

FIGURE 3.4. C_n vs. n for chains with $\theta = 112°$, $\nu = 3$, and $\phi = 180°$ and $\pm 60°$. **U** for all internal bonds is given by Eq. (3.9) with $\tau = \psi = 1$. The other statistical weights are (a) $\sigma = \omega = 1$, (b) $\sigma = 0.4$, $\omega = 1$, and (c) $\sigma = 0.4$, $\omega = 0.1$.

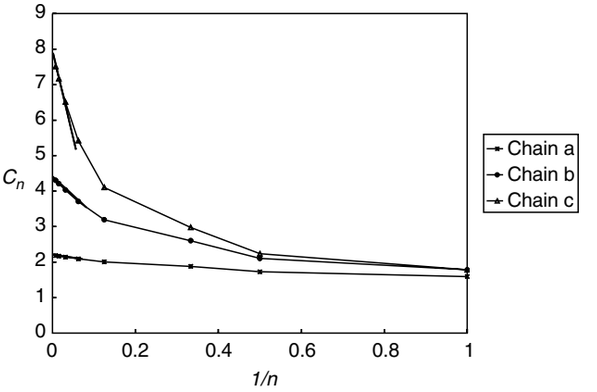

FIGURE 3.5. The data in Fig.3. 4 plotted as C_n vs. $1/n$, along with linear extrapolations to $1/n = 0$. The values of C_∞, which are (a) 2.198, (b) 4.396, and (c) 7.869, can be estimated with an error no larger than 1% by linear extrapolation of the data for n no larger than 128. The linear extrapolation shown, which uses C_{64} and C_{128}, leads to estimates for C_∞ of (a) 2.198, (b) 4.393, and (c) 7.858.

3.13 OTHER APPLICATIONS OF THE RIS MODEL

The previous portion of this chapter has focused primarily on the use of the RIS model for the computation of the mean square unperturbed dimensions, because that is the most frequent application of the model. This section describes briefly many other applications of the RIS model. All of these applications employ the conformational partition function, but the additional information incorporated in the calculation, and the manipulation of Z, depend on the application.

3.13.1 Applications That Depend Only on the Energetic Information Contained in Z

The calculation of $p_{\eta;i}$ as a function of i provides an estimate of the distance that end effects penetrate into a long unperturbed chain. This calculation shows that end effects for polyethylene are confined to the first few bonds at the end of the chain [10]. The end effects can extend much further into the chain when the second-order interactions become more severe, as is frequently the case for the probability of a helical conformation, $p_{h;i}$, in a long homopolypeptide near the midpoint of its helix-coil transition [132]. In proton NMR, the values of $p_{\eta;i}$ are helpful in understanding the values of the spin–spin coupling constants, using the Karplus relationship [111–114], and in understanding the γ effect on the chemical shift in ^{13}C NMR spectra [110,133]. The values of $p_{\eta;i}$ have also been used to interpret the optical activity exhibited by chiral poly(α-olefins) [115] and other polymers [134,135].

The combination of p_η and $p_{\xi\eta}$ gives the number of bonds in a run of state η. An illustrative use is in the determination of the average number of residues in a helical segment in a homopolypeptide as $p_h/p_c h$, where h denotes the helical state, and c denotes any other state [10,132].

The stereochemical composition of vinyl polymers after epimerization to stereochemical composition can be determined from the information contained in a more elaborate form of Z that takes account of the conformations of all stereochemical sequences, with all sequences weighted with respect to the same definition for the zero point of the conformational energy [136,137].

3.13.2 Applications That Use Properties Accessible From Z and the Geometry of the Chains

The higher even moments of the unperturbed dimensions, $\langle r^{2p}\rangle_0$ and $\langle s^{2p}\rangle_0$, $p > 1$, are accessible through an appropriate expansion in the dimensions of the generator matrices used for the simpler cases where $p = 1$ [11]. Dimensionless ratios formed from appropriate combinations of these even moments provide information about the shape of the distribution functions. Thus $\langle r^2\rangle_0$ measures the average value of r^2,$\langle r^4\rangle_0/\langle r^2\rangle_0^2$ measures the width of the distribution for r^2, and $\langle r^6\rangle_0/\langle r^2\rangle_0^3$ measures the skewness of this distribution function. All flexible homopolymers will approach the Gaussian limit of $\langle r^4\rangle_0/\langle r^2\rangle_0^2 = 5/3$ as $n \to \infty$, but narrower distributions (smaller $\langle r^4\rangle_0/\langle r^2\rangle_0^2$) are typical at finite n [138]. Macrocyclization equilibria can be understood in terms of these dimensionless ratios, via an elaboration of the Jacobson–Stockmayer approach [139,140]. More accurate results, particularly for rather short chains, are obtained when the $\langle r^{2p}\rangle_0/\langle r^2\rangle_0^p$ are supplemented by additional terms, calculated from the RIS model, that monitor the angular correlation between bonds 1 and n in the unperturbed chain as $r^2 \to 0$ [141,142].

Although the averages of many conformation-dependent physical properties of interest can be extracted rapidly from the RIS model by a matrix multiplication scheme of the type shown in Eq. (3.42), with $\boldsymbol{G}_i$ defined as appropriate for the specific property of interest, there are numerous other properties that cannot be evaluated by this simple device. For these other properties, an efficient Monte Carlo (MC) simulation can often be constructed, using the information in the RIS model. The information in Z allows rapid computation of the $p_{\eta;2}$ and $q_{\xi\eta;i}$, $2 < i < n$. These normalized probabilities and a random number generator allow rapid generation of a representative sample of unperturbed chains. If the sample is sufficiently large, the simple average of r^2 over all chains in the sample will approach the value of $\langle r^2\rangle_0$ specified by Eq. (3.42). The MC simulation is less efficient than Eq. (3.42) in the calculation of $\langle r^2\rangle_0$, but it offers the opportunity for the calculation of other physical properties that cannot be formulated as a serial matrix product. An example is provided by the angular scattering function, $P(q)$, where q is related to the scattering angle, θ, and wavelength of the radiation, λ, by Eq. (3.47).

$$P(q) = \frac{1}{(n+1)^2}\sum_{i=0}^{n}\sum_{j=0}^{n}\left\langle\frac{\sin(qr_{ij})}{qr_{ij}}\right\rangle, \tag{3.46}$$

$$q = \frac{4\pi}{\lambda}\sin\left(\frac{\theta}{2}\right). \tag{3.47}$$

An illustrative example is provided by the use of this approach to determine how the scattering function of unperturbed poly(methyl methacrylate) depends on the stereochemical composition of the chains [143]. The method can also be employed to generate accurate distribution functions for the end-to-end distance in unperturbed chains that are sufficiently short so that there are strong departures from the Gaussian distribution which would be achieved in the limit as $n \to \infty$ [144].

The representative sample of unperturbed chains can be edited to generate other useful ensembles. One of the most common examples is to discard chains with r larger than a specified cutoff. As this cutoff becomes smaller and smaller, the ensemble of surviving chains approaches the ensemble for the unperturbed macrocycle [145]. This ensemble can be used to evaluate properties of the ensemble directly, or to determine how easily polydimethylsiloxane macrocycles of a given n can be threaded [146]. The unperturbed ensemble can also be edited to discard chains that attempt placement of their atoms in regions of space that are deemed to be inaccessible. This approach generates ensembles of chains that are tethered by one end to an impenetrable surface [147], or chains in a melt that contains impenetrable spherical filler particles [148]. The complete ensemble of unperturbed chains can also be perturbed by the introduction of new interactions, not considered explicitly in the RIS model, as in the re-weighting of the ensemble to investigate the properties of bolaform electrolytes (polymer with ionic groups at their ends) [149].

The $p_{\eta;i}$ and $q_{\xi\eta;i}$ can be used to cause coarse-grained chains to mimic the conformational properties of specific real chains, because these probabilities enforce the proper distribution function for $\mathbf{r}$ for the entire coarse-grained chain, as well as all of its subchains [150,151]. This feature facilitates the recovery of atomistically detailed models from equilibrated ensembles of coarse-grained chains [152]. It also causes the coarse-grained chains to be sensitive to subtleties such as the dependence of the miscibility of polypropylene chains in the melt on their stereochemical composition [153,154].

3.13.3 Applications That Depend on Properties in Addition to Z and the Geometry of the Chains

Generator matrices are easily formulated for the computation of the mean square dipole moment, $\langle\mu^2\rangle_0$, using the analogy between formulating $\mathbf{r}$ as a sum of bond vectors and

formulating $\boldsymbol{\mu}$ as a sum of bond dipole moment vectors [10,15,130]. This analogy can be extended, via the valence optical scheme, to conformation-dependent properties that depend on the anisotropy of the polarizability of a bond [10,12]. This analogy leads to generator matrices for the optical anisotropy, stress-optical coefficient, electrical birefringence, i.e., molar Kerr constant, and magnetic birefringence, i.e., molar Cotton-Mouton constant.

3.14 WHY ARE SOME CHAINS DESCRIBED WITH MORE THAN ONE RIS MODEL?

The appearance in the literature of several RIS models for a single polymer may initially be confusing, but it is not at all surprising when one considers the objectives of the RIS approach. The exact description of the physical properties of a polymer would start from the Schrödinger equation, in a manner similar to one appropriate for small molecules. That approach is not practical. Therefore we resort to practical models that contain sufficient detailed information to let us account in a satisfactory manner for the physical properties that are of interest to us. Sometimes this objective can be obtained to a similar degree of accuracy with somewhat different values for the parameters in the model. This situation is illustrated by the first two entries in Table 3.2. The two RIS models for polyethylene place the *gauche* states at slightly different displacements, $\pm(120^\circ - \Delta\phi)$, from the *trans* state. In order to maintain the proper values for C_n, a change in the geometry of the chain, produced by a change in the value of $\Delta\phi$, requires compensating changes in the weighting of the chains, which is achieved by adjustments in the values of E_σ and E_ω [14]. If the value of $\Delta\phi$ were increased from 0 to 7.5° without any other changes in the model, C_n would increase because the g states would have been moved closer to the geometry of the t state. This increase in C_n can be avoided by increasing slightly the probability for g state, and that objective is achieved by the changes in E_σ and E_ω. The literature contains many similar examples where a given chain is described by various RIS models that have the same form, but slightly different values of the parameters.

There are also numerous examples where the RIS models have more substantial differences, because they use statistical weight matrices of different dimensions. Several examples are presented in Table 3.6. An obvious origin of the differences in dimension of the **U**'s is a difference in the number of rotational isomeric states assigned to individual bonds. Thus polyethylene has been described with RIS models that assign three [14], five [14], or seven [155] states to each internal bond. An increase in ν should lead to a more accurate model, because it permits the incorporation of more detail into the calculation. Of course, it also introduces more parameters into the model, with the added burden on the user of assigning values to these parameters. The most popular RIS models for polyethylene use $\nu = 3$ because the increased accuracy accessible with a larger value of ν usually is not justified because it makes a trivial improvement in the agreement between the calculated values and experiment. The principle here is to incorporate into the RIS model as much detail as is necessary . . . but no more detail than necessary.

TABLE 3.6. *Representative polymers that have been described by RIS models with different ν's*

Polymer	ν	References
Polyethylene	3	[14]
	5	[14]
	7	[155]
Polytetrafluoroethylene	3	[24]
	4	[25]
	6	[25]
Polyisobutylene	3	[32]
	4	[34,35]
	6	[33,35]
Poly(vinylidene chloride)	3	[156]
	6	[41]
Polypropylene	3	[69,71]
	4	[155]
	5	[72,157]
	6	[70]
Poly(methyl methacrylate)	2	[92]
	3	[94]
	6	[93]
Polycarbonate	2	[117,158]
	4	[16]

The necessary amount of detail required in the RIS model may depend on the physical property that is calculated from the model. For example, the dependence of C_∞ on stereochemical composition in poly(methyl methacrylate) is described nearly as well by a relative simple three-state model [94] and by a much more complex six state model that contains many more parameters [93]. However, the six-state model is superior to its simpler relative in the description of the scattering function, $P(\mu)$, which is sensitive to the precise description of the conformations of relatively short subchains [159]. In the case of polypropylene, the stereochemical composition achieved after epimerization to stereochemical equilibrium is captured correctly by a three-state model [71], but accurate description of the behavior of C_∞ with changes in stereochemical composition is better achieved with a five-state model [72]. The stereochemical composition at stereochemical equilibration does not depend explicitly on the geometry (l, θ, ϕ) when it is calculated with the RIS model [71], but C_∞ is obviously sensitive to this geometry [72]. In particular, the manner in which C_∞ depends on the probability of a *meso* dyad, p_m, as $p_m \to 1$ can be improved by going from a three-state to a five-state model.

The dimensions of **U** change, at constant ν, if higher order interactions are incorporated in the RIS model. Thus

polyethylene has been treated using a 9×9 representation of **U**. The calculation retains $\nu = 3$, but the increase in dimensions of **U** was necessary to test the potential importance of third-order interactions [160]. In order to introduce into **U** a statistical weight that depends on a third-order interaction, the rows are indexed by the states at bonds $i - 2$ and $i - 1$, and the columns are indexed by the states at bonds $i - 1$ and i, leading to a $\nu^2 \times \nu^2$ representation for **U**. The only nonzero elements in this **U** are those where the row and column agree on the state at bond $i - 1$. For this reason, 2/3 of the elements are zero. Any nonzero element corresponds to a unique combination of rotational isomeric states at bond $i - 2$, $i - 1$, and i. Third-order interactions have also been included in **U** for polyoxyethylene, requiring an expansion in the dimension of **U**, even though $\nu = 3$ [45]. Interactions of higher than third order are sometimes important, as illustrated by the transition from a random coil to an intramolecular antiparallel sheet with tight bends [161]. Under these circumstances, each **U** becomes a sparse matrix. The sparse character of the matrix can be exploited in writing the computer code required for numerical evaluation of the model [161].

ACKNOWLEDGMENT

Over his career, much of WLM's research using the RIS model has been supported by various sources. Current financial support for this research is from NSF DMR 0098321 and from the Collaborative Center in Polymer Photonics, funded jointly by the Air Force Office of Scientific Research, Wright-Patterson Air Force Base, and The University of Akron. Some items coauthored by WLM in the reference list were supported by FAA, NIH, and other NSF grants.

REFERENCES

1. W. L. Mattice, C. A. Helfer, and A. P. Sokolov, Macromolecules **37**, 4711 (2004).
2. P. Debye, J. Chem. Phys. **14**, 636 (1946).
3. H. A. Kramers and G. H. Wannier, Phys. Rev. **60**, 252 (1941).
4. M. V. Volkenstein, Dokl. Acad. Nauk SSSR **78**, 879 (1951).
5. Yu. Ya. Gotlib, Zh. Tekhn. Fiz. **29**, 523 (1959).
6. T. M. Birshtein and O. B. Ptitsyn, Zh. Tekhn. Fiz. **29**, 1048 (1959).
7. S. Lifson, J. Chem. Phys. **30**, 964 (1959).
8. K. Nagai, J. Chem. Phys. **31**, 1169 (1959).
9. C. A. J. Hoeve, J. Chem. Phys. **32**, 888 (1960).
10. P. J. Flory, *Statistical Mechanics of Chain Molecules* (Wiley, New York, 1969). Reprinted with the same title by Hanser, München, in 1989.
11. P. J. Flory, Macromolecules **7**, 381 (1974).
12. W. L. Mattice and U. W. Suter, *Conformational Theory of Large Molecules. The Rotational Isomeric State Model in Macromolecular Systems* (Wiley, New York, 1994).
13. M. Rehahn, W. L. Mattice, and U. W. Suter, Adv. Polym. Sci. **131/132** (1997).
14. A. Abe, R. L. Jernigan, and P. J. Flory, J. Am. Chem. Soc. **88**, 631 (1966).
15. A. Abe and J. E. Mark, J. Am. Chem. Soc. **98**, 6468 (1976).
16. M. Hutnik, A. S. Argon, and U. W. Suter, Macromolecules **24**, 5956 (1991).
17. J. H. Ko and J. E. Mark, Macromolecules **8**, 869, 874 (1975).
18. P. J. Flory, V. Crescenzi, and J. E. Mark, J. Am. Chem. Soc. **86**, 146 (1964).
19. C. A. Hoeve, J. Chem. Phys. **35**, 1266 (1961).
20. W. J. Welsh, L. DeBolt, and J. E. Mark, Macromolecules **19**, 2978 (1986).
21. J. A. Semlyen, Trans. Faraday. Soc. **63**, 743 (1967).
22. J. A. Semlyen, Trans. Faraday. Soc. **64**, 1396 (1968).
23. J. W. Mark and J. G. Curro, J. Chem. Phys. **80**, 5262 (1984).
24. T. W. Bates and W. H. Stockmayer, J. Chem. Phys. **45**, 2321 (1966).
25. G. D. Smith, R. L. Jaffe, and D. Y. Yoon, Macromolecules **28**, 3166 (1994).
26. O. Borodin, G. D. Smith, and D. Bedrov, J. Phys. Chem. B **106**, 9912 (2002).
27. R. Bohmer and C. A. Angell, Phys. Rev. B: Condens. Matter & Mater. Phys. **48**, 5857 (1993).
28. P. J. Flory and J. E. Mark, Makromol. Chem. **75**, 11 (1964).
29. G. D. Smith, R. L. Jaffe, and D. Y. Yoon, J. Phys. Chem. **98**, 9078 (1994).
30. D. Chen and W. L. Mattice, Polymer **45**, 3877 (2004).
31. M. S. Beavers and J. A. Semlyen, Polymer **13**, 385 (1972).
32. G. Allegra, E. Benedetti, and C. Pedrone, Macromolecules **3**, 727 (1970).
33. R. H. Boyd and S. M. Breitling, Macromolecules **5**, 1 (1972).
34. L. C. DeBolt and U. W. Suter, Macromolecules **20**, 1424 (1987).
35. M. Vacatello and D. Y. Yoon, Macromolecules **25**, 2502 (1992).
36. L. Carballeira, A. J. Pereiras, and M. A. Rios, Macromolecules **23**, 1309 (1990).
37. O. G. Byutner and G. D. Smith, Macromolecules **32**, 8376 (1999).
38. P. R. Sundararajan, Comput. Polym. Sci. **1**, 18 (1991).
39. I. Bahar, I. Zuniga, R. Dodge, and W. L. Mattice, Macromolecules **24**, 2986 (1991).
40. J. A. Semlyen and P. J. Flory, Trans. Faraday. Soc. **62**, 2622 (1966).
41. R. H. Boyd and L. Kesner, J. Polym. Sci., Polym. Phys. Ed. **19**, 393 (1981).
42. E. Saiz, J. Polym. Sci., Polym. Phys. Ed. **25**, 1565 (1987).
43. R. D. Patil and J. E. Mark, Comput. Theor. Polym. Sci. **10**, 189 (2000).
44. J. E. Mark and P. J. Flory, J. Am. Chem. Soc. **87**, 1415 (1965).
45. G. D. Smith, D. Y. Yoon, and R. L. Jaffe, Macromolecules **26**, 5213 (1993).
46. Y. Sasanuma, H. Ohta, I, Touma, H. Matoba, Y. Hayashi, and A. Kaito, Macromolecules **35**, 3748 (2002).
47. W. G. Miller, D. A. Brant, and P. J. Flory, J. Mol. Biol. **23**, 67 (1967).
48. A. Abe, Macromolecules **13**, 546 (1980).
49. W. L. Mattice, J. Am. Chem. Soc. **102**, 2242 (1980).
50. K. Kato, A. Araki, and A. Abe, Polym. J. **13**, 1065 (1981).
51. J. E. Mark, J. Am. Chem. Soc. **88**, 4354 (1966).
52. T. Ishikawa and K. Nagai, J. Polym. Sci., Part A-2 **7**, 1123 (1969).
53. Y. Abe and P. J. Flory, Macromolecules **4**, 219 (1971).
54. G. D. Smith and W. Paul, J. Phys. Chem. A **102**, 1200 (1998).
55. J. E. Mark, J. Am. Chem. Soc. **89**, 6829 (1967).
56. T. Ishikawa and K. Nagai, Polym. J. **1**, 116 (1970).
57. Y. Abe and P. J. Flory, Macromolecules **4**, 230 (1971).
58. J. Guzmán, E. Riande, W. J. Welsh, and J. E. Mark, Makromol. Chem. **183**, 2573 (1982).
59. E. Saiz, E. Riande, J. Guzmán, and J. de Abajo, J. Chem. Phys. **73**, 958 (1980).
60. K. Inomata, N. Phataralaoha, and A. Abe, Comput. Polym. Sci. **1**, 126 (1991).
61. E. Riande, J. Guzmán, E. Saiz, and J. de Abajo, Macromolecules **14**, 608 (1981).
62. E. Riande and J. E. Mark, Macromolecules **11**, 956 (1978).
63. E. Riande, J. Guzmán, W. J. Welsh, and J. E. Mark, Makromol. Chem. **183**, 2555 (1982).
64. E. Riande and J. Guzmán, Macromolecules **12**, 952 (1979).
65. E. Riande, J. Polym. Sci., Polym. Phys. Ed. **14**, 2231 (1976).
66. M. Mutter, U. W. Suter, and P. J. Flory, J. Am. Chem. Soc. **98**, 5745 (1976).
67. P. J. Flory, J. E. Mark, and A. Abe, J. Am. Chem. Soc. **88**, 639 (1966).
68. D. Y. Yoon, P. R. Sundararajan, and P. J. Flory, Macromolecules **8**, 776 (1975).
69. Y. Abe, A. E. Tonelli, and P. J. Flory, Macromolecules **3**, 294, 303 (1970).

70. R. H. Boyd and S. M. Breitling, Macromolecules **5**, 279 (1972).
71. U. W. Suter, S. Pucci, and P. Pino, J. Am. Chem. Soc. **97**, 1018 (1975).
72. U. W. Suter and P. J. Flory, Macromolecules **8**, 765 (1975).
73. R. M. Wolf and U. W. Suter, Macromolecules **17**, 669 (1984).
74. A. E. Tonelli, Macromolecules **18**, 1086 (1985).
75. A. E. Tonelli, Macromolecules **13**, 734 (1980).
76. W. L. Mattice, Macromolecules **10**, 1171 (1977).
77. P. R. Sundararajan, Macromolecules **23**, 3178 (1990).
78. A. Abe, T. Hirano, and T. Tsurura, Macromolecules **12**, 1092 (1979).
79. Y. Sasanuma, Macromolecules **28**, 8629 (1995).
80. A. Abe, Macromolecules **10**, 34 (1977).
81. J. E. Mark, J. Chem. Phys. **56**, 451 (1972).
82. G. D. Smith, P. J. Ludovice, R. L. Jaffe, and D. Y. Yoon, J. Phys. Chem. **99**, 164 (1995).
83. U. W. Suter, J. Am. Chem. Soc. **101**, 6481 (1979).
84. A. Abe, Macromolecules **13**, 541 (1980).
85. Y. Sasanuma, Y. Hayashi, H. Matoba, I. Touma, H. Ohta, M. Sawanobori, and A. Kaito, Macromolecules **24**, 8216 (2002).
86. E. D. Akten and W. L. Mattice, Macromolecules **34**, 3389 (2001).
87. P. R. Sundararajan, Macromolecules **11**, 256 (1978).
88. P. J. Flory, J. Am. Chem. Soc. **89**, 1798 (1967).
89. D. Y. Yoon, U. W. Suter, P. R. Sundararajan, and P. J. Flory, Macromolecules **8**, 784 (1975).
90. E. A. Ovalvo, E. Saiz, R. M. Masegosa, and I. Hernández-Fuentes, Macromolecules **12**, 865 (1979).
91. J. A. Guest, K. Matsuo, W. H. Stockmayer, and U. W. Suter, Macromolecules **13**, 560 (1980).
92. P. R. Sundararajan and P. J. Flory, J. Am. Chem. Soc. **96**, 5025 (1974).
93. M. Vacatello and P. J. Flory, Macromolecules **19**, 405 (1986).
94. P. R. Sundararajan, Macromolecules **19**, 415 (1986).
95. J. E. Mark and J. H. Ko, J. Polym. Sci., Polym. Phys. Ed. **13**, 2221 (1975).
96. A. D. Williams and P. J. Flory, J. Am. Chem. Soc. **91**, 3111 (1969).
97. R. F. Rapold and U. W. Suter, Macromol. Theory Simul. **3**, 1 (1994).
98. A. E. Tonelli, Macromolecules **18**, 2579 (1985).
99. E. Saiz, E. Riande, M. P. Delgado, and J. M. Barrales-Rienda, Macromolecules **15**, 1152 (1982).
100. A. E. Tonelli, Polymer **23**, 676 (1982).
101. P. R. Sundararajan, Macromolecules **10**, 623 (1977).
102. W. J. Welsh, J. R. Damewood, Jr., and R. C. West, Macromolecules **22**, 2947 (1989).
103. P. R. Sundararajan, Macromolecules **24**, 1420 (1991).
104. J. E. Mark, J. Chem. Phys. **56**, 458 (1972).
105. J. S. Saiz, E. Riande, J. San Román, and E. L. Madruga, Macromolecules **23**, 786 (1990).
106. P. R. Sundararajan, Macromolecles **13**, 512 (1980).
107. A. Abe, H. Kobayashi, T. Kawamura, M. Date, T. Uryu, and K. Matsuzaki, Macromolecules **21**, 3414 (1988).
108. P. R. Sundararajan, Macromolecules **21**, 1256 (1988).
109. C. A. Helfer, W. L. Mattice, and D. Chen, Polymer **45**, 1297 (2004).
110. A. E. Tonelli, *NMR Spectroscopy and Polymer Microstructures. The Conformational Connection.* (VCH, New York, 1989).
111. M. Karplus, J. Chem. Phys. **30**, 11 (1959).
112. M. Karplus, J. Chem. Phys. **33**, 1842 (1960).
113. M. Karplus, J. Am. Chem. Soc. **35**, 2870 (1963).
114. F. A. Bovey, A. I. Brewster, D. J. Patel, A. E. Tonelli, and D. A. Torchia, Acct. Chem. Res. **5**, 193 (1972).
115. A. Abe, J. Am. Chem. Soc. **90**, 2205 (1968).
116. W. K. Kim and W. L. Mattice, Comput. Theor. Polym. Sci. **8**, 339 (1998).
117. A. D. Williams and P. J. Flory, J. Polym. Sci.: Part A-2 **6**, 1945 (1968).
118. A. D. Williams and P. J. Flory, J. Polym. Sci.: Part A-2 **5**, 147 (1967).
119. F. Mendicuti, E. Saiz, and W. L. Mattice, Polymer **33**, 4908 (1992).
120. G. C. Rutledge, Macromolecules **25**, 3984 (1992).
121. E. Yurtsever and B. Erman, Polymer **34**, 3887 (1993).
122. V. S. R. Rao, N. Yathindra, and P. R. Sundararajan, Biopolymers **8**, 325 (1969).
123. D. A. Brant and W. L. Dimpfl, Macromolecules **3**, 655 (1970).
124. D. A. Brant and K. D. Goebel, Macromolecules **8**, 522 (1975).
125. W. K. Olson and P. J. Flory, Biopolymers **11**, 1 (1972).
126. D. A. Brant and P. J. Flory, J. Am. Chem. Soc. **87**, 2788 (1965).
127. W. G. Miller and P. J. Flory, J. Mol. Biol. **15**, 298 (1966).
128. D. A. Brant, W. G. Miller, and P. J. Flory, J. Mol. Biol. **23**, 47 (1967).
129. D. A. Brant, A. E. Tonelli, and P. J. Flory, Macromolecules **2**, 225, 228 (1969).
130. J. E. Mark, J. Chem. Phys. **56**, 458 (1972).
131. C. A. Helfer and W. L. Mattice, Polymer **46**, 4361 (2005).
132. D. C. Poland and H. A. Scheraga, *Theory of Helix-Coil Transitions in Biopolymers; Statistical Mechanical Theory of Order–Disorder Transitions in Biological Macromolecules* (Academic, New York, 1970).
133. A. E. Tonelli and F. C. Schilling, Acct. Chem. Res. **14**, 223 (1981).
134. A. Abe, J. Am. Chem. Soc. **92**, 1136 (1970).
135. E. Saiz and M. P. Tarazona, Macromolecules **16**, 1128 (1983).
136. U. W. Suter, Macromolecules **14**, 523 (1980).
137. U. W. Suter and P. Neuenschwander, Macromolecules **14**, 528 (1980).
138. R. L. Jernigan and P. J. Flory, J. Chem. Phys. **50**, 4178 (1969).
139. H. Jacobson and W. H. Stockmayer, J. Chem. Phys. **18**, 1600 (1950).
140. R. L. Jernigan and P. J. Flory, J. Chem. Phys. **50**, 4185 (1969).
141. P. J. Flory, U. W. Suter, and M. Mutter, J. Am. Chem. Soc. **98**, 5733 (1976).
142. U. W. Suter, M. Mutter, and P. J. Flory, J. Am. Chem. Soc. **98**, 5740 (1976).
143. M. Vacatello, D. Y. Yoon, and P. J. Flory, Macromolecules **23**, 1993 (1990).
144. J. E. Mark and J. G. Curro, J. Chem. Phys. **81**, 6408 (1984).
145. W. L. Mattice, Macromolecules **13**, 506 (1980).
146. L. C. DeBolt and J. E. Mark, Macromolecules **20**, 2369 (1987).
147. R. I. Feigin and D. H. Napper, J. Colloid. Interf. Sci. **71**, 117 (1979).
148. M. A. Sharaf, A. Kloczkowski, and J. E. Mark, Comput. Polym. Sci. **4**, 29 (1994).
149. W. M. Mattice and J. Skolnick, Macromolecules **14**, 863 (1981).
150. R. F. Rapold and W. L. Mattice, Macromolecules **29**, 2457 (1996).
151. T. Haliloglu and W. L. Mattice, J. Chem. Phys. **108**, 6989 (1997).
152. P. Doruker and W. L. Mattice, Macromolecules **30**, 5520 (1997).
153. T. C. Clancy, M. Pütz, J. D. Weinhold, J. G. Curro, and W. L. Mattice, Macromolecules **33**, 9452 (2000).
154. G. Xu, T. C. Clancy, W. L. Mattice, and S. K. Kumar, Macromolecules **35**, 3309 (2002).
155. P. J. Flory, J. Polym. Sci., Polym. Phys. Ed. **11**, 621 (1973).
156. K. Matsuo and W. H. Stockmayer, Macromolecules **8**, 650 (1975).
157. F. Heatley, Polymer **13**, 218 (1972).
158. B. C. Laskowski, D. Y. Yoon, D. MacLean, and R. L. Jaffe, Macromolecules **21**, 1629 (1988).
159. M. Vacatello, D. Y. Yoon, and P. J. Flory, Macromolecules **23**, 1993 (1990).
160. W. L. Mattice, Comput. Polym. Sci. **1**, 173 (1991).
161. W. L. Mattice and H. A. Scheraga, Biopolymers **23**, 1701 (1984).

CHAPTER 4

Computational Parameters

Joel R. Fried

Department of Chemical and Materials Engineering, University of Cincinnati, Cincinnati, OH 45221-0012

This chapter discusses the form and parameterization of the potential energy terms that are used for the atomistic simulation of polymers. The sum of potential terms constitutes a molecular force field that can be used in molecular mechanics, molecular dynamics, and Monte Carlo simulations of polymeric systems. Molecular simulation methods can be used to determine such properties as PVT data, self-diffusion coefficients, modulus, phase equilibrium, x-ray and neutron diffraction spectra, small molecule solubility, and glass transition temperatures with considerable accuracy and reliability using current force fields. Included in the coverage of Chapter 4 is a review of the fundamentals of molecular mechanics and a survey of the most widely used force fields for the simulation of polymer systems. In addition, references to the use of specific force fields in the study of important polymer groups are given.

4.1 MOLECULAR MECHANICS

Traditional molecular mechanics methods developed by Allinger [1] and others view a molecule as a series of beads (i.e., the nuclei) joined together by springs (i.e., the bonds). The total potential energy, V, of the system is the sum of all bonded and nonbonded terms as

$$V(\mathbf{r}) = V^{\mathbf{B}}(\mathbf{r}) + V^{\mathrm{NB}}(\mathbf{r}). \tag{4.1}$$

The bonded terms include bond stretching, angle bending, and dihedral (i.e., torsional) contributions as

$$V^{\mathrm{B}}(\mathbf{r}) = \sum_{\text{bonds}} V^{\mathrm{bond}}(r_{ij}) + \sum_{\text{bends}} V^{\mathrm{bend}}(\theta_{ijk}) + \sum_{\text{dihedrals}} V^{\mathrm{tors}}(\phi_{ijkl}), \tag{4.2}$$

where the summations are made over all contiguous atoms constituting bonds (i.e., two-body interactions), angles (three-body interactions), and torsions (four-body interactions) in the system. Torsional contributions also may include improper torsion and out-of-plane bending terms in some force fields as discussed in Section 4.2.

Nonbonded terms typically include steric (e.g., van der Waals) and electrostatic (e.g., Coulombic) terms but may also include polarization contributions. Force field parameters for each bonded or nonbonded term are obtained by fitting potential energy terms to ab initio (e.g., HF/6-31G*) or DFT calculations of small molecules or by fitting to experimental data such as crystal structure and the heat of vaporization[1] (ΔH_{V}) for low-molecular-weight compounds. The form of specific terms used by different commercial, public domain, and customized force fields for polymer simulations are given in the sections that follow.

4.1.1 Bonded Terms

Bond Stretching

Bond-stretching terms can have several different forms including the simple harmonic function

$$V^{\mathrm{bond}}(r_{ij}) = \frac{1}{2}\sum_{\text{bonds}} k_{ij}^{\mathrm{bond}}\left(r_{ij} - r_{ij}^{0}\right)^2, \tag{4.3}$$

where k_{ij}^{bond} is the bond-stretching parameter and r_{ij}^{0} is the equilibrium bond distance (for which the potential energy contribution is zero). The summation is taken over all bonds in the system. Alternately, additional higher order (i.e.,

[1] The heat of vaporization is related to the cohesive energy density (CED), the total intermolecular energy, through the expression

$$E_{\mathrm{CED}} = \frac{\rho}{M}(\Delta H_{\mathrm{V}} - RT)$$

where M is the molecular weight and ρ is the density of the low-molecular-weight compound.

anharmonic) terms may be included as a polynomial such as the quartic expression

$$V^{\text{bond}}(r_{ij}) = \frac{1}{2}\sum_{\text{bonds}}\left[k_2\left(r_{ij}-r_{ij}^0\right)^2 + k_3\left(r_{ij}-r_{ij}^0\right)^3 + k_4\left(r_{ij}-r_{ij}^0\right)^4\right]. \quad (4.4)$$

A Morse exponential potential [2] can also be used for the bond-stretching term in the form

$$V^{\text{bond}}(r_{ij}) = \sum_{\text{bonds}} D_{ij}\left\{\exp\left[-\alpha\left(r_{ij}-r_{ij}^0\right)\right]-1\right\}^2, \quad (4.5)$$

where D_{ij} is the bond dissociation energy and

$$\alpha = \left(\frac{k_{ij}}{2D_{ij}}\right)^{1/2}. \quad (4.6)$$

The Morse function is an accurate representation of the bond-stretching potential since the exponential term in Eq. (4.5) implicitly includes anharmonic terms.

Angle Bending

The harmonic term for (valence) angle bending can be written as

$$V^{\text{bend}}(\theta_{ijk}) = \frac{1}{2}\sum_{\text{bends}} k_{ijk}^{\text{bend}}\left(\theta_{ijk}-\theta_{ijk}^0\right)^2, \quad (4.7)$$

where θ_{ijk}^0 is the equilibrium (i.e., minimum energy) valence angle. The quartic form may be written as

$$V^{\text{bend}}(\theta_{ijk}) = \frac{1}{2}\sum_{\text{bends}}\left[k_2\left(\theta_{ijk}-\theta_{ijk}^0\right)^2 + k_3\left(\theta_{ijk}-\theta_{ijk}^0\right)^3 + k_4\left(\theta_{ijk}-\theta_{ijk}^0\right)^4\right]. \quad (4.8)$$

An alternative to the harmonic expression Eq. (4.7) is the Urey–Bradley expression

$$V_{\text{UB}} = \sum_{\text{UB}} K_{\text{UB}}(S-S_0)^2. \quad (4.9)$$

where S is the Urey–Bradley 1,3 distance (i.e., the A–C distance in bond angle ABC).

Torsion

Torsional terms can have several different forms such as

$$V^{\text{tors}}(\phi_{ijkl}) = \frac{1}{2}\sum_{\text{dihedrals}}\sum_{n=1,2,\ldots} k_{ijkl}^{\text{tors}}(n)[1-\cos(n\phi_{ijkl})], \quad (4.10)$$

where n is the periodicity of the torsional motion. Another torsional form that has been used is the Ryckaert–Bellemans potential [3,4]

$$V^{\text{tors}}(\phi_{ijkl}) = \sum_{\text{dihedrals}}\sum_{n=0}^{5} a_n\cos^n\phi_{ijkl}. \quad (4.11)$$

Improper (out-of-plane bending) torsion potentials appear in some force fields. These are used to represent potential energy required to maintain the configuration of four contiguous atoms within certain geometric limits. The form of this potential term can be written as

$$V^{\text{oop}}(\omega_{ijkl}) = \frac{1}{2}\sum_{\substack{\text{improper}\\ \text{torsions}}} k_{ijkl}^{\text{oop}}\left(\omega_{ijkl}-\omega_{ijkl}^0\right)^2, \quad (4.12)$$

where ω_{ijkl}^0 represents the equilibrium (i.e., minimum energy) improper torsion angle.

Cross-Coupling Terms

Cross-coupling terms have been used in several force fields as a means to represent the effect of one type deformation on another such as the interrelationship between bond stretching and angle bending which can be expressed in a bond–bend potential term as

$$V^{\text{b,b}}(r_{ij},\theta_{ijk}) = \frac{1}{2}\sum_{\text{bonds}}\sum_{\text{bends}} k^{\text{b,b}}\left(r_{ij}-r_{ij}^0\right)^2\left(\theta_{ijk}-\theta_{ijk}^0\right)^2. \quad (4.13)$$

Other cross-coupling terms include bond–torsion and bend–bend–torsion. Cross-coupling terms are important for accurate modeling of normal mode vibrational frequencies and to better model the potential at large deformation (i.e., positions far from the potential minimum).

4.1.2 Nonbonded Terms

Nonbonded terms include intramolecular interactions between pairs of atoms separated by three or more bonds and those belonging to different molecules (i.e., intermolecular interactions). Interactions between pairs of atoms separated by one or two bonds are contained in the bonded energy terms of the bond-stretch and angle-bending terms, respectively. All interactions in a simulation system may be included (i.e., Ewald summation) or distance cutoffs, typically in the range from 8 to 12 Å, may be used.

Steric Terms

Steric interactions are typically represented by some form of a Lennard-Jones (LJ) potential such as the LJ 6–12 potential or the LJ 6–9 potential as illustrated below

$$V^{\text{LJ}} = \sum_{i\neq j}\varepsilon_{ij}\left[2\left(\frac{r_{ij}^0}{r_{ij}}\right)^9 - 3\left(\frac{r_{ij}^0}{r_{ij}}\right)^6\right]. \quad (4.14)$$

The 6th order term in the LJ expression represents dispersion (long-range) interactions while the 9th (or 12th) order term represents short-range repulsion. Sometimes an exponential potential may be used as the short-range term in combination with a 6th order dispersion term in the form

$$V^{\exp-6} = \sum_{i \neq j} \left[A_{ij} \exp(-B_{ij} r_{ij}) - \frac{C_{ij}}{r_{ij}^6} \right]. \tag{4.15}$$

The exponential form is a better representation of repulsive interactions than the LJ inverse-12 form. The combination of an exponential and a 6th order term has been called the Buckingham potential function, the exponential-6 equation, or the modified Hill equation.

The LJ parameters ε_{ij} and r_{ij}^0 appearing in Eq. (4.14) are obtained by a combination rule using individual atomic parameters. These combination rules include the Lorentz and Berthelot rule and the 6th order combination law given as [5]

$$r_{ij}^0 = \left[\frac{(r_i^0)^6 + (r_j^0)^6}{2} \right]^{1/6} \tag{4.16}$$

and

$$\varepsilon_{ij} = \frac{2(\varepsilon_i \varepsilon_j)^{1/2} (r_i^0 r_j^0)^3}{(r_i^0)^6 + (r_j^0)^6}. \tag{4.17}$$

Electrostatic Terms

The electrostatic terms include the simple Coulombic expression in the general form

$$V^{\text{es}} = \sum_{i \neq j} \frac{f q_i q_j}{r_{ij}}, \tag{4.18}$$

where q_i represents the charge on atom i of the atom pair i,j, r_{ij} is the separation between atoms i and j, and $f = 1/\pi\varepsilon_0$ where ε_0 is the dielectric constant.

Hydrogen Bonding Contributions

An additional nonbonded term sometimes appearing in force fields for biological systems (especially older force field versions) is used to model the interaction between hydrogen donor and acceptor atoms involved in hydrogen bonding. An example is the potential energy term

$$V^{\text{HB}} = \sum_{i \neq j} \left(\frac{C_{ij}}{r_{ij}^{12}} - \frac{D_{ij}}{r_{ij}^{10}} \right) \cos^4 \theta_{\text{DHA}}, \tag{4.19}$$

where θ_{DHA} is the angle between the donor (D), hydrogen (H), and acceptor (A) atoms. Current force field versions do not explicitly treat hydrogen bonding since extensive parameterization of nonbonded terms ideally should include hydrogen bonding. Incorporation of multiple nonbonded terms, including polarization terms as discussed in the next section, significantly adds to the computational time since nonbonded interactions must be calculated between thousands of atoms at each timestep, typically 1 fs.

Polarization

Some force fields also include a polarization term, V^{pol}, along with steric (i.e., LJ or Buckingham) and electrostatic terms in the nonbonded potential expression as

$$V^{\text{NB}}(\mathbf{r}) = V^{\text{steric}}(\mathbf{r}) + V^{\text{es}}(\mathbf{r}) + V^{\text{pol}}(\mathbf{r}). \tag{4.20}$$

An example of the form of a polarization term is [6]

$$V^{\text{pol}} = \frac{1}{2} \sum_i \mu_i E_i, \tag{4.21}$$

where μ_i is the dipole moment associated with atom i and E_i is the electrostatic field experienced at atom i. A detailed discussion of polarization contributions is given by Smith and Borodin [7]. Polarizable force fields allow the charge distribution to respond to the dielectric environment [8] and are particularly important in the atomistic simulation of water and the detailed simulation of biological systems in general. A problem associated with inclusion of a polarization potential term is the additional computational cost incurred by including another nonbonded term. In the case of polymers, polarizable force fields are particularly important in the treatment of polymer electrolytes including those of poly(ethylene oxide)/Li^+ as discussed by Smith and Borodin [7] and in the atomistic simulation of systems in which chemical reactions can occur as in the case of proton transfer (e.g., fuel cell applications) or the simulation of combustion events. Force fields that can treat bond formation or breaking include ReaxxFF [9] as discussed briefly in the next section.

4.2 FORCE FIELDS

Many different force fields are now available from commercial and other sources. Some force fields like the MM series[2] of force fields developed by Allinger and the Merck MM [10] have been parameterized primarily for molecular mechanics and dynamics of small molecules. Due to their limited importance for polymer simulations, they will not be covered in this section; however, they have been used to study conformational properties of model compounds for some aromatic polymers. In some cases, force fields primarily developed for biomolecules such as AMBER, CHARMM, and GROMOS have been used in the molecular simulation of polymeric systems. Force fields having particular importance for polymers include simple but versatile

[2] The most recent version is MM4.

generic Class I force fields like DREIDING [11]. At the upper end are ab initio parameterized Class II force fields such as the consistent force field (CFF) family to which the force field COMPASS[3] [12] belongs. COMPASS has been extensively parameterized using physical property data and includes anharmonic and cross-coupling contributions in the bonded interactions (Section 4.1.1). In the discussion that follows, force fields are grouped into the categories of generic force fields, biological force fields, and Class II force fields. As shown by references given in Table 4.1 that surveys the literature from 1990 to 2005, all the force fields discussed in this section have been used for the atomistic simulation of polymeric systems. Many of these articles provide information on parameterization. References prior to 1990 were included in the previous review by Roe [13].

4.2.1 Generic Force Fields

Universal. The parameters in the Universal force field (UFF) [14–16] are calculated using general rules based only upon the element, its hybridization, and its connectivity. For this reason, the UFF has broad applicability but is inherently less accurate than extensively parameterized force fields such as COMPASS. Bond-stretching terms in the UFF are either harmonic or Morse functions. The angle-bending and torsion terms are described by a small cosine Fourier expansion. For nonbonded terms, the LJ 6–12 potential and Coulombic terms are used for steric and electrostatic terms, respectively.

DREIDING. DREIDING is another general-purpose force field that uses generalized force constants and geometry parameters. Parameterization of DREIDING is biased toward the first row elements (and carbon); however, DREIDING can be custom parameterized from ab initio or semiempircal data from calculations of model compounds with very good success in the atomistic simulation of polymers as shown by Fried and Goyal [17] and others. The default form of DREIDING uses the harmonic term, Eq. (4.3), for bond stretching and a harmonic cosine form of the angle-bend term given as

$$V^{\text{bend}}(\theta_{ijk}) = \frac{1}{2}\sum_{\text{bends}} k_{ijk}^{\text{bend}}\left(\cos\theta_{ijk} - \cos\theta_{ijk}^{0}\right)^2 \qquad (4.22)$$

The torsion term has the form

$$V^{\text{tor}}(\phi_{ijk}) = \frac{1}{2}\sum_{\text{dihedrals}} k_{jk}^{\text{tor}}\left\{1 - \cos\left[n_{jk}(\phi_{\text{jk}} - \phi_{\text{jk}}^{0})\right]\right\} \qquad (4.23)$$

where ϕ is the dihedral or torsional angle between the *ijk* and *jkl* planes formed by two consecutive bonds *ij* and *kl*. In addition, DREIDING includes an inversion term that has

[3] *C*ondensed-phase *O*ptimized *M*olecular *P*otentials for *A*tomistic *S*imulation *S*tudies.

TABLE 4.1. *Literature citations (1990–2005) for force fields used in the atomistic simulations of polymers.*

Polymer	Force field	Reference
Poly(aryl ether ether ketone)	TRIPOS	[41]
	DREIDING	[42]
Polyarylates	CHARMM	[43]
Poly(2,5-benzimidazole)	TRIPOS	[44]
Polybenzoxazoles	DREIDING	[45]
trans-1,4-Polybutadiene	CHARMM	[46]
Polycarbonate	CFF93	[36]
	DREIDING	[47,48]
	TRIPOS	[49]
Polydimethylsiloxane	TRIPOS	[50]
	ReaxxFF	[9]
Polyethersulfone	DREIDING	[51]
Polyethylene	custom	[52]
	custom	[53]
	COMPASS	[54]
Poly(ethylene oxide)	CFF93	[39]
	custom	[55]
	CVFF	[56]
	PCFF	[57]
	DREIDING	[58]
Poly(ethylene terephthalate)	CFF93+	[37]
	Custom	[59]
	DREIDING	[60]
Poly(*p*-hydroxybenzoic acid)	CFF93	[37]
Polyimides	DREIDING	[61–66]
	TRIPOS	[67]
Polyisobutylene	Custom	[53]
Polyisoprene	PCFF	[68]
Polymethacrylates	AMBER	[69]
	PCFF	[70]
Poly(methyl methacrylate)	PCFF	[70,71]
Poly(naphthalic anhydride)	DREIDING	[72]
Poly(*p*-phenylene)	DREIDING	[73]
	UFF	[74]
Poly(*p*-phenylene isophthalate)	AMBER	[75]
Poly(*p*-phenylene sulfide)	Custom	[76]
Poly(*p*-phenylene terephthalate)	COMPASS	[77]
	AMBER	[75]
Polyphosphazenes	COMPASS	[40]
	AMBER	[78]
Polypropylene	CFF91	[79]
Poly(propylene oxide)	Custom	[80]
Polypyrrole	GROMOS	[81]
Polyrotaxanes	Tripos5.2	[82]
Polysilanes	CFF93	[38]
Polystyrene	CHARMM	[83,84]
	AMBER	[85]
syndiotactic-polystyrene	Custom	[86]
Poly[1-(trimethylsilyl)-1-propyne]	DREIDING	[17]
Polyurethanes	DREIDING	[87]
Poly(vinyl chloride)	custom	[88]
	CVFF, CFF91	[89]
Poly(vinyl methyl ether)	PCFF2	[90]
Poly(vinylene fluoride)	Custom	[91]

importance for atoms that are bonded to three other atoms (e.g., N in NH_3 and P in PH_3). The inversion term represents the difficulty of forcing all three bonds for atom i bonded to exactly three other atoms j, k, l, into the same plane. For nonbonded interactions, DREIDING uses a LJ 6–12 potential, a Coulombic expression for electrostatic interactions, and a term to accommodate hydrogen bonding.

4.2.2 Biological Force Fields

Empirical force fields for biological macromolecules have been reviewed by Mackerell [6] and by Ponder and Case [18]. These include CHARMM, AMBER, OPLS, and GROMOS. All may be classified as a Class I force field of the general form given by Eg. (4.24)

$$V(\mathbf{r}) = \frac{1}{2}\sum_{\text{bonds}} k_{ij}^{\text{bond}}(r_{ij}-r_{ij}^0)^2 + \frac{1}{2}\sum_{\text{bends}} k_{ijk}^{\text{bend}}(\theta_{ijk}-\theta_{ijk}^0)^2 + \sum_{\text{torsions}} k_\phi[1+\cos(n\phi-\delta)] + \frac{1}{2}\sum_{\substack{\text{improper}\\ \text{torsions}}} k_{ijkl}^{\text{oop}}(\omega_{ijkl}-\omega_{ijkl}^0)^2 + \sum_{i\neq j}\varepsilon_{ij}\left[2\left(\frac{r_{ij}^0}{r_{ij}}\right)^{12} - 3\left(\frac{r_{ij}^0}{r_{ij}}\right)^{6}\right] + \sum_{i\neq j}\frac{q_i q_j}{\varepsilon r_{ij}}, \tag{4.24}$$

where the bonded terms are all harmonic and there are no cross-terms.

CHARMM. The CHARMM[4] [19] force field includes harmonic terms for bond stretching and angle bending. Both proper and improper torsion terms are included in CHARMM as are LJ 6–12 and Coulombic nonbonded contributions.

AMBER. AMBER [20,21] has been extensively used in the simulation of proteins and nucleic acids but recently has been generalized with parameters for most organic acid and pharmaceutical molecules [22].

OPLS. The OPLS[5] force field [23–25] was introduced in the early 1980s to simulate liquid-state properties of water and more than 40 organic liquids. The form of the OPLS-AA force field is given as [25]

$$V(\mathbf{r}) = \sum_i k_{\text{b},i}(r_i - r_i^0)^2 + \sum_i k_{\theta,i}(\theta_i-\theta_i^0)^2 + \sum_i \left[V_{0,i} + V_{1,i}(1+\cos\phi_i)/2 + V_{2,i}(1-\cos 2\phi_i)/2 + V_{3,i}(1+\cos 3\phi_i)/2\right] + \sum_i\sum_j \left\{(q_i q_j e^2/r_{ij}) + 4\varepsilon_{ij}\left[(\sigma_{ij}/r_{ij})^{12} - (\sigma_{ij}/r_{ij})^6\right]\right\}. \tag{4.25}$$

TRIPOS. A force parameterized for biomolecules and small organic molecules, but sometimes used for polymers, is the TRIPOS force field [26] in the Sybyl molecular modeling package. The TRIPOS 5.2 force field includes harmonic bond stretching and angle bending with a torsional function consisting of a single cosine term. Nonbonded terms include a LJ 6–12 potential and a Coulombic term with either a constant or distance dependent dielectric function.

GROMACS. Another force field originally targeted for the molecular simulations of biomolecules, but also useful for polymers, is GROMACS[6] that runs molecular dynamics in a message-passing parallel mode. GROMACS [27] is a new implementation of GROMOS[7] developed by van Gunsteren and Berendsen at the University of Groningen in the late 1980s [28,29]. Provisions are available in GROMACS for conversion between GROMACS and GROMOS formats including the GROMOS87 and GROMOS96 force fields that are provided in GROMACS. Current features of GROMACS 3.0 have been reviewed by Lindahl *et al*. [30].

For bonded terms, GROMACS uses either a two-body harmonic potential (Eq. (4.3)) or Morse function for bond stretching and a three-body harmonic potential for angle bending (Eq. (4.7)). For both bond stretching and angle bending, a constraint can be used in place of the potential term. Four-body potentials include proper torsions and improper torsion potentials in the form of Eqs. (4.11) and (4.12), respectively. GROMACS uses a LJ 6–12 potential (an exponential short-range term, Eq. (4.15), is optional) and a Coulombic term (Eq. (4.18)) for nonbonded interactions. Force fields options include GROMOS, OPLS, and AMBER. Any united atom (UA) or all-atom force fields based on the general types of potential functions implemented in the GROMOS code can be used. GROMACS also permits the use of arbitrary forms of interactions with spline-interpolated tables as well as external potential terms for position-restraining forces and external acceleration (for nonequilibrium molecular dynamics).

[4] *C*hemistry at *HAR*vard *M*acromolecular *M*echanics).
[5] Optimized Potentials for Liquid Simulations.
[6] *GRO*ningen *MA*chine for *C*hemical *S*imulation.
[7] *GRO*ningen *M*olecular *S*imulation.

CVFF. The consistent valence force field (CVFF) originally applied to biological systems [31] is a forerunner of the consistent force field (CFF) and its later derivatives (the polymer consistent force field PCFF and COMPASS) as discussed in Section 4.24. Terms in CVFF included a Morse potential for bond stretching, a harmonic term for angle bending, cosine torsional and out-of-plane torsional terms, four cross-coupling terms (bond–bond, angle–angle, bond–angle, and angle–torsion), and LJ 6–12 and Coulombic terms for nonbonded interactions. CVFF has been reported to perform less favorably than an early version of CFF (CFF91) for predicting the conformational energies of small molecules [32].

4.2.3 Specialized Force Field and MD Codes

ReaxFF. ReaxFF allows for bond breaking and bond formation in MD simulation so that thermal decomposition can be modeled as has been shown recently for polydimethylsiloxane [9]. ReaxxFF includes terms for traditional bonded potentials as well as nonbonded potentials (i.e., van der Waals and Coulombic). Bond breaking and bond formation are handled through a bond order/bond distance relationship. Parameterization is through high-level DFT calculations (B3LYP/6-311++G**).

DL_POLY. DL_POLY[8] is a parallel molecular dynamics simulation package originally developed at the Daresbury Laboratory in England. Parameters for the current DL_POLY_3 force field may be obtained from the GROMOS, AMBER, and DREIDING force fields that share functional forms.

LAMMPS. Another message-passing MD code is LAMMPS[9][33] used for high-performance parallelized molecular dynamics calculations. The current version (version 17) is compatible with both AMBER and CHARMM.

4.2.4 Class II Force Fields

Class II force fields make extensive use of both anharmonic and cross-coupling terms to adequately represent the ab initio potential energy surface (PES). These include the original consistent force field (CFF) that developed out of CVFF (Section 4.2.2) and subsequent variations, the most recent being the COMPASS force field.

CFF. The consistent force field (CCF) [34] developed by Biosym[10] is a descendent of CVFF but differs in the specific types of potential terms. The nonbonded terms of CFF include a quartic bond-stretch term (Eq. (4.4)), a quartic angle-bending term (Eq. (4.8)), a three-term Fourier expansion term for torsion (Eq. (4.10)), and an out-of-plane torsion term (Eq. (4.12)). CFF includes several different versions (CFF91, CFF93 [35], CFF95) and the polymer consistent force field (PCFF). CFF93 has been parameterized for polycarbonates [36], aromatic polyesters [37], polysilanes [38], and poly(ethylene oxide) [39].

COMPASS. COMPASS is an example of a Class II force field parameterized by using an analytic representation of the ab initio (e.g., HF/6-31G*) potential energy surface. The functional form of the COMPASS force field is the same as CFF93 and includes an out-of-plane potential term (angle χ), a LJ 6–9 potential as well as nonharmonic terms for bond stretching and angle bending, a Fourier cosine series for torsion, and a number of cross-coupled terms for the bonded interactions. The form of the COMPASS force field described in detail by Sun [12] is

$$
\begin{aligned}
V(\mathbf{r}) = {} & \sum_b \left[k_2(b-b_0)^2 + k_3(b-b_0)^3 + k_4(b-b_0)^4\right] + \\
& \sum_\theta \left[k_2(\theta-\theta_0)^2 + k_3(\theta-\theta_0)^3 + k_4(\theta-\theta_0)^4\right] + \\
& \sum_\phi \left[k_1(1-\cos\phi) + k_2(1-\cos 2\phi) + k_3(1-\cos 3\phi)\right] + \\
& \sum_\chi k_2\chi^2 + \sum_{b,b'} k(b-b_0)\left(b'-b_0^{'}\right) + \sum_{b,\theta} k(b-b_0)(\theta-\theta_0) + \\
& \sum_{b,\phi} (b-b_0)\left[k_1(1-\cos\phi) + k_2(1-\cos 2\phi) + k_3(1-\cos 3\phi)\right] + \\
& \sum_{b,\theta} k\left(\theta'-\theta_0^{'}\right)(\theta-\theta_0) + \sum_{\theta,\theta,\phi} k(\theta-\theta_0)\left(\theta'-\theta_0^{'}\right)\cos\phi + \\
& \sum_{i,j} \frac{q_i q_j}{r_{ij}} + \sum_{i,j} \varepsilon_{ij}\left[2\left(\frac{r_{ij}^0}{r_{ij}}\right)^9 - 3\left(\frac{r_{ij}^0}{r_{ij}}\right)^6\right].
\end{aligned}
\tag{4.26}
$$

The partial charge for atom i in COMPASS is the sum of all charge bond increments, δ_{ij}, as

$$q_i = \sum_j \delta_{ij}. \tag{4.27}$$

The LJ parameters are obtained from the 6th order combination law (Eqs. (4.16) and (4.17)).

The parameterization of COMPASS for bonded potential terms includes a fitting of the total energies as well their first derivatives (gradients) and second derivatives (Hessians) to ab initio (HF/6–31G*) calculations of low-molecular-weight analogs. Examples of such analogs in the parameterization of COMPASS terms for polycarbonate are diphenyl carbonate, dimethyl carbonate, and 2,2-diphenylpropane [36]. Nonbonded parameters are obtained from ab initio calculations and by parameter fitting to crystal structures. Valence parameters and charges are further scaled to fit experimental data. Full descriptions of the parameterization procedures and a tabulation of force constants for COMPASS have been given in several sources [12,40].*

[8] http://www.cse.clrc.ac.uk/msi/software/DL_POLY/.

[9] *L*arge-scale *A*tomic/*M*olecular *M*assively *P*arallel *S*imulator; http://www.cs.sandia.gov/~sjplimp/lammps.html.

[10] Biosym was merged with Molecular Simulations into the current company Accelrys.

REFERENCES

1. N. L. Allinger, in *Physical Advances in Organic Chemistry*, edited by V. Gold (Academic Press, London, 1976), Vol. 13, pp. 1–82.
2. P. M. Morse, Phys. Rev. **34**, 57 (1929).
3. J. P. Ryckaert and A. Bellemans, Faraday Discuss. Chem. Soc. **66**, 95 (1978).
4. J. P. Ryckaert and A. Bellemans, Chem. Phys. Lett. **30**, 123 (1984).
5. M. Waldman and A. T. Hagler, J. Comput. Chem. **14**, 1077 (1993).
6. A. Mackerell Jr., J. Comput. Chem. **25**, 1584 (2004).
7. G. D. Smith and O. Borodin, in *Molecular Simulation Methods for Predicting Polymer Properties*, edited by V. Galiatsatos, (Wiley-Interscience, Hoboken, 2005), pp. 47–94.
8. T. A. Halgren and W. Damm, Curr. Opin. Struct. Biol. **11**, 236 (2001).
9. K. Chenoweth, S. Cheung, A. C. T. van Duin, *et al*. J. Am. Chem. Soc. **127**, 7192 (2005).
10. T. A. Halgren, J. Comput. Chem. **17**, 490 (1996).
11. S. L. Mayo, B. D. Olafson and W. A. Goddard III, J. Phys. Chem. **94**, 8897 (1990).
12. H. Sun, J. Phys. Chem. B **102**, 7338 (1998).
13. R.-J. Roe, in *Physical Properties of Polymers Handbook*, edited by J. E. Mark, AIP Press, Woodbury, NY, 1996.
14. A. K. Rappe, C. J. Casewit, K. S. Colwell *et al*., J. Am. Chem. Soc. **114**, 10024 (1992).
15. C. J. Casewit, K. S. Colwell and A. K. Rappe, J. Am. Chem. Soc. **114**, 10047 (1992).
16. C. J. Casewit, K. S. Colwell and A. K. Rappe, J. Am. Chem. Soc. **114**, 10035 (1992).
17. J. R. Fried and D. K. Goyal, J. Polym. Sci., Part B: Polym. Phys. **36**, 519 (1998).
18. J. W. Ponder and D. A. Case, Adv. Protein Chem. **66**, 27 (2003).
19. B. R. Brooks, R. E. Bruccoleri, B. D. Olafson, *et al*., J. Comput. Chem. **4**, 187 (1983).
20. C. J. Weiner, P. A. Kollman, D. A. Case, *et al*., J. Am. Chem. Soc. **106**, 765 (1984).
21. D. A. Perlman, D. A. Case, J. W. Caldwell, *et al*., Comput. Phys. Commun. **91**, 1 (1995).
22. J. Wang, R. M. Wolf, J. W. Caldwell, *et al*., J. Comput. Chem. **25**, 1157 (2004).
23. W. L. Jorgenson and J. Tirado-Reeves, J. Am. Chem. Soc. **110**, 1657 (1988).
24. W. L. Jorgensen, D. S. Maxwell and J. Tirado-Rives, J. Am. Chem. Soc. **118**, 11225 (1996).
25. N. A. McDonald and W. L. Jorgensen, J. Phys. Chem. B **102**, 8049 (1998).
26. M. Clark, R. D. Cramer III and N. van Opdenbosch, J. Comput. Chem. **10**, 982 (1989).
27. H. J. C. Berendsen, D. van der Spoel and R. van Drunen, Comput. Phys. Commun. **91**, 43 (1995).
28. J. Hermans, H. J. C. Berendsen, W. F. van Gunsteren, *et al*., Biopolymers **23**, 1513 (1984).
29. W. R. P. Scott, P. H. Hunenberger, I. G. Tironi, *et al*., J. Phys. Chem. A **103**, 3596 (1999).
30. E. Lindahl, B. Hess and D. van der Spoel, J. Mol. Model. **7**, 306 (2001).
31. P. Dauber-Osguthorpe, V. A. Roberts, D. J. Osguthorpe, *et al*., Proteins: Struct. Funct. Genet. **4**, 31 (1988).
32. K. Gundertofte, T. Liljefors, P.-O. Norrby, *et al*., J. Comput. Chem. **17**, 429 (1996).
33. S. Plimpton and B. Hendrickson, J. Comput. Chem. **17**, 326 (1996).
34. J. R. Maple, M.-J. Hwang, T. P. Stockfisch, *et al*., J. Comput. Chem. **15**, 162 (1994).
35. M. J. Hwang, T. P. Stockfisch and A. T. Hagler, J. Am. Chem. Soc. **116**, 2515 (1994).
36. H. Sun, S. J. Mumby, J. R. Maple, *et al*., J. Am. Chem. Soc. 2978 (1994).
37. H. Sun, J. Comput. Chem. **15**, 752 (1994).
38. H. Sun, Macromolecules **28**, 701 (1995).
39. D. Rigby, H. Sun and B. E. Eichinger, Polym. Int. **44**, 331 (1997).
40. H. Sun, P. Ren and J. R. Fried, Comput. Theor. Polym. Sci. **8**, 229 (1998).
41. C. L. Chen, C. L. Lee, H. L. Chen, *et al*., Macromolecules **27**, 7872 (1994).
42. J. Kendrick, E. Robson and M. Weave, J. Chem. Soc., Faraday Trans. **91**, 2609 (1995).
43. S. G. Charati, R. Vetrivel, M. G. Kulkarni, *et al*., Macromolecules **25**, 2215 (1992).
44. J. Cho, J. Blackwell, S. N. Chvalun, *et al*., J. Polym. Sci., Part B: Polym. Phys. **42**, 2576 (2004).
45. V. J. Vasudevan and J. E. McGrath, Macromolecules **29**, 637 (1996).
46. R. Dodge and W. L. Mattice, Macromolecules **24**, 2709 (1991).
47. C. F. Fan, T. Cagin, Z. M. Chen, *et al*., Macromolecules **27**, 2383 (1994).
48. S. Kim and J. Liu, Korean Polym. J. **9**, 129 (2001).
49. J. H. Shih and C. L. Chen, Macromolecules **28**, 4509 (1995).
50. I. Bahar, I. Zuniga, R. Dodge, *et al*., Macromolecules **24**, 2986 (1991).
51. T. Shi and W. Jiang, Macromol. Theory Simul. **10**, 232 (2001).
52. D. W. Noid, B. G. Sumpter and B. Wunderlich, Macromolecules **24**, 4148 (1991).
53. P. V. K. Pant and R. H. Boyd, Macromolecules **26**, 679 (1993).
54. G. Zifferer and A. Kornherr, J. Chem. Phys. **122**, 204906 (2005).
55. G. D. Smith, R. L. Jaffe and D. Y. Yoon, J. Phys. Chem. **97**, 12752 (1993).
56. K. Tasaki, Macromolecules **29**, 8922 (1996).
57. J. Ennari, J. Hamara and F. Sundholm, Polymer **38**, 3733 (1997).
58. L. J. A. Siqueira and M. C. C. Ribeiro, J. Chem. Phys. **122**, 194911 (2005).
59. S. U. Boyd and R. H. Boyd, Macromolecules **34**, 7219 (2001).
60. D. Pavel and R. Shanks, Polymer **46**, 6135 (2005).
61. J. W. Kang, K. Choi, W. H. Jo, *et al*., Polymer **39**, 7079 (1998).
62. Y. Kitano, I. Usami, Y. Obata, *et al*., Polymer **36**, (1995).
63. M. V. Brillhart, Y. Y. Cheng, P. Nagarkart, *et al*., Polymer **38**, 3059 (1997).
64. R. Zhang and W. L. Mattice, Macromolecules **26**, 6100 (1993).
65. U. Natarajan and W. L. Mattice, Macromol. Theory Simul. **6**, 949 (1997).
66. A. Shimazu, T. Miyazaki and K. Ikeda, J. Phys.: Condens. Matter **166**, 113 (2000).
67. T.-M. Wu, S. Chvalum, J. Blackwell, *et al*., Polymer **36**, 2123 (1995).
68. F. Alvarez, A. Alegria, J. Colmenero, *et al*., Macromolecules **33**, 8077 (2000).
69. K.-Y. Jung, H.-I. Kim and J. Liu, Korean Polym. J. **8**, 59 (2000).
70. A. Soldera, Polymer **43**, 4269 (2002).
71. T. M. Nicholson and G. R. Davies, Macromolecules **30**, 5501 (1997).
72. J. Liu and P. H. Geil, J. Polym. Sci., Part B: Polym. Phys. **35**, 1575 (1997).
73. S. Hill, I. Hamerton and B. J. Howlin, Polymer **43**, 4103 (2002).
74. K. C. Park, L. R. Dodd, K. Levon, *et al*., Macromolecules **29**, 7149 (1996).
75. M. Depner and B. L. Schurmann, Polymer **33**, 398 (1992).
76. R. Napolitano, B. Pirozzi and A. Salvione, Macromolecules **32**, 7682 (1999).
77. T. Launne, I. Neelov and F. Sundholm, Macromol. Theory Simul. **10**, 1371 (2001).
78. H. R. Allcock, M. E. Napierala, D. L. Olmeijer, *et al*., Macromolecules **32**, 732 (1999).
79. B. Kuhn, M. Ehrig and R. Ahlrichs, Macromolecules **29**, 4051 (1996).
80. P. Ahlstrom, O. Borodin, G. Wahnstrom, *et al*., J. Chem. Phys. **112**, 10669 (2000).
81. J. J. L. Cascales and T. F. Otero, J. Chem. Phys. **120**, 1951 (2004).
82. J. Pozuelo, F. Mendicuti and W. L. Mattice, Macromolecules **30**, 3685 (1997).
83. R. Khare, M. E. Paulaitus and S. R. Lustig, Macromolecules **26**, 7203 (1993).
84. R. Khare and M. E. Paulaitis, Macromolecules **28**, 4495 (1995).
85. M. Mondello, H.-J. Yang, H. Furuya, *et al*., Macromolecules **27**, 3566 (1994).
86. Y. Tamai and M. Fukuda, Polymer **44**, 3279 (2003).
87. H. Yang, Z.-s. Li, Z.-y. Lu, *et al*., Polymer **45**, 6753 (2004).
88. G. D. Smith, R. L. Jaffe and D. Y. Yoon, Macromolecules **26**, 298 (1993).
89. R. J. Meier and L. C. E. Struik, Polymer **39**, 31 (1998).
90. C. Saelee, T. M. Nicholson and G. R. Davies, Macromolecules **33**, 2258 (2000).
91. N. Karasawa and W. A. Goddard III, Macromolecules **25**, 7268 (1992).

CHAPTER 5

Theoretical Models and Simulations of Polymer Chains

Andrzej Kloczkowski* and Andrzej Kolinski†

*L .H. Baker Center for Bioinformatics and Biological Statistics, Iowa State University, Ames, IA 50011, USA**; *Faculty of Chemistry, Warsaw University, Pasteura 1, 02-093 Warsaw, Poland*†

5.1 INTRODUCTION

In the first part of this article the review of various theoretical models for polymer chains is given. The models of freely jointed chains, freely rotating chains (including wormlike chains), and chains with fixed bond angles and independent rotational potentials and with interdependent potentials, including rotational isomeric state approximation, are presented.

In the second part various theories of polymer networks are presented. The affine network model, phantom network, and theories of real networks are discussed. Scattering from polymer chains is also briefly presented.

The third part of this article covers computer simulations of polymer chains. Methods of simulation of chains on lattices are presented and the equivalence between lattice chains and off-lattice chain models is discussed. The simulation of excluded volume effect is examined. The polymer chain collapse from random coil to dense globular state, and simulations of dense polymer systems are discussed.

This article describes models for linear chains of homopolymers and for unimodal, unfilled polymer networks. Theoretical models for other systems, such as star, branched, and ring polymers, random and alternating copolymers, graft and block copolymers are discussed in the book by Mattice and Suter [1]. Block copolymers are discussed in Chap. 32 of this Handbook [2]. Theories of branched and ring polymers are presented in the book by Yamakawa [3]. Liquid–crystalline polymers are discussed in the book by Grosberg and Khokhlov [4], and liquid crystalline elastomers in the recent book of Warner and Terentjev [5]. Bimodal networks are discussed by Mark and Erman [6,7]. Molecular theories of filled polymer networks are presented by Kloczkowski, Sharaf and Mark [8] and recently by Sharaf and Mark [9].

This first part of this article deals only with treatment of ''bonded'' interactions of polymer chains, appropriate only for modeling chains under Θ-point conditions. Problems connected with effects of excluded volume are presented at the end of this chapter. The excluded volume effect for chains in good solvents are also presented in Chaps. IIB [10] and IIID [11] of this handbook and in books by Freed [12], de Gennes [13], des Cloizeaux and Jannink [14], and

Forsman [15]. More information about computer modeling of polymers is provided by Binder [16,17], Baumgartner [18], Kolinski and Skolnick [19], and most recently by Kotelyanskii and Therodorou [20].

5.2 THE FREELY JOINTED CHAIN

The freely jointed chain model (known also as random flight model) was proposed for polymers by Kuhn in 1936. The chain is assumed to consist of n bonds of equal length l, jointed in linear succession, where the directions (θ, ϕ) of bond vectors may assume all values $(0 \le \theta \le \pi; 0 \le \phi \le 2\pi)$ with equal probability (see Fig. 5.1).

This means that directions of neighboring bonds are completely uncorrelated. The freely jointed chain model corresponds to a chain with fixed bond lengths and with unconstrained, free to adjust valence angles and with free torsional rotations. The mean square end-to-end vector $\langle r^2\rangle_0$ in the unperturbed state (denoted by subscript 0) for the freely jointed chain is

$$\langle r^2\rangle_0 = \langle (\sum_{i=1}^{n} \mathbf{l}_j)\cdot(\sum_{j=1}^{n}\mathbf{l}_j)\rangle_0 = nl^2 \tag{5.1}$$

because

$$\langle \mathbf{l}_i \cdot \mathbf{l}_j\rangle_0 = 0 \quad \text{for } i \neq j. \tag{5.2}$$

It is convenient to compare real polymer chains with freely jointed chain by using the concept of the characteristic ratio defined as the ratio of the mean-square end-to-end vectors of a real chain and freely jointed chain with the same number of bonds

$$C_n = \frac{\langle r^2\rangle_0}{nl^2}. \tag{5.3}$$

The characteristic ratio is a measure of chain flexibility. Flexible chains have C_n close to unity, while semiflexible and rigid polymers have usually much larger values of C_n. The mean-square radius of gyration for freely jointed chain is:

$$\langle s^2\rangle_0 \equiv \frac{\sum\limits_{0 \le i < j \le n} \langle r_{ij}^2\rangle_0}{(n+1)^2} = \frac{(n+2)nl^2}{6\ (n+1).} \tag{5.4}$$

For longer chains (in the limit $n \to \infty$) we have

$$\frac{\langle s^2\rangle_0}{\langle r^2\rangle_0} = \frac{1}{6}. \tag{5.5}$$

The freely jointed chain model has an exact analytical solution for the distribution function of the end-to-end vector. The probability that the chain of n bonds has the end-to-end vector $\mathbf{r}$ is

$$P(\mathbf{r},n) = \int \mathrm{d}\mathbf{l}_1\mathrm{d}\mathbf{l}_2\ldots\mathrm{d}\mathbf{l}_n\delta[(\sum_{i=1}^{n}\mathbf{l}_i) - \mathbf{r}]\prod_{j=1}^{n}\exp\left(\frac{-\mathrm{u}(\mathbf{l}_j)}{kT}\right), \tag{5.6}$$

where T is the absolute temperature, k is the Boltzmann constant, $u(\mathbf{l}_j)$ is the potential energy of two segments connected by the j-th bond $\mathbf{l}_j$, and δ denotes Dirac delta function. For the freely jointed chain model we have

$$\exp\left(\frac{-\mathrm{u}(\mathbf{l}_j)}{kT}\right) = \frac{1}{4\pi l^2}\delta(|\mathbf{l}_j| - \ell). \tag{5.7}$$

By using the Fourier representation of the δ function we obtain

$$\begin{aligned} P(\mathbf{r},\ n) &= \frac{1}{8\pi^3}\int \mathrm{d}\mathbf{k}\,\mathrm{e}^{-\mathrm{i}\mathbf{k}\cdot\mathbf{r}}\left[\frac{\sin(kl)}{kl}\right]^n \\ &= \frac{1}{2\pi^2 r}\int_0^\infty \sin(kr)\left[\frac{\sin(kl)}{kl}\right]^n k\mathrm{d}k. \end{aligned} \tag{5.8}$$

The solution of Eq. (5.8) is

$$\begin{aligned} P(\mathbf{r},\ n) = \frac{1}{2^{n+1}\pi l^2 r(n-2)!}\sum_{i=0}^{i\le(n-r/l)/2} \\ (-1)^i\frac{n!}{i!(n-i)!}(n-2i-r/l)^{n-2}. \end{aligned} \tag{5.9}$$

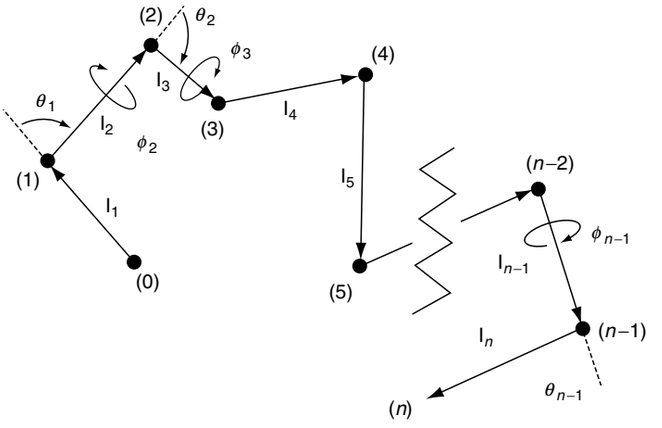

FIGURE 5.1. Polymer chain composed of n bonds. Angles θ are defined as complementary angles.

In the limit $n \to \infty$ the distribution function of the end-to-end vector for freely jointed chain asymptotically approaches a Gaussian function

$$P(\mathbf{r}, n) = \left(\frac{3}{2\pi n l^2}\right)^{3/2} \exp\left(\frac{-3r^2}{2nl^2}\right). \tag{5.10}$$

5.3 THE FREELY ROTATING CHAIN

The freely rotating chain model is a freely-jointed chain with fixed bond angles. It is assumed that all bond have equal length l and all bond angles are equal. The angle θ_i is defined as a supplementary angle of the skeletal bond angle at segment i as seen in Fig. 5.1, and therefore

$$\langle \mathbf{l}_{i+1} \cdot \mathbf{l}_j \rangle = l^2 \cos\theta. \tag{5.11}$$

Similarly for two bonds i and $i+k$ we have

$$\langle \mathbf{l}_{i+k} \cdot \mathbf{l}_i \rangle = l^2 (\cos\theta)^k. \tag{5.12}$$

This result follows from the fact that the projection of a given bond on the preceding bond is $\cos\theta$, while projections in two transverse directions averaged over free rotations are zero. This means that the projection of the $k+i$ bond on the $k+i-1$ bond is $\cos\theta$, the projection of this projection on the $k+i-2$ bond is $(\cos\theta)^2$, etc., which finally leads to the Eq. (5.12). The mean square end-to-end vector for freely rotating chain is

$$\begin{aligned}\langle r^2 \rangle &= \sum_{i=1}^{n} \langle \mathbf{l}_i \rangle^2 + 2 \sum_{i=1}^{n} \sum_{k=1}^{n-i} \langle \mathbf{l}_i \cdot \mathbf{l}_{j+k} \rangle \\ &= nl^2 \left[\frac{1+\cos\theta}{1-\cos\theta} - \frac{2\cos\theta[1-(\cos\theta)^n]}{n(1-\cos\theta)^2} \right].\end{aligned} \tag{5.13}$$

For infinitely long chains the second term in Eq. (5.13) may be neglected and the characteristic ratio defined by Eq. (5.3) becomes:

$$C_\infty = \frac{1+\cos\theta}{1-\cos\theta}. \tag{5.14}$$

The mean square radius of gyration (defined by Eq. (5.4)) for freely rotating chain is

$$\begin{aligned}\frac{\langle s^2 \rangle_0}{nl^2} &= \frac{(n+2)(1+\cos\theta)}{6(n+1)(1-\cos\theta)} - \frac{\cos\theta}{(n+1)(1-\cos\theta)^2} \\ &\quad + \frac{2(\cos\theta)^2}{(n+1)^2(1-\cos\theta)^3} \\ &\quad - \frac{2(\cos\theta)^3[1-(\cos\theta)^n]}{n(n+1)^2(1-\cos\theta)^4}.\end{aligned} \tag{5.15}$$

For very long chains the last three terms in Eq. (5.15) become negligible and $\langle s^2 \rangle_0 = \langle r^2 \rangle_0 / 6$.

5.3.1 Worm-like Chain Model

The projection of the end-to-end vector of a chain $\mathbf{r}$ on the direction of the first bond $\mathbf{l}_1/l$ for the freely rotating chain is

$$\begin{aligned}\left\langle \frac{\mathbf{r} \cdot \mathbf{l}_1}{l} \right\rangle &= \frac{1}{l} \sum_{i=1}^{n} \langle \mathbf{l}_1 \cdot \mathbf{l}_i \rangle = l \sum_{i=0}^{n-1} (\cos\theta)^i \\ &= l \frac{1-(\cos\theta)^n}{1-\cos\theta},\end{aligned} \tag{5.16}$$

where θ is the angle between bonds. In the limit $n \to \infty$ this converges to

$$\lim_{n\to\infty} \left\langle \frac{\mathbf{r} \cdot \mathbf{l}}{l} \right\rangle = \frac{1}{1-\cos\theta} \equiv a. \tag{5.17}$$

The quantity a is called the persistence length and is a measure of chain stiffness. The wormlike chain model (sometimes called the Porod-Kratky chain) is a special continuous curvature limit of the freely rotating chain, such that the bond length l goes to zero and the number of bonds n goes to infinity, but the contour length of the chain $L = nl$ and the persistance length a are kept constant. In this limit

$$\left\langle \frac{\mathbf{r} \cdot \mathbf{l}_1}{l} \right\rangle = a(1 - e^{-L/a}) \tag{5.18}$$

and

$$\frac{\langle r^2 \rangle_0}{L} = 2a\left[1 - \frac{a}{L}(1 - e^{-L/a})\right]. \tag{5.19}$$

When the chain length L is much larger than the persistance length a, the effect of chain stiffness becomes negligible. In the limit $L \to \infty$ we have $\langle r^2 \rangle_0 / L \to 2a$ and the wormlike chain reduces to a freely-jointed chain.

5.4 CHAINS WITH FIXED BOND ANGLES AND INDEPENDENT POTENTIALS FOR INTERNAL BOND ROTATION

The more realistic model than freely rotating chain is a chain with fixed bond angles and hindered internal rotations. For simplicity it is assumed that the total configurational energy of the chain is a sum of configurational energies of chain bonds, and the energy of a given bond is independent on the configurational states of other bonds in the chain including the neighboring bonds. We should note that this is an approximation and for real polymer chains because of the steric interactions the energy of a given bond depends on the energy of its neighbors.

We define a local Cartesian coordinate system for each of the bonds. We assume that the axis x_i is directed along the bond i, and the y_i axis lies in the plane formed by bonds i and $i-1$, while the z_i axis is directed to make the coordinate system right-handed. The components of the $(i+1)$th bond $\mathbf{l}_{i+1}$ can be expressed in the coordinate system of the preceding bond i

$$\mathbf{l}'_{i+1} = \mathbf{T}_i \mathbf{l}_{i+1}, \tag{5.20}$$

where $\mathbf{T}_i$ is the orthogonal matrix of the rotational transformation

$$\mathbf{T}_i = \begin{bmatrix} \cos\theta_i & \sin\theta_i & 0 \\ \sin\theta_i\cos\phi_i & -\cos\theta_i\cos\phi_i & \sin\phi_i \\ \sin\theta_i\sin\phi_i & -\cos\theta_i\sin\phi_i & -\cos\phi_i \end{bmatrix} \quad (5.21)$$

Here θ_i is the supplementary bond angle (see Fig. 5.1) and ϕ_i is a dihedral angle between two planes defined by two pairs of bonds: bonds $i-1$ and i, and i and $i+1$.

The scalar product of two bonds $\mathbf{l}_i \cdot \mathbf{l}_j$ written in the matrix notation is $\mathbf{l}_i^{\mathrm{T}}\mathbf{l}_j$ where $\mathbf{l}_j$ is the column vector and $\mathbf{l}_i^{\mathrm{T}}$ is the transpose of $\mathbf{l}_i$ (i.e., the row vector)

$$\mathbf{l}_j = l_j \begin{bmatrix} 1 \\ 0 \\ 0 \end{bmatrix} \quad \mathbf{l}_i^{\mathrm{T}} = \mathbf{l}_j[100], \quad (5.22)$$

where l_i and l_j are lenghts of bonds i and j ($l_i = l_j = l$ in our model but for polymers with different types of bonds in the backbone they may differ). Transforming successively over the intervening bonds the vector representation of the bond j to the coordinate system of bond i ($j > i$) we have

$$\langle \mathbf{l}_i \cdot \mathbf{l}_j \rangle = \langle \mathbf{l}_i^{\mathrm{T}} \mathbf{T}_i \mathbf{T}_{i+1} \cdots \mathbf{T}_{j-1} \mathbf{l}_j \rangle = l_i l_j \langle \mathbf{T}_i \mathbf{T}_{i+1} \cdots \mathbf{T}_j \rangle_{11}. \quad (5.23)$$

Here $\langle \mathbf{T}_i \mathbf{T}_{i+1} \ldots \mathbf{T}_{j-1} \rangle_{11}$ denotes configurational average of the (1–1) element of the matrix product $\mathbf{T}_i \mathbf{T}_{i+1} \ldots \mathbf{T}_{j-1}$. The configurational average of the product of rotational transformation matrices is generally given by

$$\langle \mathbf{T}_i \mathbf{T}_{i+1} \cdots \mathbf{T}_{j-1} \rangle = \frac{\int \cdots \int (\mathbf{T}_i \mathbf{T}_{i+1} \cdots \mathbf{T}_{j-1}) \exp\left[\frac{-E(\mathbf{l}_1, \mathbf{l}_2, \cdots, \mathbf{l}_n)}{kT}\right] \mathrm{d}\mathbf{l}_1 \mathrm{d}\mathbf{l}_2 \cdots \mathrm{d}\mathbf{l}_n}{\int \cdots \int \exp\left[\frac{-E(\mathbf{l}_1, \mathbf{l}_2, \cdots, \mathbf{l}_n)}{kT}\right] \mathrm{d}\mathbf{l}_1 \mathrm{d}\mathbf{l}_2 \cdots \mathrm{d}\mathbf{l}_n}, \quad (5.24)$$

where k is the Boltzmann constant, T is the absolute temperature and $E(\mathbf{l}_1, \mathbf{l}_2, \ldots, \mathbf{l}_n)$ is the conformational energy of the whole chain of n bonds. For a chain with fixed bond lenghts this energy depends only on the orientations of bonds described by bond angles θ_i and rotational angles ϕ_i, where $1 \le i \le n-1$, since the orientation of the last n-th bond is fully determined by the orientation of preceding bonds. For a chain with fixed bond angles the conformational energy is only a function of rotational angles ϕ_i, with $2 \le i \le n-1$, because ϕ_1 is undefined. For chains with independent potentials for internal bond rotation the conformational energy of the chain is a sum of bond energies $E_i(\phi_i)$

$$E(\phi_2, \phi_3, \cdots, \phi_{n-1}) = \sum_{i=2}^{n-1} E_i(\phi_i) \quad (5.25)$$

and

$$\langle \mathbf{T}_i \mathbf{T}_{i+1} \cdots \mathbf{T}_{j-1} \rangle = \prod_{k=1}^{j-1} \langle \mathbf{T}_k \rangle, \quad (5.26)$$

where for symmetric rotational potentials with $u_i(\phi_i) = u_i(-\phi_i)$ we have

$$\langle \mathbf{T}_k \rangle = \begin{bmatrix} \cos\theta_k & \sin\theta_k & 0 \\ \sin\theta_k\langle\cos\phi_k\rangle & -\cos\theta_k\langle\cos\phi_k\rangle & 0 \\ 0 & 0 & -\langle\cos\phi_k\rangle \end{bmatrix}. \quad (5.27)$$

Here $\langle \cos\phi_k \rangle$ is

$$\langle \cos\phi_k \rangle = \frac{\int_0^{2\pi} \cos\phi_k \exp\left[\frac{-E_k(\phi_k)}{kT}\right] \mathrm{d}\phi_k}{\int_0^{2\pi} \exp\left[\frac{-E_k(\phi_k)}{kT}\right] \mathrm{d}\phi_k}. \quad (5.28)$$

Using Eqs. (5.23) and (5.27) we may calculate the mean-square end-to-end vector for fixed bond angles and independent potentials for internal bond rotation

$$\langle r^2 \rangle_0 = nl^2 + 2l^2 \left[\sum_{i=1}^{n} \sum_{k=1}^{n-i} \langle \mathbf{T} \rangle^k \right]_{11} = nl^2 \left[\frac{\mathbf{E} + \langle \mathbf{T} \rangle}{\mathbf{E} - \langle \mathbf{T} \rangle} - 2\langle \mathbf{T} \rangle \frac{(\mathbf{E} + \langle \mathbf{T} \rangle^n)}{n(\mathbf{E} - \langle \mathbf{T} \rangle)^2} \right]_{11}, \quad (5.29)$$

where $\mathbf{E}$ is the unit matrix, and the subscript 11 denotes the (1–1) element of the matrix in square parenthesis. Equation (5.29) resembles Eq. (5.13) for freely rotating chain with $\cos\theta$ replaced by $<\mathbf{T}>$. Similarly to Eq. (5.15) the mean square radius of gyration is

$$\frac{\langle s^2 \rangle_0}{nl^2} = \left[\frac{(n+2)(\mathbf{E} + \langle \mathbf{T} \rangle)}{6(n+1)(\mathbf{E} - \langle \mathbf{T} \rangle)} - \frac{\langle \mathbf{T} \rangle}{(n+1)(\mathbf{E} - \langle \mathbf{T} \rangle)^2} + \frac{2\langle \mathbf{T} \rangle^2}{(n+1)^2(1 - \langle \mathbf{T} \rangle)^3} - \frac{2\langle \mathbf{T} \rangle^3 [1 - \langle \mathbf{T} \rangle^n]}{n(n+1)^2(1 - \langle \mathbf{T} \rangle)^4} \right]_{11}. \quad (5.30)$$

The general solution of eqs. (5.27) and (5.28) is possible by diagonaliziation of the matrix $<\mathbf{T}>$ defined by Eq. (5.27). The eigenvalues of $<\mathbf{T}>$ are

$$\lambda_{1,2} = \frac{1}{2}\left[\cos\theta(1 - \langle\cos\phi\rangle) \pm \sqrt{\cos^2\theta(1 - \langle\cos\phi\rangle)^2 + 4\langle\cos\phi\rangle} \right]. \quad \lambda_3 = -\langle\cos\phi\rangle \quad (5.31)$$

For example, the expression for $\langle r^2 \rangle_0$ in terms of eigenvalues of $<\mathbf{T}>$ is

$$\frac{\langle r^2 \rangle_0}{nl^2} = \frac{(1 + \cos\theta)(1 + \langle\cos\phi\rangle)}{(1 - \cos\theta)(1 - \langle\cos\phi\rangle)} - \frac{2\lambda_1(\cos\theta\langle\cos\phi\rangle + \lambda_1)(1 - \lambda_1^n)}{n(\lambda_1 - \lambda_2)(1 - \lambda_1)^2} + \frac{2\lambda_2(\cos\theta\langle\cos\phi\rangle + \lambda_2)(1 - \lambda_2^n)}{n(\lambda_1 - \lambda_2)(1 - \lambda_2)^2}. \quad (5.32)$$

For very long chains only first terms in Eqs. (5.29) and (5.30) are important and we have

$$C_\infty = \lim_{n\to\infty} \frac{\langle r^2 \rangle_0}{nl^2} = \left[\frac{\mathbf{E} + \langle \mathbf{T} \rangle}{\mathbf{E} - \langle \mathbf{T} \rangle} \right]_{11} = \frac{(1 + \cos\theta)(1 + \langle\cos\phi\rangle)}{(1 - \cos\theta)(1 - \langle\cos\phi\rangle)} \quad (5.33)$$

and

$$\frac{\langle s^2\rangle_0}{nl^2} = \frac{n+2}{6(n+1)} = \left[\frac{\mathbf{E}+\langle\mathbf{T}\rangle}{\mathbf{E}-\langle\mathbf{T}\rangle}\right]_{11} = \frac{(n+2)(1+\cos\theta)(1+\langle\cos\phi\rangle)}{6(n+1)(1-\cos\theta)(1-\langle\cos\phi\rangle)}. \tag{5.34}$$

5.5 CHAINS WITH INTERDEPENDENT ROTATIONAL POTENTIALS. THE ROTATIONAL ISOMERIC STATE APPROXIMATION

In real polymer chains the rotational potentials depend on the steric interactions between pendant groups of neighboring bonds, and are generally not mutually independent. In the simplest case of hydrocarbons the bond rotational potential has three minima as shown in Fig. 5.2. The global minimum at the torsional angle 0° corresponds to the *trans* two other minima with the same energies at torsional angle around $+120^\circ$ and -120° correspond to the *gauche*$^+$ and the *gauche*$^-$ states (g^+ and g^-). The energy difference between the *trans* the *gauche*$^\pm$ states for *n*-alkanes is about 500 cal/(mole). We may use the rotational isomeric state approximation that each bond in the chain occur in one of these rotational states. This assumption enables us to replace all integrals over rotational angles in the partition function and statistical averages by summations over bonds rotational states. Additionally steric interactions between pendant groups of neighboring bonds become important, e.g., the sequence $g^\pm g^\pm$ becomes energetically very unfavorable.

We may neglect the longer range interactions and assume that the configurational energy is a sum of energies of nearest-neighbor pairs

$$E(\phi_2,\phi_3,\cdots,\phi_{n-1}) = \sum_{i=2}^{n-1} E_i(\phi_{i-1},\phi_i). \tag{5.35}$$

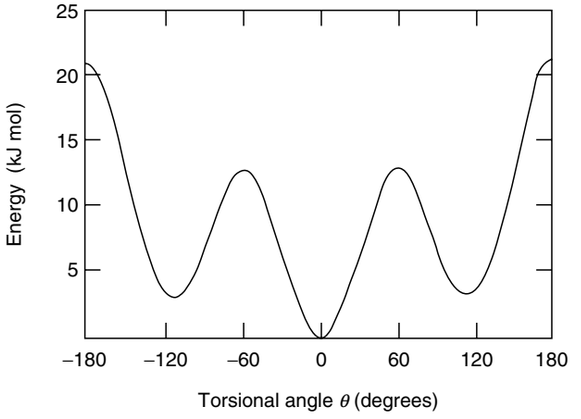

FIGURE. 5.2. The dependence of the conformational energy on the torsional angle in *n*-alkanes.

The configurational partition function becomes

$$Z = \int\cdots\int \exp\left[-\frac{1}{kT}E(\phi_2,\cdots,\phi_{n-1})\right] d\phi_2\cdots d\phi_{n-1} = \sum_{\{\phi\}}\prod_{i=2}^{n-1}\exp\left[-\frac{1}{kT}E_i(\phi_{i-1},\phi_i)\right], \tag{5.36}$$

where $\{\phi\}$ denotes the set of all available states (t,g^+,g^-) for all bonds in the chain. We define the statistical weight corresponding to bond i being in the η state while bond $i-1$ being in the ζ state (where η and ζ are sampled from the t,g^+,g^- set)

$$u_{\zeta\eta,i} = \mathbf{exp}\left(\frac{-E_{\zeta\eta,i}}{kT}\right) \tag{5.37}$$

and the statistical weight matrix

$$\mathbf{U}_i = \begin{bmatrix} u_{tt,i} & u_{tg^+,i} & u_{tg^-,i} \\ u_{g^+t,i} & u_{g^+g^+,i} & u_{g^+g^-,i} \\ u_{g^-t,i} & u_{g^-g^+,i} & u_{g^-g^-,i} \end{bmatrix}. \tag{5.38}$$

It is convenient to express the energy of a given single bond relative to the energy of the *trans* state. The energy of a pair of bonds $E_{\eta\zeta,i}$ is defined relative to the state where the bond i is in the *trans* state, and all subsequent bonds $j > i$ are also in the *trans* states. From this definition follows $E_{\eta t} = 0$ for $\zeta = t,g^+,g^-$. Additionally $E_{tg^+} = E_{tg^-} = E_{g^+g^+} = E_{g^-g^-}$ ($\approx$ 500 cal/mol for *n*-alkanes), and $\mathrm{E_{g^+g^-}} = \mathrm{E_{g^-g^+}}$ ($\approx$ 3,000 cal/mole for *n*-alkanes). This means that the statistical weight matrix may be written as

$$\mathbf{U} = \begin{bmatrix} 1 & \sigma & \sigma \\ 1 & \sigma\psi & \sigma\omega \\ 1 & \sigma\omega & \sigma\psi \end{bmatrix}, \tag{5.39}$$

where $\sigma\psi$ and $\sigma\omega$ denote $u_{g^+g^+}$ and $u_{g^+g^-}$, respectively.

By using the statistical weight matrices we may express the configuration partition function as

$$\mathbf{Z} = \sum_{\{\phi\}}\prod_{i=2}^{n-1} u_{\eta\zeta,i} = \mathbf{J}^*\left[\prod_{i=2}^{n-1}\mathbf{U_i}\right]\mathbf{J}, \tag{5.40}$$

where $\mathbf{J}^*$ and $\mathbf{J}$ are row and column vectors, respectively

$$\mathbf{J}^* = [\,1 \quad 0 \quad 0\,] \quad \mathbf{J} = \begin{bmatrix} 1 \\ 1 \\ 1 \end{bmatrix}. \tag{5.41}$$

For very long chains (in the limit $n \to \infty$) the partition function is determined by the largest eigenvalue λ_1 of the statistical weight matrix $\mathbf{U}$

$$Z \cong \lambda_1^{n-2}. \tag{5.42}$$

The largest eigenvalue of the matrix $\mathbf{U}$ defined by Eq. (5.39) is

$$\lambda_1 = \frac{1}{2}\left[1+\sigma(\psi+\omega)+\sqrt{[1-\sigma(\psi+\omega)]^2+8\sigma}\right]. \tag{5.43}$$

The probability that bonds $i-1$ and i occur in states η and ζ, respectively is

$$p_{\eta\zeta,i} = \frac{1}{Z}\mathbf{J}^*\left[\prod_{k=2}^{i-1}\mathbf{U}_k\right]\frac{\partial \mathbf{U}_i}{\partial \ln u_{\eta\zeta,i}}\left[\prod_{k=i+1}^{n-1}\mathbf{U}_k\right]\mathbf{J} \cong \frac{\partial \ln \lambda_1}{\partial \ln u_{\eta\zeta}}. \tag{5.44}$$

The probability that bond i is in the state ζ, irrespective of the state of bond $i-1$ is

$$p_{\zeta,i} = \sum_{n=t,g^+,g^-} p_{\eta\zeta,i} \cong \sum_{\eta=t,g^+,g^-}\frac{\partial \ln \lambda_1}{\partial \ln u_{\eta\zeta}}. \tag{5.45}$$

The conditional probability that bond i is in ζ state, given that bond $i-1$ is in state η is

$$q_{\eta\zeta,i} = \frac{p_{\eta\zeta,i}}{p_{\eta,i-1}}. \tag{5.46}$$

In order to calculate the mean square end-to-end vector or a radius of gyration we have to calculate averages $\langle \mathbf{T}_i\mathbf{T}_{i+1}\ldots\mathbf{T}_{j-1}\rangle$ (Eq. (5.24)). For bonds with independent rotational potentials this average is a product of averages $\langle \mathbf{T}\rangle$ for single bonds. For chains with interactions between neighboring bonds we define for each bond i the supermatrix $\| \mathbf{T}_i \|$ of the order 9×9

$$\| \mathbf{T}_i \| = \begin{bmatrix} \mathbf{T}(\phi_1) & & \\ & \mathbf{T}(\phi_2) & \\ & & \mathbf{T}(\phi_3) \end{bmatrix}_i, \tag{5.47}$$

where $\mathbf{T}$ is rotation matrix given by Eq. (5.21), and the $\phi_1 = 0^\circ, \phi_2 = 120^\circ, \phi_3 = -120^\circ$, are the torsional angles corresponding to the *trans*, *gauche*$^+$ and *gauche*$^-$ states.

We define also a direct product $\mathbf{U}_i \otimes \mathbf{E}_3$ of the statistical weight matrix $\mathbf{U}_i$ (defined by Eq. (5.38)) and the unit matrix of order three $\mathbf{E}_3$.

$$\mathbf{U}_i \otimes \mathbf{E}_3 = \begin{bmatrix} u_{tt}\mathbf{E}_3 & u_{tg^+}\mathbf{E}_3 & u_{tg^-}\mathbf{E}_3 \\ u_{g^+t}\mathbf{E}_3 & u_{g^+g^+}\mathbf{E}_3 & u_{g^+g^-}\mathbf{E}_3 \\ u_{g^-t}\mathbf{E}_3 & u_{g^-g^+}\mathbf{E}_3 & u_{g^-g}\mathbf{E}_3 \end{bmatrix}. \tag{5.48}$$

The statistical average of the product of rotation matrices may then be written as

$$\langle \mathbf{T}_i\mathbf{T}_{i+1}\ldots\mathbf{T}_{j-1}\rangle = \langle \mathbf{T}_i^{(j-i)}\rangle = \frac{1}{Z}\left[(\mathbf{J}^*\mathbf{U}_2^{(i-2)})\otimes\mathbf{E}_3\right]\times [(\mathbf{U}\otimes\mathbf{E}_3)\parallel \mathbf{T} \parallel]_i^{(j-i)}\left[(\mathbf{U}_j^{(n-j)}\mathbf{J})\otimes\mathbf{E}_3\right] \tag{5.49}$$

Then the mean-square end-to-end vector and the mean square radius of gyration are

$$\langle r^2\rangle_0 = nl^2 + 2\sum_{i=1}^{n-1}\sum_{j=i+1}^{n}\mathbf{l}_i^T\langle \mathbf{T}_i^{(j-i)}\rangle\mathbf{l}_j \tag{5.50}$$

and

$$\langle s^2\rangle_0 = \frac{1}{(n+1)^2}\sum_{0\le h\le k\le n}\sum_{i=h+1}^{k}\sum_{j=h+1}^{k}\mathbf{l}_i^T\langle \mathbf{T}^{(j-i)}\rangle\mathbf{l}_j \tag{5.51}$$

with $\langle \mathbf{T}_i^{(j-i)}\rangle$ given by Eq. (5.49). Both $\langle r^2\rangle_0$ and $\langle s^2\rangle_0$ may be written in a more compact form in terms of proper supermatrices. The details are given in Flory's monograph [21]. Additional information is given in the Handbook chapter by Honeycutt [22].

5.6 THEORIES OF POLYMER NETWORKS

5.6.1 The Affine Network

The theory of affine networks was developed by Kuhn and improved by Treloar, and is based on the assumption that the network consists of ν freely-jointed Gaussian chains and the mean-square end-to-end vector of network chains in the undeformed network is the same as of chains in the uncross-linked state. This assumption is supported by experimental data. It is also assumed that there is no change in volume on deformation and the junctions displace affinily with macroscopic deformation. The intermolecular interactions in the model are neglected, i.e., the system is similar to the ideal gas.

The elastic free energy of a chain is related to the distribution function of the end-to-end vector $P(\mathbf{r})$

$$A_{\text{el}} = c(T) - kT\ln P(\mathbf{r}) = A^*(T) + \frac{3}{2}kT\frac{\langle r^2\rangle}{\langle r^2\rangle_0} \tag{5.52}$$

for the Gaussian distribution given by Eq. (5.10). Here $c(T)$ and $A^*(T)$ are constants dependent only on the temperature T, k is a Boltzmann constant, and $\langle r^2\rangle_0$ is the average of the mean-square end-to-end vector in the undeformed state.

The elastic free energy of the network ΔA_{el} relative to the undeformed state is a sum of free energies of individual chains

$$\Delta A_{\text{el}} = \frac{3kT}{2\langle r^2\rangle_0}\sum_{\nu}(r^2 - \langle r^2\rangle_0) = \frac{3}{2}\nu kT\left(\frac{\langle r^2\rangle}{\langle r^2\rangle_0} - 1\right) \tag{5.53}$$

Here $\langle r^2\rangle$ is the end-to-end vector in the deformed state averaged over the ensemble of chains

$$\langle r^2\rangle = \langle x^2\rangle + \langle y^2\rangle + \langle z^2\rangle. \tag{5.54}$$

In the affine model of the network it is assumed all junction points are imbedded in the network, and each Cartesian component of the chain end-to-end vector transforms linearly with macroscopic deformation

$$x = \lambda_x x_0, \quad y = \lambda_y y_0, \quad z = \lambda_z z_0 \tag{5.55}$$

$$\langle x^2\rangle = \lambda_x^2\langle r^2\rangle_0, \quad \langle y^2\rangle = \lambda_y^2\langle y^2\rangle_0, \quad \langle z^2\rangle = \lambda_z^2\langle z^2\rangle_0 \tag{5.56}$$

and therefore

$$\Delta A_{\text{el}} = \frac{1}{2}\nu kT(\lambda_x^2 + \lambda_y^2 + \lambda_z^2 - 3). \tag{5.57}$$

Here, λ_x, λ_y, and λ_z are the components of the deformation tensor $\boldsymbol{\lambda}$, defined as the ratios of the final length of the

sample L_t to the initial length $L_{t,0}$ in $t = x$, y, and z direction, respectively. (The more rigorous statistical mechanical analysis by Flory [23] has shown that Eq. (5.57) should contain additional logarithmic term $-\mu kT \ln(V/V_0)$, where μ is the number of junctions, V is the volume of the network, and V_0 is volume of the network at the state of formation).

The force f under uniaxial tension in direction z is obtained from the thermodynamic expression:

$$f = \left(\frac{\partial \Delta A_{\mathrm{el}}}{\partial L}\right)_{T,V} = L_0^{-1}\left(\frac{\partial \Delta A_{\mathrm{el}}}{\partial \lambda}\right)_{T,V}, \tag{5.58}$$

where $\lambda = \lambda_z = L_z/L_{z,0}$. Because the volume of the sample is constant during deformation the x and y components of the deformation are $\lambda_x = \lambda_y = \lambda^{-1/2}$. Performing the differentiation in Eq. (5.58) leads to the elastic equation of state

$$f = \left(\frac{\nu kT}{L_0}\right)(\lambda - 1/\lambda^2). \tag{5.59}$$

5.6.2 The Phantom Network Theory

The theory of phantom network was formulated by James and Guth [24] in the forties. They assumed that chains are Gaussian with the distribution $P(\mathbf{r})$ of the end-to-end vector

$$P(\mathbf{r}) = \left(\frac{\gamma}{\pi}\right)^{3/2} \exp(-\gamma r^2), \tag{5.60}$$

where

$$\gamma = \frac{3}{2\langle r^2\rangle_0} \tag{5.61}$$

and interact only at junction points. This means that chains may pass freely through one another, i.e., are ''phantom'', the excluded volume effects and chain entanglements are neglected in the theory. They assumed also that all junctions at the surface of the network are fixed and deform affinely with macroscopic strain, while all junctions and chains inside the bulk of the network fluctuate around their mean positions. The idea of the phantom network is very similar to the concept of the ideal gas. The theory based on these simple assumptions leads to significant improvements in the understanding of the properties of networks, such as microscopic fluctuations and neutron scattering behavior.

The configurational partition function Z_N of the phantom network is the product of the configurational partition functions of its individual chains. junctions i and j:

$$\begin{aligned} Z_N &= C\prod_{i<j} \exp(-3r_{ij}^2/2\langle r_{ij}^2\rangle_0) \\ &= C\prod_{i<j} \exp\left(-\frac{1}{2}\sum_i \sum_j \gamma_{ij}^*|\mathbf{R}_i - \mathbf{R}_j|^2\right). \end{aligned} \tag{5.62}$$

Here, $\mathbf{R}_i$ and $\mathbf{R}_j$ are positions of junctions i and j, $\gamma_{\mathrm{ij}}^* = 3/2\langle r_{\mathrm{ij}}^2\rangle_0$ if junctions i and j are connected by a chain, and zero otherwise, and C is a normalization constant. The position vectors $\mathbf{R}_i$ with i ranging from 1 to μ, where μ is a number of junctions, may be arranged in column form, represented as $\{\mathbf{R}\}$. Equation (5.62) may then be written

$$Z_N = C\exp(-\{\mathbf{R}\}^T\mathbf{\Gamma}\{\mathbf{R}\}), \tag{5.63}$$

where the superscript T denotes the transpose. The symmetric matrix $\mathbf{\Gamma}$ known as the Kirchhoff valency-adjacency matrix in the graph theory describes the connectivity of the network and its elements γ_{ij} are

$$\mathbf{\Gamma} = \begin{cases} \gamma_{ij} = -\gamma_{ij}^*, & i \neq j \\ \gamma_{ii} = \sum\limits_j \gamma_{ij}^* = \sum\limits_j \gamma_{ij}^*. \end{cases} \tag{5.64}$$

James and Guth assumed that all μ junctions in the network may be divided into two sets of junctions: (i) μ_σ fixed junctions at the bounding surface of the polymer and (ii) μ_τ free junctions fluctuating about their mean positions $\{\bar{\mathbf{R}}_\tau\}$ inside the polymer. The partition function of the network due to fluctuating junctions is

$$Z_N = C\exp(-\{\Delta\mathbf{R}_\tau\}^T\mathbf{\Gamma}_\tau\{\Delta\mathbf{R}_\tau\}), \tag{5.65}$$

where $\{\Delta\mathbf{R}_\tau\}$ denotes fluctuations of free junctions

$$\{\Delta\mathbf{R}_\tau\} = \{\mathbf{R}_\tau\} - \{\overline{\mathbf{R}}_\tau\}. \tag{5.66}$$

The product of the fluctuations of two junctions i and j averaged over the network may be obtained from Eq. (5.65) as

$$\begin{aligned} \langle \Delta\mathbf{R}_i \cdot \Delta\mathbf{R}_j\rangle &= \frac{\int \Delta\mathbf{R}_i \cdot \Delta\mathbf{R}_j \exp[-\{\Delta\mathbf{R}_\tau\}^{\mathrm{T}}\mathbf{\Gamma}_\tau\{\Delta\mathbf{R}_\tau\}]\mathrm{d}\{\Delta\mathbf{R}_\tau\}}{\int \exp[-\{\Delta\mathbf{R}_\tau\}^{\mathrm{T}}\mathbf{\Gamma}_\tau\{\Delta\mathbf{R}_\tau\}]\mathrm{d}\{\Delta\mathbf{R}_\tau\}} \\ &= -\frac{\partial \ln Z_\tau}{\partial \gamma_{ij}}, \end{aligned} \tag{5.67}$$

where $\mathrm{d}\{\Delta\mathbf{R}_\tau\} \equiv \mathrm{d}\Delta\mathbf{R}_{1\tau}\mathrm{d}\Delta\mathbf{R}_{2\tau}\ldots\mathrm{d}\Delta\mathbf{R}_{\mu\tau}$ and

$$Z_\tau = \int \exp[-\{\Delta\mathbf{R}_\tau\}^{\mathrm{T}}\mathbf{\Gamma}_\tau\{\Delta\mathbf{R}_\tau]\mathrm{d}\{\Delta\mathbf{R}_\tau\} = \left(\frac{\pi^{\mu_\tau}}{\det\mathbf{\Gamma}_\tau}\right)^{3/2}. \tag{5.68}$$

This leads to the expression

$$\langle \Delta\mathbf{R}_i \bullet \Delta\mathbf{R}_j\rangle = \frac{3}{2}\frac{\partial}{\partial \gamma_{ij}} \ln|\det\mathbf{\Gamma}_\tau| = \frac{3}{2}(\mathbf{\Gamma}_\tau^{-1})_{ij}, \tag{5.69}$$

where $(\mathbf{\Gamma}_\tau^{-1})_{ij}$ denotes the $(i-j)$-th element of the inverse matrix $\mathbf{\Gamma}_\tau^{-1}$. Fluctuations of junctions from their mean positions in a phantom network depend on the network's functionality ϕ and are independent of macroscopic deformation.

For example for the infinitely large network with the symmetrical tree-like topology (such as shown in Fig. 5.3) the mean-square fluctuations of junctions $\langle(\Delta\mathrm{R})^2\rangle$ and

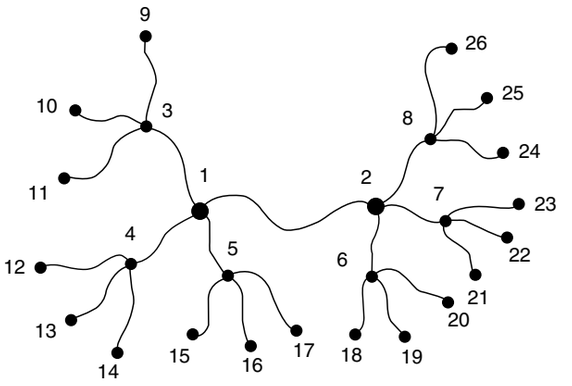

FIGURE 5.3. First three tiers of a unimodal, symmetrically grown, tetrafunctional network ($\phi = 4$) with tree-like topology.

correlations between fluctuations of two junctions i and j $\langle \Delta\mathbf{R}_i \cdot \Delta\mathbf{R}_j \rangle$ separated by m other junctions are:

$$\begin{bmatrix} \langle (\Delta \mathrm{R}_i)^2 \rangle & \langle \Delta\mathbf{R}_i \cdot \mathbf{R}_j \rangle \\ \langle \Delta\mathbf{R}_j \cdot \Delta\mathbf{R}_i \rangle & \langle (\Delta \mathrm{R}_j)^2 \rangle \end{bmatrix} = \frac{3}{2} \begin{bmatrix} (\Gamma_\tau^{-1})_{ii} & (\Gamma_\tau^{-1})_{ij} \\ (\Gamma_\tau^{-1})_{ji} & (\Gamma_\tau^{-1})_{jj} \end{bmatrix}$$

$$= \frac{3}{2\gamma} \begin{bmatrix} \frac{\phi-1}{\phi(\phi-2)} & \frac{1}{\phi(\phi-2)(\phi-1)^m} \\ \frac{1}{\phi(\phi-2)(\phi-1)^m} & \frac{\phi-1}{\phi(\phi-2)} \end{bmatrix}. \tag{5.70}$$

The mean-square fluctuations of the distance $r_{ij} = |\mathbf{R}_i - \mathbf{R}_j|$ between junctions i and j are

$$\begin{aligned} \langle (\Delta r_{ij})^2 \rangle &= \langle (\Delta\mathbf{R}_i - \Delta\mathbf{R}_i)^2 \rangle \\ &= \frac{3}{2}[(\Gamma_\tau^{-1})_{ii} + (\Gamma_\tau^{-1})_{jj} - 2(\Gamma_\tau^{-1})_{ij}] \\ &= \frac{2[(\phi-1)^{m+1} - 1]}{\phi(\phi-2)(\phi-1)^m} \langle r^2 \rangle 0. \end{aligned} \tag{5.71}$$

For a special case of mean-square fluctuations of the end-to-end vector ($m = 0$) we have

$$\langle (\Delta r)^2 \rangle = \frac{2}{\phi} \langle r^2 \rangle_0. \tag{5.72}$$

Equations (5.70) and (5.71) may be easily generalized for fluctuations of points along the chains in the network, since each point along the chain may be considered as bi-functional junction. As a consequence the valence-adjacency matrix in this generalized case contains additional elements describing the connectivity of bi-functional junctions. More details is provided in the review article by Kloczkowski, Mark, and Erman [25].

The vector $\mathbf{r}_{ij}$ between junctions i and j is

$$\boldsymbol{r}_{ij} = \bar{\boldsymbol{r}}_{ij} + \Delta\boldsymbol{r}_{ij}, \tag{5.73}$$

where $\Delta\mathbf{r}_{ij}$ is the instantaneous fluctuation of $\mathbf{r}_{ij}$ and $\bar{\mathbf{r}}_{ij}$ is the time average of $\mathbf{r}_{ij}$. Squaring both sides of the above equation and taking the ensemble average leads to

$$\langle r_{ij}^2 \rangle = \langle \bar{r}_{ij}^2 \rangle + \langle (\Delta r_{ij})^2 \rangle \tag{5.74}$$

since instantaneous fluctuations and mean values are uncorrelated. From Eqs. (5.72) and (5.74) follows:

$$\langle \bar{r}^2 \rangle = (1 - \frac{2}{\phi}) \langle r^2 \rangle_0. \tag{5.75}$$

According to the theory the mean positions of junctions transform affinely with macroscopic strain while the fluctuations are strain independent:

$$\boldsymbol{r}_{ij} = \bar{\boldsymbol{r}}_{ij} + \Delta\boldsymbol{r}_{ij} \tag{5.76}$$

i.e.,

$$\langle r^2 \rangle = \left[(1 - \frac{2}{\phi}) \frac{\lambda_x^2 + \lambda_y^2 + \lambda_z^2}{3} + \frac{2}{\phi} \right] \langle r^2 \rangle_0. \tag{5.77}$$

Using Eq. (5.53) for the elastic free energy, we obtain the following expression for the free energy of the phantom network

$$\Delta A_{\mathrm{el}} = \frac{1}{2}(1 - \frac{2}{\phi}) \nu kT (\lambda_x^2 + \lambda_y^2 + \lambda_z^2 - 3). \tag{5.78}$$

Equation (5.78) is very similar to Eq. (5.57) for the affine network. The only difference is that the so called front factor (equal $\nu/2$ for affine network model) is replaced by $\xi/2$ for the phantom network model where

$$\xi = (1 - \frac{2}{\phi}) \nu. \tag{5.79}$$

The equation for the elastic force is similar to Eq. (5.59) for the affine network with ν replaced by ξ.

5.7 STATISTICAL THEORIES OF REAL NETWORKS

In real polymer network the effects of excluded volume and chain entanglements should be taken into account. In 1977 Flory [26] formulated the constrained junction model of real networks. According to this theory fluctuations of junctions are affected by chains interpenetration, and as the result the elastic free energy is a sum of the elastic free energy of the phantom network ΔA_{ph} (given by Eq. (5.78)) and the free energy of constraints ΔA_{c}

$$\Delta A_{\mathrm{el}} = \Delta A_{\mathrm{ph}} + \Delta A_{\mathrm{c}} \tag{5.80}$$

with ΔA_{c} given by the formula

$$\Delta A_{\mathrm{c}} = \frac{1}{2} \mu kT \sum_{t=x,y,z} [B_t + D_t - \ln(1 + B_t) - \ln(1 + D_t)], \tag{5.81}$$

where

$$B_t = \frac{\kappa^2(\lambda_t^2 - 1)}{(\lambda_t^2 + \kappa^2)^2} \tag{5.82}$$

and

$$D_t = \frac{\lambda_t^2 B_t}{\kappa}. \tag{5.83}$$

Here κ is a parameter which measures the strength of the constraints. For $\kappa = 0$ we obtain the phantom network limit, and for infinitely strong constraints ($\kappa = \infty$) the affine limit is obtained. Erman and Monnerie [27] developed the constrained chain model, where constraints effect fluctuations of the centers of the mass of chains in the network. Kloczkowski, Mark, and Erman [28] proposed a diffused-constraint theory with continuous placement of constraints along the network chains.

A different statistical–mechanical approach based on so called replica formalism was developed by Edwards and coworkers [29,30]. They studied the effect of topological entanglements between chains on the elastic free energy of the network and formulated the slip-link model. The elastic energy of constraints in the slip-link theory is

$$\Delta A_{\mathrm{c}} = \frac{1}{2} N_{\mathrm{s}} kT \sum_{t=x,y,z} \left[\frac{(\lambda_t^2 - 1)}{1 + \eta\lambda_t^2} + \ln\left[\frac{1 + \eta\lambda_t^2}{1 + \eta} \right] \right], \quad (5.84)$$

where N_{s} is the number of slip-links and η is the slipage parameter. Equation (5.84) is very similar to Eq. (5.81) for the constrained junction model. Vilgis and Erman [31] showed that for small deformations both equations have the same form (except minor volume term) with $\kappa = 1/\eta$.

5.8 SCATTERING FROM POLYMER CHAINS

The scattering form factor $S(\mathbf{q})$ from a labeled chain in the network is given by the Fourier transform of the distribution function $\Omega(\mathbf{r}_{ij})$ of the vector $\mathbf{r}_{ij}$ between two scattering centers i and j averaged over all pairs of scattering centers along the chain:

$$S(\mathbf{q}) = \frac{1}{N^2} \sum_{i,j=1}^{N} \int \exp(i\mathbf{q} \cdot \mathbf{r}_{ij}) \Omega(\mathbf{r}_{ij}) \mathrm{d}\mathbf{r}_{ij}. \quad (5.85)$$

Here $\mathbf{q}$ is the scattering vector representing the difference between the incident and scattered wave vectors $\mathbf{k}_0$ and $\mathbf{k}$, respectively, and N is the total number of scattering centers along the chain.

The distribution function $\Omega(\mathbf{r}_{ij})$ of the vector $\mathbf{r}_{ij}$ between scattering centers in the undeformed state is assumed to be Gaussian. The distribution function $\Omega(\mathbf{r}_{ij})$ in the deformed state is

$$\Omega(\mathbf{r}_{ij}) = [(2\pi)^3 \langle x_{ij}^2 \rangle \langle y_{ij}^2 \rangle \langle z_{ij}^2 \rangle]^{-1/2} \exp(- x_{ij}^2/2\langle x_{ij}^2 \rangle - y_{ij}^2/2\langle y_{ij}^2 \rangle - z_{ij}^2/2\langle z_{ij}^2 \rangle), \quad (5.86)$$

where $\langle x_{ij}^2 \rangle$, $\langle y_{ij}^2 \rangle$, and $\langle z_{ij}^2 \rangle$ are the mean-square components of the vector $\mathbf{r}_{ij}$ in the deformed state. Substituting the expression for $\Omega(\mathbf{r}_{ij})$ given by Eq. (5.86) into Eq. (5.85) leads to

$$S(\mathbf{q}) = \frac{1}{N^2} \sum_{i,j=1}^{N} \exp(- q_x^2 \langle x_{ij}^2 \rangle/2 - q_y^2 \langle y_{ij}^2 \rangle/2 - q_z^2 \langle z_{ij}^2 \rangle/2), \quad (5.87)$$

where q_x, q_y, and q_z are the components of the scattering vector $\mathbf{q}$. The vector $\mathbf{r}_{ij}$ between two scattering centers may be written for a phantom network as $\mathbf{r}_{ij} = \bar{\mathbf{r}}_{ij} + \Delta\mathbf{r}_{\mathrm{ij}}$ where $\bar{\mathbf{r}}_{ij}$ is the time average of $\mathbf{r}_{ij}$, and $\Delta\mathbf{r}_{ij}$ is the instantaneous fluctuation of $\mathbf{r}_{ij}$ from its mean time-averaged value. Assuming that mean-square fluctuations are strain independent and that mean positions transform affinely with macroscopic strain and applying Eqs. (5.74)–(5.77) leads to

$$\langle x_{ij}^2 \rangle = \left[\lambda_x^2 + (1 - \lambda_x^2) \frac{\langle \Delta x_{ij}^2 \rangle_0}{\langle x_{ij}^2 \rangle_0} \right] \langle x_{ij}^2 \rangle_0, \quad (5.88)$$

where λ_x is the x component of the principal deformation gradient tensor $\boldsymbol{\lambda}$, with similar expressions for the y and z components. For a freely jointed chain

$$\langle x_{ij}^2 \rangle_0 = \langle r_{ij}^2 \rangle_0 / 3 = \eta \langle r^2 \rangle_0 / 3,$$

where $\eta = |i - j|/N$ is the fractional distance, and $\langle r^2 \rangle_0$ is the mean-square end-to-end vector for the undeformed chain. Substituting these results to Eq. (5.87) leads to

$$S(\mathbf{q}) = \frac{1}{N^2} \sum_{i,j=1}^{N} \exp\left[-\upsilon \frac{|i-j|}{N} \left(1 - (1 - \lambda^{*2}) \frac{(\phi - 2)}{\phi} \frac{|i-j|}{N} \right) \right]. \quad (5.89)$$

In this equation

$$\upsilon = q^2 \langle r^2 \rangle_0 / 6 \quad (5.90)$$

and the *vector* $\boldsymbol{\lambda}^*$ is

$$\boldsymbol{\lambda}^* = \boldsymbol{\lambda}\mathbf{q}/q. \quad (5.91)$$

For scattering parallel to the direction of extension $\lambda^* = \lambda_{\parallel}$ and for scattering perpendicular to the direction of extension $\lambda^* = \lambda_{\perp} = 1/\sqrt{\lambda_{\parallel}}$. Replacing the double summation by integration and evaluating one of the integrals leads to

$$S(\mathbf{q}) = 2 \int_0^1 \mathrm{d}\eta (1 - \eta) \exp\left[-\upsilon\eta \left[1 - \eta(1 - \lambda^{*2}) \frac{\phi - 2}{\phi} \right] \right] \quad (5.92)$$

the result obtained by Pearson [32]. As the strain goes to zero Eq. (5.92) has the limiting form

$$\lim_{\lambda \to 1} S(\mathbf{q}) = \frac{2}{\upsilon} (\mathrm{e}^{-\upsilon} + \upsilon - 1) \quad (5.93)$$

derived by Debye [33], corresponding to the scattering from an unperturbed Gaussian coil. Readers interested in scattering from labeled cross-linked paths in unimodal and bimodal networks should consult the review article by Kloczkowski, Mark, and Erman [25].

5.9 SIMULATIONS OF POLYMERS

System composed of polymers or containing polymers immersed in low molecular media are extremely complex

for many reasons. First, polymer chains (linear, branched, or cyclic) have often a huge molecular mass. Large fraction of single covalent bonds in the main chain imply at least a limited internal rotational freedom for each such bond, and consequently lead to an enormous number of available conformational isomers. Second, due to the excluded volume effect polymer chains are non-Markovian, i.e., conformational space accessible to a selected portion of the chain depends on the actual conformation of the remaining fragments. Consequently, a rigorous analytical treatment of polymer conformational statistics and dynamics is essentially impossible; although various aspects of polymer physics could be quite successfully addressed within framework of approximate theories (see the previous sections). Third, the chain connectivity imposes a complex network of topological obstacles. A moving chain cannot cross its own contour or the paths of the other chains present in the system. This has pronounced consequences for polymer dynamics in solutions and polymeric melts, where motion of polymers has to be extremely correlated and the correlation distances are several orders of magnitude larger than it is observed in typical disordered low molecular systems. The nature of these correlations could be extremely complex.

For the above reasons computer simulations are very important components of methodology of theoretical polymer physics. Properly designed computational experiments expand our understanding of these complex systems, provide excellent test of the existing theories and stimulate development of new theoretical approaches. Due to the large size, time scales involved, and complexity of polymeric systems numerous new simulation techniques have been developed to meet these extreme computational demands. This way theoretical physics of polymers had significant influence on progress in computational physics in general.

Simulations of polymers could be designed on various levels of molecular details treated in an explicit way [16–20, 34–36]. Molecular Dynamics (or Brownian Dynamics) of all-atom systems are limited to short chains or/and to studies of local and fast relaxation processes. It is rather impractical, and often nonfeasible, to do MD simulations of long polymer collapse or a self diffusion of polymer chain in a melt, to give just a couple of typical examples. Monte Carlo simulations of the all-atom systems have a bit less limitations, but still large scale rearrangements are difficult to study. For these reasons frequently reduced representations of polymer conformational space are employed. These range from united atom models, where groups of atoms are treated as single interaction units, to lattice models where entire mers (or large united atoms) are restricted to a lattice, thereby enormously reducing the number of available states and simplifying energy calculations. While simple lattice models are of very limited utility in the physics of low molecular mass system, for polymers they provided general solutions to very fundamental problems. This qualitative difference is strictly related to the difference in the correlation length scales in the two types of systems. In polymers the local details become usually irrelevant at large distances. Because of their importance for general physics of polymers and educational values we start from a discussion of simple lattice models of polymers and polymer dynamics.

5.9.1 Ideal Lattice Chains are Equivalent to Off-lattice Models

Let us consider a chain restricted to a simple cubic lattice, with the lattice spacing equal to 1. The chain is a string of vectors with the six allowed orientations belonging to the following set $\{|1,0,0|, |-1,0,0|, |0,1,0|, |0,-1,0|, 0,0,1, |0,0,-1|\}$. A chain vector could be followed by any of the vectors from the set. Thus, there is no any average orientational correlation between the chain vectors, in spite of the lattice restrictions. Note, that for this ideal model a lattice site can be occupied by more than one bead of the chain. It could be immediately seen that the Eqs. (5.1) and (5.2) written for the freely joined chain are true as well for the ideal lattice chain. The models are equivalent, and an exact analytical theory of their conformational statistics exists. Such analogy goes much further. Let us now consider a chain restricted to the diamond lattice with a constant tetrahedral value of the valence angle and three discrete values of the torsional angle corresponding to the *trans* and two *gauche* states. Again, it is easy to note that this model is equivalent (in respect to its global properties) to the ideal, freely rotating chain with the tetrahedral value of the planar angle. It is also easy to show that such chain can mimic the chain with restricted rotations and interdependent rotations, provided Boltzmann weights are assigned to the *trans* and *gauche* conformations and proper correlations between the weights are taken into account.

Equivalence of the ideal continuous and the lattice models extends also on the dynamic properties of a single chain. The Rouse model [37,38] , (or the bead and spring model) consists of a string of points (or beads) of equal mass connected by harmonic springs of equal length and equal strength of the harmonic potentials, although without any angular interactions. An exact analytical solution for the relaxation spectrum of this model is relatively easy to derive. For the ideal (without excluded volume limitations) lattice chain a simple model of dynamics, simulated by a long random sequence of small local conformational changes, could be formalized in a stochastic Master Equation of motion. It has been shown by Verdier and Stockmayer [39], that such model is equivalent to the Rouse model [37,38] in almost entire relaxation spectrum, except the fastest local oscillations involving a couple of chain segments.

5.9.2 Simulation of the Excluded Volume Effect in a Single Chain

The ideal models described in the previous sections ignored a very important fact, that a polymer has its own volume, i.e., two segments cannot occupy the same place in space. Using a series of approximations Flory has shown that the exclude volume leads to a significant increase of the average random coil dimensions and changes the number of accessible conformers. Flory, has also shown that in a thermodynamically ''poor'' solvent the proper volume of the chain segments could be balanced by their mutual attractions, leading to a pseudoideal state, very similar to the Boyle point for the real gases. Typical, however, is the situation of a ''good'' solvent, where the effect of excluded volume is large. Exact analytical solution to the excluded volume problem does not exist. It is unknown how to calculate partition function of a single chain, since the probability of a given conformation of the $(n+1)$th bond added to a chain depends on the conformation of the preceding n bonds. The process of virtual growth of a ''real'' (with excluded volume, in contrast to the ideal, lacking volume chains) chain is non-Markovian. This is exactly a situation where the data from computer simulations are needed for estimations of true (in silico) experimental properties of the model system and for subsequent evaluation of the assumptions and predictions of various approximate theories.

In the context of a simple lattice model the problem could be formulated as follows. Compute the number of non-self-intersecting random walks on the lattice and the distribution of the segment density, size, shape, etc., of the resulting random coils as a function of the chain length. The first thought is to use computer for an exact enumeration of all possible conformations of a n-segment chain. Unfortunately, the number of possible random walks grows exponentially with the chain length. Exact enumeration is possible only for n range of few tens of segments. In this range the finite length effects are still large and an extrapolation of the obtained (exact) data to higher values of n is uncertain. Another approach is to employ a stochastic sampling (Monte Carlo method) to get a ''representative'' ensemble of non-self-intersecting random walks of the assumed length n. There the result is not exact, however avoids any systematic errors. The magnitude of the statistical error could be always reduced by the increase of the sample size. The algorithm is very simple.

1. Start from the first bond.
2. Add the next bond in a randomly selected direction (the simple ''back'' step could be a priori prohibited and the resulting bias easily removed from the results).
3. Check for non-self-intersection and repeat from (2) if a double occupancy of a lattice site is not detected, otherwise erase the chain and start from (1).
4. Stop the chain growth when the requested length n is reached and add the chain to the statistical ensemble.
5. Repeat the entire process starting from (1) until the required number of chain in the sample is collected.
6. Perform statistical analysis of the collected ensemble.

The process of the MC chain growth is illustrated in Fig. 5.4.

Situations, as that schematically depicted in Fig. 5.4B happen quite frequently. Therefore, the algorithm outlined above has a huge sample attrition rate; only a small fraction of the staring chains are finally accepted in the statistical

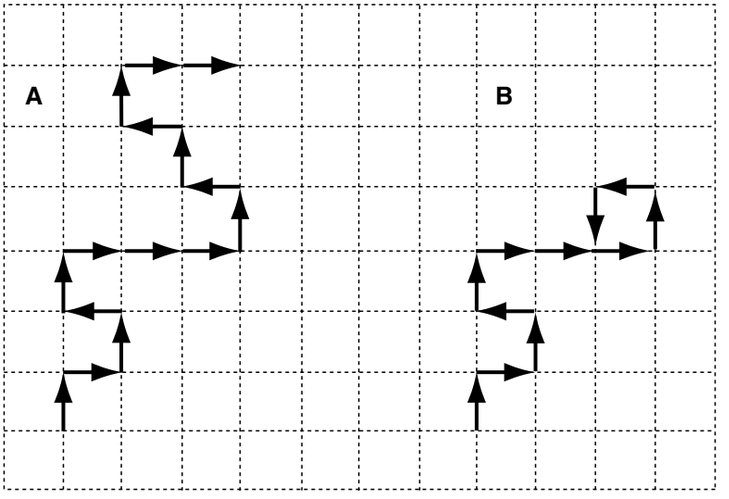

FIGURE 5.4. Two dimensional illustration of the MC growth of non-self-intersecting walks (see the text for details). On the left side (A) an example of the successful structure composed of $n = 15$ segments is shown. On the right side (B) an intersection has been detected before reaching $n = 15$, the final chain length, and the chain has to be removed from the statistical ensemble.

pool. To overcome this problem Rosenbluth and Rosenbluth [40] proposed a modified approach. The segments are selected only from the set of orientations which do not cause the intermediate chain clash. In the case shown in Fig. 5.4B the segment number 11 would be selected only from the following two possibilities; to the left, and to the top of the plane. Obviously, this introduces a bias to the sample. This bias could be easily removed with a proper weighting of the particular conformation with a factorials depending on the number of the allowed continuations at each step. The R&R method allows for generation of much longer chains. Their length is limited by the ''cull-the-sack'' effect, where the growing chain end is surrounded by the chain segments, blocking all the possibilities for the further continuation of the growth process. A number of extensions of the original R&R method have been proposed since then. In general, these methods look into possibility of a continuation in a larger perspective than just one segment ahead.

There are several qualitatively different ways of sampling the polymer conformational space. One may start from a chain of a given length and successively modify its conformation. Two examples of such types of algorithms are illustrated in Fig. 5.5. One of them is the ''pivot'' algorithm, where a single step consist of a random selection of a bond and a rotation (in two dimensional case it is reduced just to a flip; vertical or horizontal) of the selected end of the chain. Advantage of this algorithm is that in a single step a large modification of the chain conformation is attempted. However the acceptance rate for longer chain could be rather small. A number of different global rearrangements of the chain conformations were designed aiming on a more efficient sampling. An example is the ''reptation'' algorithm, where a bond (or a small number of bonds) is cut-off from one end of the chain and added in a random direction on the opposite end. The acceptance ratio for this type of global update algorithms could be quite high. Yet another example is a technique that could be viewed as a complex ''pivot-like'' algorithm, where a part of the chain on one end is erased and then re-grown in a random or semirandom fashion. Of course, the statistical sample is collected in along series of attempts (sometimes successful) to successive modifications of subsequently generated conformations. In the second type of algorithms (Fig. 5.5A) local micromodiffications of the chain conformation are randomly selected at random position of the chain. Marginally, let us note that the local move algorithm could be interpreted as a simulated Brownian motion of a polymer chain. This is a ''real'' chain version of the before mentioned Verdier–Stockmayer model [39] of polymer dynamics. Again, it should be stressed out, that an accurate analytical theory for the real chain dynamics does not exist. The local move algorithms are powerful tools for study of long-time (and large scale) polymer dynamics. There are however several problems with the models employing a limited set of local moves and low coordination number lattices. The algorithms could be nonergodic, or rather ergodic in a subset of its full conformational space. This is explained in Fig. 5.6. There is no path to- and no path from the conformation shown in the drawing. The problem may be cured using a higher coordination lattices and/or a larger set of ''less-local'' micromodiffications. An example of such larger scale move is shown in Fig. 5.6B. The backfire of such update of the local move algorithms is a less clear relation with the model of the Brownian motion. Perhaps, the ''wave-like'' move, when attempted rarely could be interpreted as a particular coincidence of a series of local moves, which somehow were able to pass the local conformational barriers. An additional flaw of the low coordination lattice models (beside the ergodicity

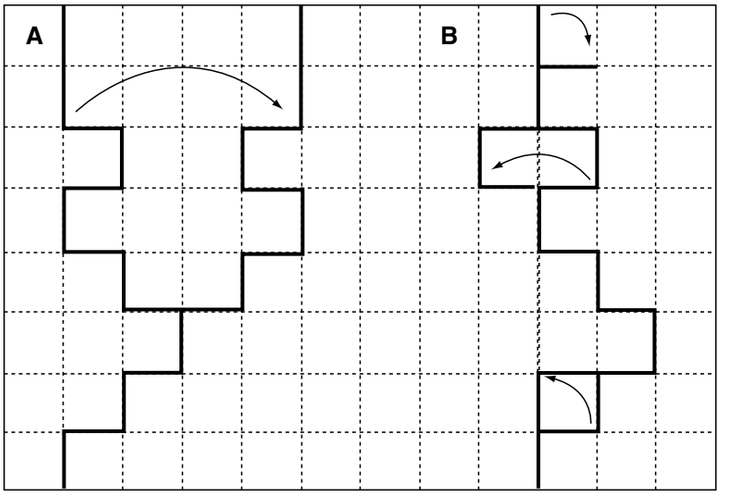

FIGURE 5.5. The idea of the pivot algorithm (A), and the local moves algorithm (B). The black contours indicate the initial structures, the lighter bonds show the accepted modifications. The local moves include (from top to the bottom of B): random chain end modification, a crankshaft move and a corner move.

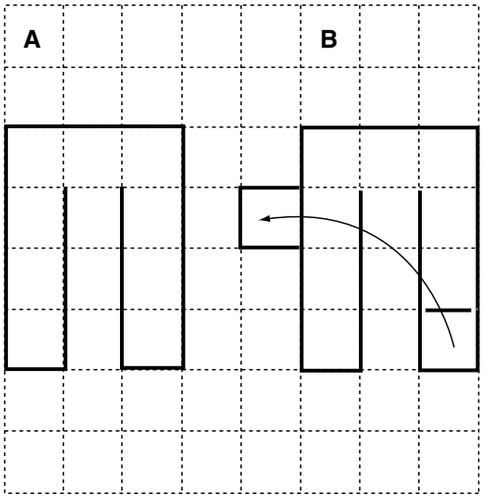

FIGURE 5.6. A trapped conformation for the algorithm with only local moves for a chain on the simple square lattice (A). A longer distance move that guarantees the ergodicity of the algorithm, where a U shaped fragment at one part of the chain is cut-off and attached somewhere else (B).

problems) of polymer dynamics is the difficulty of controlling the effects of the lattice anisotropy on the observed motion. Obviously, simple models of polymer conformations and dynamics, very similar to those described above could be design in the continuous space. Such models could be sampled using MD, MC, or via various hybrid sampling techniques based on a combination of genetic algorithms (GA) and molecular mechanics (usually MC dynamics). The results from simplified lattice and off-lattice models are essentially equivalent. For instance, the average chain dimensions of the real chain models scale as $\langle S^2 \rangle \sim n^{\gamma}$. Interestingly, the value of the universal constant for the 3-dimensional chains is close (but not identical) to the value resulting from the mean-field analytical theory of Flory. More qualitative differences are observed between the results of the "real" chain simulation of the polymer dynamics and the ideal chain theory of Rouse [37].

5.9.3 Simulations of Polymer Chain Collapse

Polymer chains in solution can undergo a collapse transition from an expanded random coil state to a dense globular state. The transition could be induced by decrease of temperature or by adding a "poor" solvent to the solution [41]. This process is difficult to describe analytically, but could be studied in details via computer simulations. Let us again consider a very simple lattice model. Representation of protein conformational state could be done using any kind of simple lattice. In such context it is easy to design a very simple potential mimicking the balance between the volume of the chain segments and their mutual attractions in the solution. The simplest form of such potential is given below:

$$E_{ij} = \begin{cases} \infty, for\ r_{ij} < 1 \\ \varepsilon, for\ r_{ij} = 1 \\ 0, for\ r_{ij} > 1. \end{cases} \quad (5.94)$$

In the formula above r_{ij} is the distance between two beads of the chain, 1 is the lattice spacing, and ε is a negative constant. With $\varepsilon = 0$ the model reduces to the model of a "real" chain in a good solvent, where mutual attractions of the chain segments could be ignored. Energy of the entire chain is a sum of the binary contributions ΣE_{ij}.

With decreasing temperature (or with increasing strength of the long-range interactions ε) the mean dimensions of the chain decrease (the solid curve in Fig. 5.7). The curves become steeper with increasing chain length; nevertheless the collapse transition remains continuous. The dashed horizontal line corresponds to the dimensions of an ideal chain of the same local geometry. The vertical dashed line denotes the collapse transition temperature. Slightly higher than ideal dimensions of the real chain at the transition midpoint are due to a bit higher prefactor – the scaling of the mean dimension with the chain length is at this point the same as for an ideal chain i.e., $\langle S^2 \rangle \sim n$. At very low temperatures, the globular state is a dense droplet with $\langle S^2 \rangle \sim n^{2/3}$. Obviously, at very high temperatures the chain behaves as the thermal "real" chain discussed in the previous section, i.e., $\langle S^2 \rangle \sim n^{\gamma}$.

Very interesting are the models where on top of the long range interactions a local stiffness of the model chain is superimposed. Let us assume that we are dealing now with a simple chain restricted to the diamond lattice (although any other lattice or off-lattice model can include the short-range interactions that simulate the polymer limited flexibility). Then let us assume that the *trans* conformation is favored energetically in respect to the two *gauche* conformations. At some critical ratio of the potential energy

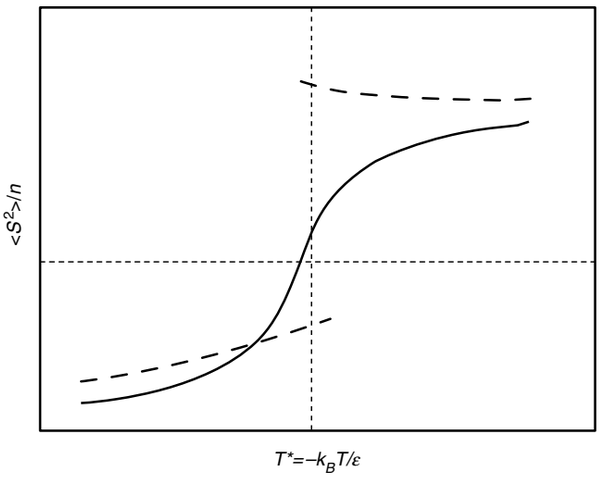

FIGURE 5.7. Collapse transition of a flexible polymer chain (solid line) and a semiflexible chain (dashed line) of a limited length (see the text for an explanation).

of these two types of local geometries the behavior of a chain of a limited length changes dramatically. In the range of high temperatures with decreasing temperature the chain dimensions increase due to increasing effect of the stiffness. Relatively long expanded segments could be seen at this range. At a critical temperature, these ''rods'' of fluctuating length coalesce due to a huge decrease of the potential energy of the long-range interactions for a small entropic expense. The transition is abrupt, highly cooperative (the average length of the expanded sequences jumps up at the transition), and has all features of the first-order phase transition, including easily detected metastable region, an ''almost'' singularity of the heat capacity and an extremely low population of the intermediate states. At the transition midpoint the simulated molecules adopt essentially only two types of conformations; swollen random coils with a short sequences of expanded states and a densely packed, highly ordered globular state, with much longer sequences of the expanded local conformations. This behavior of the semiflexible model has a number of essential properties of globular proteins. First, the collapse transition is pseudo first-order (all-or-none in the language of protein biophysics). Second, it is cooperative and the collapse induces a sudden increase of the length of the regular expanded fragments, very much as the formation of secondary structure during the protein folding transition. Third, the collapsed structure is highly ordered with relatively well defined (however not unique) number of ''secondary structure'' expanded elements. Note, that these striking similarities are observed in the homopolymer model where all polymer units are the same. This leads to the conclusion that one of the most important general aspects of protein folding is a competition between the long-range and the short-range (stiffness) interactions. In this picture, differentiation of the interactions along the polypeptide chains (sequence of amino acids) plays a ''fine-tuning'' role, selecting the structural detail of the globular state. This analogy to protein folding extends even further. As the length of the semiflexible chain increases the ordering of the globular state becomes modular – domains are formed upon the collapse. Each domain can form at slightly different temperature, within the range of the metastable states shown in Fig. 5.7. When the number of domains becomes large the collapse transition becomes continuous, as it should be for any infinitely long flexible (or semiflexible) polymer chain. Such detailed insight into the collapse transition of semiflexible polymers could be gain only from computer simulations, although a very approximate theories for a single globule collapse of semiflexible polymers were published in past.

A single polymer simulations could address also the issues of chain topology, including the effect of polymer branching and macrocycles on the thermodynamics of the collapse transition and the dynamics in a diluted media. This can be addressed on various levels of details, from a large scale conformational sampling within a framework of reduced models to a detailed molecular mechanics study of local conformational transitions. For instance, a very interesting simulation of DNA collapse has been recently performed using the bead and string model with a short range bending potential and the Brownian Dynamics as a sampling technique. These simulations led to a very plausible and nontrivial picture of the DNA collapse pathway. It is also possible to employ a multiscale sampling, where the large scale relaxations are modeled on a low resolution level and the details are studied with the all-atom representation.

Finally, it is worth to mention a very broad class of approaches to a specific problem of polymer collapse transition, the protein folding transition. This field attracts a lot of researches due to its importance for molecular biology, and biotechnology, genetics, and molecular medicine (including new drugs design in particular). In the case of the protein folding problem, the details of physics and the pathway description of the collapse transition are (at least by now) of a lesser importance. The mean goal is to predict the unique structure of protein globular state. The task is nontrivial, since the copolymers of interest are composed of twenty different mers (amino acids) and the sequence of these mers dictates a vast variety of three-dimensional globular structures, with a very specific local conformations and their well defined mutual packing in the globule. Two types of algorithms are now the most successful. The first one uses a large set of ''prefabricated'' protein fragments, extracted from a collection of known three-dimensional structures, and the sampling scheme are based on an iterative shuffling of these fragments within the simulated chain. Another approach is more in spirit of the classic polymer algorithms. It employs a local move schemes, however with a complex representation of the polypeptide conformational space and elaborated set of mean field potentials, derived either from the physical properties of the small molecules or from statistical analysis of the structural regularities seen in known structures of globular proteins. An amazing progress was achieved in this field during the last few years. The second approach is probably somewhat more general; it opens a possibility of a qualitative study of protein folding pathways and molecular mechanisms, not only the predictions of the globular structure. The predictive power of the both type of approaches are similar. Nevertheless, the second one seems to be a bit more open for a wider range of applications. These applications include the bootstrapped (resolution- and time-vise multiscale) implementations of the polypeptide representation and dynamics. Coupling of the various levels of resolution enables for a quite detailed study of protein dynamics and thermodynamics. The simulation techniques and models developed specifically for proteins are easily adaptable for more general applications in polymer computational physics. [43]

5.9.4 Simulations of Dense Polymeric Systems

Dense polymeric systems include polymer solutions, polymer networks, polymer melts, polymer liquid crystals

and solids, and many more. There is a vast body of literature on each of these subjects [42]. The modeling approaches are also of great variety, from a simple reduced models (lattice and continuous) to the detailed molecular mechanics and even a quantum mechanics. It is beyond scope of this chapter to go through the detail of various applications. Let us just outline some of problems that could be addressed in computer simulations, increasing our understanding of complex systems and providing important stimuli for theoretical studies and practical applications in material science and biotechnology.

Typical dense polymer solutions and melts are globally disordered; however the level of local ordering could be relatively high. This is a very complex phenomenon that involves long-range correlations that are the results of specific local interactions. A general insight could be gain from the low resolution models that allow for study of the large scale conformational rearrangements; although specific details could be very sensitive to the atomic structure and require extensive molecular mechanic study of carefully selected starting conformations. The same could be said about the phase transitions in bulk polymers.

The rate polymer diffusion in polymer media spans orders of magnitude. The mechanism of the process is unclear. It is very difficult to provide even a qualitative mechanistic picture how a long chain can move throughout a complex network of entanglements superimposed by the other macromolecules. The reptation theory of DeGennes [13] is probably only qualitatively true and only for very specific conditions. Simulations could be extremely helpful in at lest qualitative understanding of this process.

Another challenging (however not really macromolecular) polymeric system are biological membranes. It is known from various experiments that the spectrum of relaxation processes in membranes is extremely wide; from local cooperative motion of phospholipide chain and occasional jumping of molecules from one side of a membrane to the other one to a global flexing of the membrane and formation of vesicles. Simulations are done on various levels of generalization. There are mesoscopic model which treat the membrane as a kind of elastic network, but also a very detailed all-atom study of membrane structure and local dynamics. Bootstrapped, multiscale simulations could be a very promising way to attack this problem.

REFERENCES

1. W.L. Mattice and U.W. Suter, *Conformational Theory of Chain Molecules*, Wiley, New York, 1994.
2. M.F. Schulz and F.S. Bates, this volume, Chap. 32
3. H. Yamakawa, *Modern Theory of Polymer Solutions*, Harper & Row, New York, 1971.
4. A.Y. Grosberg and A.R. Khokhlov, *Statistical Physics of Macromolecules*, AIP, New York, 1994.
5. M. Warner and E.M. Terentjev, *Liquid Crystal Elastomers*, Oxford University Press, Oxford, 2003.
6. J.E. Mark and B. Erman, *Rubberlike Elasticity. A Molecular Primer*, Wiley, New York, 1988.
7. B. Erman and J.E. Mark, *Structures and Properties of Rubberlike Networks*, Oxford University Press, Oxford, 1997.
8. A. Kloczkowski, M.A. Sharaf and J.E. Mark, *Chem. Eng. Sci*. **49**, 2889 (1994).
9. M.A. Sharaf and J.E. Mark, *Polymer*, **45**, 3943 (2004).
10. W. Zhao and J.E. Mark, this volume, Chap. IIB.
11. J.D. Honeycutt, this volume, Chap. IIID.
12. K.F. Fried, *Renormalization Group Theory of Macromolecules*, Wiley, New York, 1987.
13. P.G. DeGennes, *Scaling Concepts in Polymer Physics*, Cornell University Press, New York, 1979.
14. J. des Cloizeaux and C. Jannink, *Polymers in Solutions: Their Modeling and Structure*, Clarendon, Oxford, 1990.
15. W.C. Forsman, Ed., *Polymers in Solution*, Plenum, New York, 1986.
16. K. Binder, Ed., *Monte Carlo Methods in Statistical Physics*, Springer-Verlag, Berlin Heidelberg New York, 1986.
17. K. Binder, *Monte Carlo and Molecular Dynamics Simulations in Polymer Sciences*, Oxford University Press, Oxford, 1995.
18. A. Baumgaertner, Simulation of polymer motion, *Ann. Rev. Phys. Chem*. **35**, 419 (1984).
19. Kolinski and J. Skolnick, *Lattice Models of Protein Folding, Dynamics and Thermodynamics*. R.G. Landes, Austin, TX, 1996.
20. M. Kotelyanskii and D.N. Therodorou, Ed., *Simulation Methods for Polymers*, Marcel Dekker, New York, 2004.
21. P.J. Flory,*Statistical Mechanics of Chain Molecules*, Interscience, New York, 1969.
22. J.D. Honeycutt, this volume, Chap. XX.
23. P.J. Flory, *Proc. Roy. Soc. London, Ser. A* **351**, 351 (1974).
24. H.M. James and E. Guth, *J. Chem. Phys*. **15**, 669 (1947).
25. A. Kloczkowski, J.E. Mark and B. Erman, *Comput. Polym. Sci*. **2**, 8 (1992).
26. P.J. Flory, *J. Chem. Phys*. **66**, 5720 (1977).
27. B. Erman and L. Monnerie, *Macromolecules*, **22**, 3342 (1989), **25**, 4456 (1992).
28. A. Kloczkowski, J.E. Mark and B. Erman, *Macromolecules*, **28**, 5089 (1995).
29. R.T. Deam and S.F. Edwards, *Phil. Trans. R. Soc, A,* **280**, 317 (1976).
30. R.C. Ball, M. Doi and S.F. Edwards, *Polymer*, **22**, 1010 (1981).
31. T. Vilgis and B. Erman, *Macromolecules*, **26**, 6657 (1993).
32. D.S. Pearson, *Macromolecules*, **10**, 696 (1977).
33. P. Debye, *J. Phys. Colloid. Chem*. **51**, 18 (1947).
34. R.H. Boyd and P.J. Philips, *The Science of Polymer Molecules*, Cambridge, New York, 1993.
35. P.R. Schleyer, Ed. *Encyclopedia of Computational Chemistry*, Wiley, New York, 1998.
36. W.F. van Gunsteren and P.K. Weiner, *Computer Simulations of Biomolecular Systems. Theoretical and Experimental Applications*. Escom, Leiden, 1989.
37. P.E. Rouse, *J. Chem. Phys*. **21**, 1272 (1953).
38. M. Doi and S.F. Edwards, *The Theory of Polymer Dynamics*, Clarendon, Oxford, 1986.
39. P.H. Verdier and W.H. Stockmayer, *J. Chem. Phys*. **36**, 227 (1962).
40. M. Rosenbluth and N. Rosenbluth, *J. Chem. Phys*. **23**, 356 (1955).
41. A. Montesi, M. Pasquali and M.C. MacKintosh, *Phys. Rev. E* **69**, 021916 (2004).
42. J.E. Mark, K. Ngai, W. Graessley, L. Mandelkern, E. Samulski, J. Koenig and G. Wignall, *Physical Properties of Polymers,* Cambridge University Press, Cambridge 2004.
43. A. Kolinski, Acta Biochim. Polonica **51**, 349 (2004).

CHAPTER 6

Scaling, Exponents, and Fractal Dimensions

Mohamed Daoud,* H. Eugene Stanley,† and Dietrich Stauffer‡

* *Laboratorie Léon Brillouin (CEA-CNRS), CE Saclay; Gif-sur-Yvette, Cedex, France*
† *Center for Polymer Studies and Department of Physics, Boston University, Boston, MA 02215*
‡ *Institute of Theoretical Physics, Cologne University, D-50923 Köln, Euroland*

6.1 LINEAR POLYMERS

Textiles, much of living matter, plastics, and many other materials consist of linear or branched polymers. Each polymer usually is a carbon chain consisting of many monomers like -CH_2-. We emphasize here the modeling of such polymers and compare the theoretical results with experiments.

First, we consider the conformation of a random linear chain, which is a model for a dilute solution of a polymer in a solvent [1–6]. Typical examples are polystyrene in benzene or polydimethylsiloxane in toluene or cyclohexane. We assume that the macromolecules are made of N statistical units which are randomly oriented with respect to each other. Because the actual monomers have to respect chemical bond angles, independent units can be regarded as made of several monomers. It is possible to define such independent units which will be used in all cases. This procedure was first presented by Kuhn, who defined the concept of local rigidity of a polymer [1]. Here, we consider the chains as completely flexible, and we do not distinguish between actual monomers and statistically independent units.

6.1.1 The Random Walk

The simplest model to describe the structure of a linear chain made of N units of length l each is the random walk. This is an ideal chain where no interactions are present between monomers. The distribution function $P(r,N)$, which is the probability that a chain made of N steps starts at the origin and ends at point r, is a Gaussian. In three-dimensional space,

$$P(r, N) = (3/2\pi N\ell^2)^{3/2} \exp\{-3r^2/2N\ell^2\}. \tag{6.1}$$

From the second moment we define the fractal dimension d_f of the walk by $\langle r^2\rangle^{d_f/2} \sim N$. For any spatial dimension d, the second moment $R_0^2 \equiv \langle r^2\rangle$ of $P(r, N)$ is

$$R_0^2 \sim N\ell^2, \tag{6.2a}$$

Thus the fractal dimension [6] is

$$d_f = 2 \tag{6.2b}$$

for any d. It is important to stress that any definition of a characteristic length for the random walk leads to this result.

What is a fractal and its dimension? A long spaghetti is one dimensional since its mass increases linearly with the length. A pizza has a mass proportional to the square of the radius, if its thickness is constant, and thus is two dimensional. A glass of red wine has a volume and mass proportional to the third power of the length, and is three dimensional. Thus an object with mass proportional to $(\text{radius})^{d_f}$ has a dimension d_f. It is called a fractal with the fractal dimension d_f if d_f differs from the Euclidean dimension (usually 3) of the space into which the object is embedded. The apple-like Mandelbrot set is perhaps the most famous deterministic fractal, whereas the random walks of Eq. (6.2a) are random fractals with mass $\propto N \propto (\text{radius})^2$. In deterministic fractals, small parts are mathematically similar to suitably chosen large parts; in random fractals this "self-similarity" (a large branch of a tree looks similar to a small twig on it) is often described but seldom defined in any precise way.

For a polymer chain, it is possible to use the mean square end-to-end distance, as we did above. It is also possible to

define the average radius of gyration. One finds that these lengths are proportional to each other if both are long, and that the fractal dimension is 2 (for a discussion, see Chapter 1 in [7]). This is the reason for using the sign $\sim$, which denotes asymptotic proportionality, and scaling laws are assumed to be valid only asymptotically. It is important that the precise way the length is defined will change the prefactor, but not the exponents. In this sense, we can say that there is only one characteristic length, and we will not be interested in the differences between the prefactors.

The fractal dimension may be observed experimentally by light or neutron scattering [8]. The scattered intensity $S(\vec{q})$ is the Fourier transform of the pair correlation function

$$S(\vec{q}) = \sum_{i,j=1}^{N} \langle \exp[i\vec{q} \cdot (\vec{r}_i - \vec{r}_j)] \rangle, \tag{6.3}$$

where the brackets $\langle \cdots \rangle$ represent an average over all configurations, and $\vec{q}$ is the momentum transfer in the scattering experiment: for a neutron with wavelength λ elastically scattered with an angle θ, we have

$$q \equiv |\vec{q}| = \frac{4\pi}{\lambda} \sin\frac{\theta}{2}. \tag{6.4}$$

Because Eq. (6.1) is valid for any pair of units in a random walk, Eq. (6.3) may be calculated exactly. This was done by Debye [1] some years ago. He found

$$S(q) = \frac{2}{X^2}(e^{-x} - 1 + X), \tag{6.5}$$

with

$$X = q^2 R_0^2/3. \tag{6.6}$$

Here, R_0 is the radius of gyration of the ideal chain. In the intermediate range, $l^{-1} \gg q \gg R_0^{-1}$, where the fractal nature of the walk appears, relation (6.5) may be approximated by

$$S(q) \sim q^{-2}. \tag{6.7}$$

This relation provides a convenient way to measure the fractal dimension of a single polymer, whenever the intermediate range may be reached experimentally. Neutron scattering is an excellent technique for this: The available wave vector range is particularly well suited for polymers; since the typical unit size is around 10*A*, and the radius of gyration is several hundred Ångströms. Linear chains behave actually as random walks in two cases: in a melt, when no solvent is present, and in a theta solvent [9]. The latter is introduced in Section 6.1.2 when we discuss the actual interactions between monomers.

6.1.2 The Self-Avoiding Walk

Random walks are ideal chains in the sense that there is no interaction between monomers. For actual polymers, there is an interaction between any two monomers. The interaction consist of an attractive part for large distances, goes through a minimum at intermediate distances, and becomes a repulsive core at short distances. Because of this ''steric'' constraint, two monomers cannot be in the same location.

At high temperatures, the repulsive core is dominant, and the local minimum may be neglected completely. This is the excluded volume effect, and corresponds to what is called a good solvent [10,11]. There exists a critical temperature called the Flory theta temperature, where the excluded volume effect and the attractive part compensate each other. Such solutions are said to be in a theta solvent [12–14]. For still lower temperatures, the attractive part of the potential becomes dominant, and although two monomers are not allowed to be in the same location, they tend to be in the vicinity of each other. As a consequence, the chain tends to collapse on itself [15–17]. Solvents in which this happens are known as poor solvents.

As mentioned above, at the theta temperature, because of the compensation between attractive and repulsive parts of the potential, the random walk model gives an adequate description of a chain in three-dimensional space [1–6]. Actually, there are still logarithmic corrections, but they may be neglected. In two dimensions, a chain at theta temperature is still not equivalent to a random walk [18]. In what follows, we will be concerned with solutions in a good solvent. It was realized by Edwards [10] that the exact shape of the potential is not important, and that it could be described by a parameter $v(T)$, where T is the temperature, called the excluded volume parameter, defined as

$$v(T) = \int \{1 - e^{V(r)/\kappa T}\} dr, \tag{6.8}$$

like the classical second virial coefficient, where $V(r)$ is the effective monomer–monomer potential. This parameter is positive in a good solvent, vanishes at the theta temperature and becomes negative in a poor solvent.

In the good solvent, steric interactions are dominant, as mentioned above, and the polymer is swollen compared to the ideal chain. This swelling corresponds to a change in the fractal dimension of the chain, which now becomes smaller than 2.

The fractal dimension was calculated by various renormalization group techniques and by computer simulations [19,20]. Here, we describe the Flory approximation which, although being wrong [1–6], gives the fractal dimension within a very good accuracy for all dimensions. In this approximation one assumes that the free energy can be written as

$$F/\kappa T = \frac{R^2}{R_0^2} + v\frac{N^2}{R^d}. \tag{6.9}$$

The first term is the elastic energy, in which one considers the chain as a spring with spring constant $1/R_0^2$, where R_0 is

the ideal radius from Eq. (6.2). The radius R is the actual radius of the chain, to be determined. The second term is the interaction energy which can be estimated as follows. In a unit volume, the number of monomers is N/R^d, the number of pair interactions scales as $(N/R^d)^2$, and the interaction energy is therefore $v(N/R^d)^2$. Thus, the total interaction energy in the volume R^d scales as $R^d v(N/R^d)^2$, which is the second term in Eq. (6.9). Minimizing F with respect to R gives the fractal dimension d_f of a linear chain in the Flory approximation,

$$N \sim R^{d_f}, \tag{6.10a}$$

$$d_f = \frac{d+2}{3}. \tag{6.10b}$$

This prediction $d_f = 5/3$ in three dimensions is close to the actual value near 1.7; $d_f = 1$ and 4/3 for $d = 1$ and 2, respectively, is even exact. Note that we recover the ideal chain dimension for $d = 4$. This is the upper critical dimension above which the excluded volume interaction becomes irrelevant, and the chain is ideal. For higher dimensions, the interaction with itself is negligible for the exponents, because space is sufficiently large that the polymer almost does not cross itself. Therefore, for $d \geq d_c$ chains with or without interactions are equivalent.

Equation (6.10) was checked directly, using polymers with different masses. It was also tested using scattering experiments, by measuring the Fourier transform $S(q)$ of the pair correlation function. As above Eq. (6.7), one can show that the scattered intensity is related to the wave vector q by the fractal dimension. In $d = 3$ one finds, using Eq. (6.10), that

$$S(q) \sim q^{-\frac{5}{3}} (\ell^{-1} \gg q \gg R_0^{-1}). \tag{6.11}$$

Relations (6.10) and (6.11) were tested experimentally by small angle neutron scattering. Let us mention that star-shaped polymers are in this same universality class: the mass dependence of their radius of gyration also follows relations (6.10). However, it also depends on the number f of branches, indicating the special geometry of the object. For more details, the reader is referred to Refs. [21–25].

6.1.3 Dilute Solutions

So far, we have considered only a single polymer chain. Actual solutions contain many chains! We expect the above results to hold as long as the various polymers are far from each other. This is the case for dilute solutions, where we expect the concentration effects to be only perturbations to the various laws that we found.

Let C be the monomer concentration. It is common to define the overlap concentration C^* where the distance between centers of masses of the chains is of the order of the radius of the macromolecules. Assuming the polymers are randomly distributed, the average distance between their centers of masses is

$$\delta \sim (C/N)^{-1/d}. \tag{6.12}$$

Equating Eq. (6.12) to the radius of gyration, and using Eq. (6.10), we get

$$C^* \sim N^{1-d/d_f} \approx N^{-4/5} \quad (d = 3). \tag{6.13}$$

Relation (6.13) exhibits the fractal character of the chains; because they are fractals, their volume grows faster than their mass. Therefore, the overlap concentration decreases as the polymers become larger.

As mentioned above, we expect two concentration regimes, with C/C^* smaller or larger than unity. Therefore, we do not expect N and C to act as independent variables for all the properties, but to appear only through the ratio C/C^*. This scaling behavior occurs in many properties, but we will consider here only the scaling behavior of the radius of gyration R and of the osmotic pressure π. In both cases, one may write a scaling relation deduced from the definition of the fractal dimension, Eq. (6.10):

$$R(N,C) \sim N^{1/d_f} f(C/C^*), \tag{6.14a}$$

and

$$\pi(N,C) = \frac{C}{N} g(C/C^*). \tag{6.14b}$$

Here the prefactor $C_p \equiv C/N$ in Eq. (6.14b) is merely the pressure of an ideal gas that is obtained for very low concentrations when the chains are very far from each other.

The unknown functions $f(x)$ and $g(x)$ may be expanded for small x in the dilute regime but have singular behavior for large x in the semidilute regime. Therefore, in the dilute concentration regime, one expects corrections both for the radius and the osmotic pressure.

In the latter case, we may write

$$\pi(N,C) = \frac{C}{N}\{1 + \alpha C/C^* + \beta(C/C^*)^2 + \dots\}, \tag{6.15a}$$

where $\alpha, \beta, \dots$ are constants. This may be identified with a virial expansion,

$$\pi(N,C) = \frac{C}{N} + A_2 C^2 + \dots \tag{6.15b}$$

Comparing Eqs. (6.15a) and (6.15b) and using Eqs. (6.13) and (6.10) leads to the following expression for the second virial coefficient:

$$A_2 \sim (NC^*)^{-1} \sim N^{3/d_f}. \tag{6.16}$$

A similar expansion can be obtained for scattering intensity $S(q,C) \propto 1/(1 + q^2R^2 + \dots)$. For very low q, in the Guinier regime $qR \ll 1$, this expansion is the basis for the so-called Zimm plots that are commonly used to determine the radius of a chain and the second virial coefficient of a solution.

6.1.4 Semidilute Solutions

When the concentration C is increased above the overlap concentration C^*, one reaches a different regime where the macromolecules interpenetrate each other, and we expect the concentration effects to become dramatic. In dilute solutions, the concentration effects are represented by corrections to the power laws. Because the chains are fractals, the volume they occupy grows much faster than their mass. As indicated by Eq. (6.13), the larger the macromolecule, the smaller is C^*. For a typical polymer of 10^5 units, C^* is of the order of $10^{-2}\mathrm{g/cm^3}$.

For infinite chains, the overlap concentration vanishes, and one is left only with the semidilute range. In this range, because the chains are flexible, they overlap each other, and we expect the simple laws we discussed above to break down. Still, the scaling laws (6.14) are valid, but one has to look for other limits. The basic idea to understand the behavior of a polymer in this regime was given in the limit of a melt by Flory [1] and was later generalized to semidilute solutions by Edwards [26].

In a melt, the average interaction should cancel, since each monomer is surrounded by other monomers, and therefore the polymer should behave as an ideal chain.

We will see below that although this argument is valid for linear chains, it turns out to be wrong for branched polymers. The reason for this is related to the interpenetration of the various chains. For linear chains, this interpenetration effect was studied by Edwards [10], who introduced the concept of a screening length ξ. The idea here is that if we consider two monomers on a given chain, their total interaction is the sum of the direct excluded volume interaction and all the contributions coming from indirect interactions between them via other monomers belonging to other chains. This is equivalent to Debye–Hückel screening in an electrolyte solution. Because of this, the notion of "blob" was introduced. It corresponds to a part of the chain, made of g units, with radius ξ. Thus one may consider a polymer in a semidilute solution as an ideal chain if the blob is chosen as a statistical unit. Inside the blob, excluded volume interactions are still present. Note that at the overlap concentration, the blob is identical to the whole chain. Using these ideas, it was shown that

$$\xi \sim C^{-3/4} \tag{6.17}$$

and

$$R \sim \left(\frac{N}{g}\right)^{1/2} \xi \sim N^{1/2} C^{-1/8}. \tag{6.18}$$

Note that as concentration increases, the sizes of the blob and of the chain decrease. In the bulk, we recover Flory's results: the interaction completely screened, the size of the blob is the step length, and the chain is ideal. Thus the present model ensures a gradual cross-over from the swollen to the ideal behaviors for increasing concentrations.

The next quantity we will consider is the osmotic pressure [27]. We may use the same arguments as above to determine its dependence on C, starting with relation (6.14b). In the semidilute regime, we do not expect the expansion (6.15) to be valid, since the variable $x = C/C^*$ is larger than unity. Instead, we assume that $g(x)$ behaves as a power law. Its exponent is determined by the following condition. In this concentration range, we expect the osmotic pressure to be given by the density of contacts between polymers. This is again a collective property of the solution that should depend only on concentration and not on the mass of the individual chains. Using this condition, we find

$$\pi \sim C^{-d/(d_f - d)} \approx C^{9/4}, \tag{6.19}$$

a relation that was found first by des Cloizeaux [28]. Equation (6.19) was tested experimentally by Noda *et al.* [29].

Many points are remarkable in Eq. (6.19). The first is that these results differ strongly from what one would expect in a mean field approach. The second, and most remarkable result is that the fractal dimension controls the thermodynamic properties of the solution. This is extremely interesting because the fractal dimension was introduced to describe the properties of a single chain, where only small concentrations and distances in the order of several hundreds of Ångströms were considered. We are now discussing thermodynamic, macroscopic, properties of a solution that is semidilute, and where the polymers strongly interact. Thus what was introduced to describe a local property of a single chain controls a solution that may be rather concentrated: even a 20% solution may be in this concentration range.

6.2 GELATION FOR BRANCHED POLYMERS

So far we have considered polymers made of bifunctional units. These may react by two ends, or functionalities. When the monomers are more than bifunctional, polymerization leads to branched structures, and eventually to a solid called a gel [48]. In this section we will consider this case. As we will see, every polymer has still a fractal behavior. In addition to this, there is a very broad distribution of molecular weights, called polydispersity. Because of this, what is observed is an effective dimension that depends also on the dimension of the distribution. This holds for many polydisperse systems, with restrictions that will be discussed below. We will first present the distribution of molecular weights that is naturally found in the reaction bath. We will turn to dilute solutions, where the fractal dimension is smaller because of swelling. We will discuss the effective dimension that is observable. Then we will turn to the semidilute solutions and to the swollen gels. Finally, we will discuss the dynamics of these systems in the reaction bath.

6.2.1 The Sol–Gel Transition

Let us consider a vessel with multifunctional monomers. Each monomer may react by one or more of its f functional groups. As time proceeds, there is a formation of dimers, trimers, ..., polymers; this is the sol. This process makes the solution more and more viscous, because of the presence of large macromolecules. The viscosity diverges, and this defines a threshold time t_c. For $t > t_c$, in addition to the sol, there is an infinite molecule, the gel. Thus, there appears an elastic modulus due to the presence of a solid-like phase.

Although there are probably other universality classes, this transition was successfully modeled by bond percolation [6]. Generally, bond percolation on a lattice has each bond (line connecting two neighboring lattice sites) present randomly with probability p and absent with probability 1–p. Clusters are groups of sites connected by present bonds. For $p > p_c$ an infinite cluster is formed. Percolation theory (in a Bethe lattice approximation) was invented by Flory (1941) to describe gelation for three-functional polymers.

Sites are the unreacted monomers, bonds are the reacted functionalities. Clusters are the polymers, and the infinite cluster is the gel. We recall very briefly some results of percolation. The main result concerns the distribution of cluster sizes. This corresponds to what we called polydispersity. The distribution is very broad. If we call p the probability that a bond is reacted, p_c is its value at the gelation threshold, the average probability $P(N, \varepsilon)$ that a randomly selected monomer belongs to a large polymer with N monomers each at a small "distance" $\varepsilon \equiv p - p_c$ from the threshold is

$$P(N,\varepsilon) \sim N^{1-\tau} f(\varepsilon N^{\sigma}), \tag{6.20}$$

where τ and σ are percolation exponents [30] to be discussed below. The moments of the distribution have several interesting properties. The first moment is normalized below p_c. The higher moments diverge with different exponents

$$N_w \equiv \frac{\int NP(N,\varepsilon)\mathrm{d}N}{\int P(N,\varepsilon)\mathrm{d}N} \sim \varepsilon^{-\gamma} \tag{6.21}$$

and

$$N_z \equiv \frac{\int N^2 P(N,\varepsilon)\mathrm{d}N}{\int NP(N,\varepsilon)\mathrm{d}N} \sim \varepsilon^{-1/\sigma}. \tag{6.22}$$

Higher order moments defined the same way as above are proportional to N_z. The number of polymers with N units each is proportional to $P(N,\varepsilon)/N$

The exponent γ is the susceptibility exponent in percolation. Similarly, one may also define a characteristic length, corresponding to the size of the typical polymers in the sol, dominating in diverging moments like N_z. This length diverges as

$$\xi \sim \varepsilon^{-\nu}. \tag{6.23}$$

Using relations (6.22) and (6.23), we find the fractal dimension d_f for percolation clusters,

$$1/d_f = \sigma\nu. \tag{6.24}$$

Let us stress that this is the fractal dimension of the polymers in the reaction bath. We assume that all polymers that constitute the sol have this same fractal dimension. This was calculated by renormalization group techniques and computer simulations [31,32,33,34]. We will give a simple Flory derivation [35] that is close to the former results for all space dimensions. The polydispersity exponent τ can be shown to be related to the fractal dimension,

$$\tau = 1 + d/d_f. \tag{6.25}$$

This hyperscaling relation is valid for space dimensions $d \leq 6$.

Equation (6.25) implies that the distribution is very special; if one considers polymers with a given mass, they are in a C^* situation, i.e., they are in a space-filling configuration. Since they are fractals, however, voids are left in the structure. These voids are filled by polymers with smaller masses, with the same requirement for every mass: each one is in a C^* situation. Therefore, if one looks at the distribution, for any size considered, one always observes polymers at C^*. In this sense, the distribution is fractal [36,37]. Note that it is possible to relate the "masses" N_z and N_w (in units of the monomer mass) defined above by eliminating ε,

$$N_z \sim N_w^{d_f/(2d_f-d)}. \tag{6.26a}$$

Using relation (6.25), we get

$$N_z \sim N_w^{1/(3-\tau)}. \tag{6.26b}$$

Note that both relations (6.26a) and (6.26b) hold only if $d_f < d$, or equivalently if $\tau > 2$. If $d_f = d$, or $\tau = 2$, both masses become proportional to each other, and in our definitions, there is only one mass present in the problem. This will prove to be important in the discussion for the scattered intensity for dilute solutions below.

6.2.2 The Flory Approximation

Let us consider the large polymers, with mass N_z and radius ξ in the distribution. In the Flory approximation, one writes down a free energy made of two contributions

$$F = \frac{\xi^2}{\xi_0^2} + \frac{v}{N_w}\frac{N_z^2}{\xi^d}. \tag{6.27}$$

The first one is an entropic term where we assume that the polymer behaves like a spring with constant ξ_0^2, where ξ_0 is the radius of an ideal chain when no interactions are present. The second term is the interaction energy in which v is the excluded volume interaction, discussed for linear chains. Except for the presence of N_w, this is very similar to what we considered for chains. The presence of this factor is due

to the fact that the large polymers are penetrated by the small ones. Because of this, there is a screening of the interactions, as in the semidilute case for linear chains. The precise form for the energy was evaluated by Edwards [26] and de Gennes [38] in a Debye–Huckel approximation. The ideal chain radius ξ_0 was calculated on a Cayley tree [39] and was shown to be

$$N_z \sim \xi_0^4. \tag{6.28}$$

In the Flory approximation, all quantities, except the radius which is to be calculated, are assumed to have a mean-field behavior. Therefore there is a relation between N_z and N_w,

$$N_z \sim N_w^2. \tag{6.29}$$

Minimizing the free energy with respect to ξ and using relations (6.23) and (6.24), we get the fractal dimension d_f of the large percolation clusters,

$$d_f = \frac{1}{2}(d+2). \tag{6.30}$$

This was tested indirectly by measurements of the mass distribution and the exponent τ (6.25).

6.2.3 Dilute Solutions

Once the distribution of polymer sizes is known, it is possible to dilute the sol, and to consider dilute solutions. Let us stress that the growth of the polymers is quenched before dilution and that the distribution function is given. Because of the excluded volume interactions the polymers swell and their fractal dimension changes from d_f to d_f^a. The new fractal dimension d_f^a may be obtained within a Flory approximation by considering a free energy similar to that in Eq. (6.27). The difference between a dilute solution and the reaction bath which was considered above is in the interaction term. We expect that the excluded volume interactions are present in the dilute case whereas they are fully screened in the previous case [40]. Therefore, this contribution has the same form as in relation (6.9) for linear chains. It is straightforward to minimize the free energy with respect to the radius, which yields,

$$d_f^a = \frac{2}{5}(d+2). \tag{6.31}$$

The observation of this fractal dimension, however, is not easy, as we discuss now. Any experiment provides the average of the observed quantity over the whole distribution of masses. This averaging procedure leads to an effective dimension [41–44] that is different from the actual one. In order to see this, let us consider the scattered intensity. For a single mass, we have

$$S_1(q, N) = Ng[qR(N)]. \tag{6.32a}$$

where the function $g(x)$ behaves as a power law in the fractal range, $qR > 1$ and $qa \ll 1$, in such a way that the mass dependence disappears. For a distribution of masses, and in the dilute regime where one may neglect correlations between monomers belonging to different polymers, the total scattered intensity [45] is

$$S_{\text{total}}(q) = \sum P(N,\varepsilon) S_1(q, N). \tag{6.32b}$$

Using relations (6.32), (6.20), and (6.21), we get

$$S_{\text{total}}(q) = CN_w g(qR_z), \tag{6.32c}$$

where C is the monomer concentration and R_z is the radius of the largest polymers,

$$R_z \equiv \frac{\int NR^2(N)P(N,\varepsilon)\mathrm{d}N}{\int NP(N,\varepsilon)\mathrm{d}N}. \tag{6.33}$$

The radius R_z can be related to the largest masses N_z, Eq. (6.22), through the fractal dimension

$$R_z \sim N_z^{d_f^a} \approx N_w^{5/8} \quad (d=3). \tag{6.34}$$

This relation was tested by light scattering measurements and found to be in good agreement with experimental results. In the intermediate scattering range, $l^{-1} \gg q \gg R_z^{-1}$, the function $g(x)$ in Eq. (6.32) behaves as a power law. The exponent of $S_{\text{total}}(q)$ is determined by the requirement that we are now in the fractal regime where no explicit mass dependence should appear. Using relations of Eq. (6.26), we get

$$S_{\text{total}}(q) \sim q^{-d_f^a(3-\tau)} \approx q^{-8/5} (l^{-1} \gg q \gg R_z^{-1}) \quad (d=3). \tag{6.35}$$

Therefore, an effective fractal dimension appears, that describes the behavior of the polydisperse system. As can be seen from Eq. (6.32), this effective dimension is related to the actual one, but also to the exponent τ characterizing the distribution of masses. Note that this holds for percolation and for other distributions, as long as $\tau > 2$, as discussed above. The polydispersity effect disappears when $\tau = 2$. In this sense, we will say that such systems are not polydisperse.

This has an important implication. Measuring an exponent in a scattering experiment does not necessarily imply that one gets the fractal dimension directly. First one has to check the polydispersity by independent measurements, either with viscosity, or with second virial coefficient experiments. The latter may be calculated following the same steps as above and taking into account the interactions between the centers of masses of different polymers.

Finally, we define two more exponents related to the viscosity η and the elastic modulus G

$$\eta \sim \varepsilon^{-\kappa} G \sim \varepsilon^f \tag{6.36}$$

for which the theory is less clear [46–51]. Note that for crosslinks between very long linear chains one expects the Bethe lattice or Cayley tree exponents to be valid except in an unmeasurably small interval at the transition. We end by

noting that recently, very similar ideas were successfully applied to the diffusion of cancer cells in tissues modelled by a gel [52,53].

ACKNOWLEDGMENTS

The authors are much indebted to M. Adam, E. Bouchaud, W. Burchard, R. Colby, M. Delsanti, D. Durand, B. Farnoux, P.G. de Gennes, O. Guiselin, G. Jannink, L.T. Lee, L. Leibler, J. E. Martin, and M. Rubinstein for many discussions.

REFERENCES

1. P. J. Flory, *Principles of Polymer Chemistry* (Cornell University Press, Ithaca, 1953).
2. P. G. de Gennes, *Scaling Concepts in Polymer Physics* (Cornell University Press, Ithaca, 1979).
3. M. Doi and S. F. Edwards, *The Theory of Polymer Dynamics* (Oxford Science Publications, London, 1986).
4. J. des Cloizeaux and G. Jannink, *Les polymers en solutions* (ed. de Physique, Paris, 1987) [Engl. Transl: *Polymers in Solution*, Oxford University Press, 1990].
5. A. Yu. Grosberg and A. R. Khokhlov, *Statistical Physics of Macromolecules*, translated by Y. A. Atanov (AIP Press, New York, 1994).
6. D. Stauffer and H. E. Stanley, *From Newton to Mandelbrot: A Primer in Theoretical Physics* (Springer-Verlag, Heidelberg & New York, 1990).
7. A. Bunde and S. Havlin, eds., *Fractals and Disordered Systems* (Springer, Berlin, 1991).
8. J. Teixeira, in *On Growth and Form*, edited by H. E. Stanley and N. Ostrowsky (Martinus, Nijhoff, 1985).
9. J. P. Cotton, D. Decker, H. Benoit, B. Farnoux, J. Higgins, G. Jannink, R. Ober, C. Picot, and J. des Cloizeaux, Macromolecules **7**, 863 (1974).
10. S. F. Edwards, Proc. Phys. Soc. **65**, 613 (1965).
11. P. G. de Gennes, Phys. Lett. **38A**, 339 (1972).
12. M. J. Stephen, Phys Lett. **53A**, 363 (1975).
13. M. Daoud and G. Jannink, J. Phys. Lett. **37**, 973 (1976).
14. M. Moore, J. Phys. A **10**, 305 (1977).
15. I. M. Lifshitz, A. Grosberg, and A. Khoklov, Rev. Mod. Phys. **50**, 685 (1978).
16. M. Nierlich, J. P. Cotton, and B. Farnoux, J. Chem. Phys. **69**, 1379 (1978).
17. C. Williams, F. Brochard, and H. L. Frisch, Ann. Rev. Phys. Chem. **32**, 433 (1981).
18. B. Duplantier, Phys. Rev. Lett. **59**, 539 (1987).
19. B. Derrida, J. Phys. A **14**, L5 (1981).
20. H. J. Hilhorst, Phys. Rev. B **16**, 1253 (1977).
21. M. Daoud and J. P. Cotton, J. Phys. **43**, 531 (1982).
22. T. Birstein and E. Zhulina, Polymer **25**, 1453 (1984).
23. G. S. Grest, K. Kremer, and T. A. Witten, Macromolecules **20**, 1376 (1987).
24. J. Roovers, N. Hadjichristidis, and L. J. Fetters, Macromolecules **16**, 214 (1983).
25. A. Halperin, M. Tirrell, and T. P. Lodge, Adv. Polym. Sci. **100**, 31 (1991).
26. S. F. Edwards, Proc. Phys. Soc. **88**, 265 (1966).
27. M. Daoud, J. P. Cotton, B. Farnoux, G. Jannink, G. Sarma, H. Benoit, R. Duplessix, C. Picot, and P. G. de Gennes, Macromolecules **8**, 804 (1975).
28. J. des Cloizeaux, J. Phys. **36**, 281 (1975).
29. I. Noda, N. Kato, T. Kitano, and M. Nagasawa, Macromolecules **14**, 668 (1981).
30. H. Nakanishi and H. E. Stanley, Phys. Rev. B **22**, 2466 (1980).
31. T. C. Lubensky and J. Isaacson, Phys. Rev. Lett. **41**, 829 (1978); Phys. Rev. A **20**, 2130 (1979).
32. G. Parisi and N. Sourlas, Phys. Rev. Lett. **46**, 891 (1981).
33. P. J. Reynolds, W. Klein, and H. E. Stanley, J. Phys. C **10**, L167 (1977).
34. B. Derrida and J. Vannimenus, J. Phys. Lett. **41**, 473 (1980).
35. J. Isaacson and T. C. Lubensky, J. Phys. **42**, 175 (1981).
36. M. E. Cates, J. de Phys. Lett. **38**, 2957 (1985).
37. M. Daoud and J. E. Martin, in *The Fractal Approach to Heterogeneous Chemistry,* edited by D. Avnir (John Wiley, New York, 1990).
38. P. G. de Gennes, J. Polym. Sci. Polym., Symp. **61**, 313 (1977).
39. B. H. Zimm and W. H. Stockmayer, J. Chem. Phys. **17**, 1301 (1949).
40. M. Daoud and J. F. Joanny, J. de Phys. **42**, 1359 (1981).
41. M. Daoud, F. Family, and G. Jannink, J. de Phys. Lett. **45**, 119 (1984).
42. S. J. Candau, M. Ankrim, J. P. Munch, P. Rempp, G. Hild, and R. Osaka, in *Physical Optics of Dynamical Phenomena in Macromolecular Systems* (W. De Gruyter, Berlin, 1985), p. 145.
43. F. Schosseler and L. Leibler, J. Phys. Lett. **45**, 501 (1984).
44. F. Schosseler and L. Leibler, Macromolecules **18**, 398 (1985).
45. J. E. Martin and B. J. Ackerson, Phys. Rev. A **31**, 1180 (1985).
46. L. de Arcangelis, Comput. Sci. Eng. **5**, 78 (2004).
47. B. Ratajska-Gadomska and W. Gadomski, J. Phys. Cond. Matter 16, 9191 (2004).
48. J. P. Cohen, *Physical Properties of Polymeric Gels* (Addad, Wiley and Sons, 1996).
49. F. Prochazka, T. Nicolai and D. Durand, Macromolecules **29**, 2260 (1996).
50. T. Nicolai, H. Randrianantoandro, F. Prochazka and D. Durand, Macromolecules **30**, 5897 (1997).
51. D. Durand, and T. Nicolai, in *Encyclopaedia of Materials Science and Technology*, edited by K. H. J. Bushow, R. W. Cahn, M. C. Fleming, B. Ilschner, E. J. Kramer and S. Mahajan (Elsevier, **6**, 6116, 2001).
52. G. C. Fadda, D. Lairez, B. Arrio, J. P. Carton and V. Larreta-Garde, Biophys. **85**, 2808 (2003).
53. T. Abete, A. de Candia, D. Lairez and A. Coniglio, Phys. Rev. Lett. **93**, 228302 (2004).